Bioreactor Conditioning for Accelerated Remodeling of Fibrin-Based Tissue Engineered Heart Valves

A DISSERTATION
SUBMITTED TO THE FACULTY OF THE
UNIVERSITY OF MINNESOTA
BY

Jillian Beth Schmidt

IN PARTIAL FULFILLMENT OF THE REQUIREMENTS
FOR THE DEGREE OF
DOCTOR OF PHILOSOPHY

Dr. Robert T. Tranquillo, Advisor

May 2015

Acknowledgements

This Ph.D. thesis would not have been possible without assistance and guidance from colleagues, mentors, friends, and family, and I want to thank all who have provided me with technical and financial support as well as those who have encouraged me throughout my graduate career.

First, I must begin by thanking my advisor, Bob Tranquillo, for supporting me as I developed as a researcher, providing me with the opportunity to work in such an exciting research area, and guiding my thesis project. Thank you for your patience, advice, and encouragement throughout my time as a Ph.D. student.

Thank you to all members of the Tranquillo lab past and present who offered support and instruction, particularly Dr. Justin Weinbaum and Dr. Zeeshan Syedain for serving as mentors, Susan Saunders and Sandy Johnson for technical assistance, and Naomi Ferguson for culturing countless flasks of cells on behalf of my project. Many thanks to Jay Reimer for being my partner in crime on the valve project and helping out with almost every valve casting I performed over the course of six years. I truly value your support, friendship, and especially your ability to reach the top shelf. I am grateful to the hardworking undergraduate students who helped out on various projects related to this thesis: Alex, Kelley, Annica, Dejia, Jake, Stefani, and Kristina – thank you for your enthusiasm, dedication, and willingness to lend a hand. I also want to thank Dr. Cristine Charlesworth and the Mayo Proteomics Core for technical support with the NanoPro system.

This work would not have been possible without financial support from several sources. Thank you to the National Science Foundation for providing three years of fellowship support, the University of Minnesota Graduate School for a year-long fellowship, and the National Institutes of Health for funding the tissue engineered heart valve project.

I am so grateful to my family and friends for all of their support and for cheering me on throughout my graduate career. I especially want to thank my mom for helping me learn biology on the fly, my talented sister, Kiley, for taking my paint drawings and turning them into high quality graphics for papers and presentations, and my dad for bringing me a home-cooked meal whenever I decided I was in “crisis mode.” I would not be where I am today without your guidance and encouragement!

Abstract

Fibrin is a promising scaffold material for tissue engineered heart valves, as it is completely biological, allows for engineered matrix alignment, and is able to be degraded and replaced with collagen by entrapped cells. However, the initial fibrin matrix is mechanically weak, and extensive *in vitro* culture is required to create valves with sufficient mechanical strength and stiffness for *in vivo* function. Culture in bioreactor systems, which provide cyclic stretching and enhance nutrient transport, has been shown to increase collagen production by cells entrapped in a fibrin scaffold, accelerating strengthening of the tissue and reducing the required culture time. In the present work, steps were taken to improve bioreactor culture conditions with the goal of accelerating collagen production in fibrin-based tissue engineered heart valves using two approaches: (i) optimizing the cyclic stretching protocol and (ii) developing a novel bioreactor system that permits transmural and lumenal flow of culture medium for improved nutrient transport. The results indicated that incrementally increasing strain amplitude cyclic stretching with small, frequent increments in strain amplitude was optimal for collagen production in our system. In addition, proof of concept studies were performed in the novel bioreactor system and increased cellularity and collagen deposition near the lumenal surface of the tissue were observed.

Table of Contents

List of Tables

List of Figures

Chapter 1. Introduction

1.1. Anatomy and Function of Native Heart Valves

The heart has four chambers that coordinate the pumping of blood throughout the pulmonary and systemic circulations and likewise four heart valves that act as one way valves, preventing backward flow of blood into each chamber. As shown in Figure 1-1, blood in enters the right atrium through the superior vena cava and travels through the tricuspid valve into the right ventricle. Then the blood is pumped out through the pulmonary valve to the lungs where it is oxygenated. The oxygenated blood enters the left atrium and passes through the mitral valve into the left ventricle. From the left ventricle, the blood is pumped out through the aortic valve and delivered to the rest of the body. Each of these four heart valves is of key importance in maintaining the directional flow of blood through the heart. While the basic function of the four heart valves is the same, the hemodynamics and loading conditions are different. Each of the four valves has a unique location-specific anatomy which enables its function.[1]

1.1.1. The Atrioventricular Valves

The right atrium and ventricle and the left atrium and ventricle are connected by the tricuspid and bicuspid (mitral) valves, respectively. These two valves are referred to as the atrioventricular valves. Both atrioventricular valves consist of a valve annulus with leaflets. These leaflets are anchored to the ventricular walls by tendinous cords and the papillary muscles. During diastole, when the heart muscle is relaxed, blood flows

through the atrioventricular valves into the ventricles. During systole, the contraction phase, the leaflets close, preventing backflow of blood. The tendinous cords support the leaflets during systole and ensure coaptation. The tricuspid valve has three leaflets that are supported by three papillary muscle complexes while the mitral valve has two leaflets and two papillary muscle complexes. The leaflets of both the tricuspid and mitral valves are layered structures. The atrium facing surface of the leaflet, the atrialis layer, consists of aligned collagen and elastic fibers. Beneath the atrialis lies the spongiosa layer containing glycosaminoglycans (GAGs) and proteoglycans, which cushion the leaflets during closure. Finally, the fibrosa layer, consisting of aligned collagen fibers, provides the majority of the mechanical strength. The main cell type within the leaflet is the valvular interstitial cell (VIC) and both the atrial and ventricular surfaces of the leaflets are covered by valvular endothelial cells (VECs). The leaflets of the atrioventricular valves are attached to an annulus that is highly dynamic, changing shape throughout the cardiac cycle.[2,3]

1.1.2. The Semilunar Valves

The pulmonary and aortic valves direct the forward flow of blood from the ventricles to the lungs and body, respectively. Both valves are tri-leaflet valves, and because of the curved “half moon” shape of the junctions between the leaflets and the arterial wall, they are referred to as the semilunar valves. The pressure across the closed pulmonary valve is approximately 10 mmHg while the aortic valve sustains much higher pressure gradients of around 80 mmHg[4] and has thicker leaflets than the

pulmonary valve.[5] The valve leaflets are tri-layered structures consisting of the ventricularis layer (analogous to the atrialis in AV leaflets) which contains aligned collagen and elastic fibers, the shock absorbing spongiosa layer consisting of GAGs and proteoglycans, and the load bearing fibrosa layer containing aligned collagen fibers. As in the AV valves, the cells in the leaflets are comprised of VICs and VECs.[2,3]

The collagen fibers in the fibrosa layer are primarily aligned from commissure to commissure, and this collagen alignment gives the leaflet greater strength and stiffness in the commissural direction as compared to the radial direction.[2,6] The Young's modulus for the native human aortic valve leaflet is approximately 15 MPa in the circumferential direction, while in the radial direction the Young's modulus is only 1-2MPa.[6] During diastole, it is estimated that the leaflet strain in the radial direction is more than two times the strain in the circumferential direction, and this mechanical anisotropy is important for proper valve function under physiological loading.[7-9]

1.2. Heart Valve Defects and Disease

More than 85,000 heart valve related procedures are performed annually in the United States, and it is estimated that heart valve disease affects 2.5% of the population. While the prevalence of heart valve disease increases with age and is most prevalent in patients over 65, there are a variety of congenital heart defects that affect the valves of pediatric patients as well. The prevalence of congenital heart defects is approximately 8 in 1000 live births, and many of these defects require extensive reconstruction or replacement of one or more of the heart valves.[10]

1.2.1. Congenital Heart Defects

There several congenital heart defects that affect one or more of the heart valves and require valve repair or complete replacement. Atrioventricular septal defect is a condition in which the atrioventricular junction is malformed. Patients with this defect may have improperly formed tricuspid and mitral valves, and in many severe cases the tricuspid and mitral valves are combined into a common atrioventricular valve, instead of existing as two separate valves. In other congenital heart malformations patients may lack a tricuspid valve (tricuspid atresia) or suffer from insufficiency, malformation, or stenosis (narrowing) of one or more atrioventricular valves. The majority of the atrioventricular valve defects are repaired by restructuring the existing valves or re-routing the circulation. Several of these repairs involve multiple surgeries over the course of the first several years of the patient's life.

Stenosis of the semilunar valves is one of the more commonly occurring abnormalities. Although this stenosis can take various forms, a two-leaflet (bicuspid) aortic valve is one of the most prevalent congenital malformations. This defect prevents the valve from opening fully, resulting in altered pressure and flow characteristics. Tetralogy of Fallot is another common congenital heart defect that affects the semilunar valves. In patients with Tetralogy of Fallot the pulmonary valve is typically stenotic with a small annulus and thickened leaflets. Reconstruction or replacement of the semilunar valves is often required, either as a neonate or later in life for patients with stenotic semilunar valves.[11]

1.2.2. Acquired Valvular Disease

In addition to congenital valve defects, acquired valvular disease can also lead to valve insufficiency in adult patients. Heart valve disease is prevalent in the United States, comprising 10-20% of cardiac surgical interventions.[12] Risk for valvular disease is associated with increased age, and as the average age of the population continues to increase, incidence of valvular disease is expected to rise. Mitral valve regurgitation is the most common valve disease, affecting 1.7% of the adult population in the U.S.[10] This condition is ameliorated by mitral valve repair or replacement. Another common valve affliction in older patients is the progressive calcification of the aortic valve leaflets resulting in stenosis. This narrowing of the valve opening produces an increase in ventricular pressure and in turn results in left ventricular hypertrophy, a process in which the left ventricular wall thickens to compensate for the increased pressure. Left untreated, severe aortic stenosis can result in heart failure. Once a patient begins showing symptoms of aortic stenosis, the only current treatment option is replacement of the aortic valve with a prosthetic.[13]

1.3. Heart Valve Replacement: Current State of the Art

For many pediatric and adult patients with malformed or deteriorated heart valves, valve replacement is the standard treatment. There are currently two options for replacement valves: mechanical prosthetic valves and bioprosthetic valves. These prosthetic valves have been used successfully for several decades, increasing life span and improving the quality of life for many patients. However, each of the currently

available options has a unique set of advantages and drawbacks. The current gold standard for mechanical prosthetic valve design is a bileaflet valve that was initially manufactured by St. Jude Medical. The valve is made from pyrolytic carbon, and it consists of two leaflets, which open and close in response to the pressure difference across the valve. While these prosthetics are highly durable, patients receiving mechanical valves require lifelong anticoagulation therapy, which creates a bleeding risk and may require changes in lifestyle. The alternative is a bioprosthetic valve, which typically consists of a fixed porcine valve or tissue. In some cases human tissue homografts or autografts may be used, though these are limited in availability. While bioprosthetic valves are more biocompatible and do not require chronic anticoagulation, the valves are not living tissue, and over time they are prone to calcification and deterioration.[13] In addition, neither bioprosthetic nor mechanical prosthetic valves are capable of growth, which is particularly problematic for pediatric patients. With these drawbacks in mind, it is clear that there is room for innovative improvement in prosthetic heart valve design.

1.4. Heart Valve Tissue Engineering: Current Approaches

In order to address these shortcomings, researchers have begun work to develop a living tissue engineered heart valve (TEHV) that could be used as a replacement valve, particularly for young patients. Design criteria for a TEHV include sufficient mechanical properties, high durability, native-like hemodynamic behavior, and an ability to grow and adapt with the patient. The TEHV must also be non-thrombogenic

and non-immunogenic to prevent clot formation and immune rejection, respectively. Research groups have developed different methods to produce a TEHV that meets these demanding design criteria, but all approaches have certain aspects in common. All TEHVs are based on a scaffold material, which provides the mechanical support and correct heart valve geometry. These scaffold materials can be degradable synthetic polymers, such as polyglycolic acid or polylactic acid,[14-16] or biopolymers like fibrin or collagen.[17-19] In the classical tissue engineering approach, a TEHV is created by seeding or entrapping a relevant cell type, such as fibroblasts, mesenchymal stem cells, or smooth muscle cells, in the scaffold. This construct is then cultured *in vitro*, during which time the cells produce their own extracellular matrix (ECM) as the scaffold material is degraded.[15-20] The cell-produced ECM components, specifically collagen, provide the mechanical strength necessary to maintain valve structure and function. Various biochemical and mechanical stimuli can be used to guide the maturation process of the TEHV during the *in vitro* culture period,[20-24] and because a TEHV consists of living tissue, it has the ability to adapt and remodel in response to *in vivo* stimuli upon implantation.[14, 25-29]

Historically, the bulk of TEHV research focused on developing methods to create cellular tissue, preferably containing autologous cells to avoid an adverse immune response.[15-20, 28, 29] In this approach, a patient's cells would be isolated and used to produce an implantable TEHV. After weeks of *in vitro* culture, the TEHV could then be implanted back into the same patient from whom the cells were isolated. In recent years, there has been increased research into developing a TEHV that is available "off-

the-shelf," eliminating the long wait time between cell isolation and heart valve implantation[30-33] Decellularization, or removal of cells from the TEHV after *in vitro* culture, is one method of removing antigens that produce an immune response upon being implanted into a different patient. These TEHVs can be implanted acellular, or after seeding with patient specific cells such as mesenchymal stem cells (MSCs). Research is ongoing to determine how these decellularized TEHVs, both with and without seeded MSCs, are repopulated and remodeled by host cells *in vivo*.

In the Tranquillo Lab, TEHVs are created using a fibrin gel scaffold with neonatal human dermal fibroblasts (nhdfs) entrapped. Our TEHVs are completely biological, as fibrin is a biopolymer, isolated from the blood, which undergoes controllable, natural enzymatic degradation. Fibrin scaffolds are additionally advantageous because the cell-mediated fibrin gel contraction can be used to achieve tissue anisotropy similar to that of the native heart valve root and leaflets.[18] The entrapped nhdfs are capable of remodeling and compacting the fibrin gel, and with the appropriate geometric constraints, the alignment of the fibrin fibrils and cell-produced ECM can be controlled.[18,31] This is a major advantage over the commonly used isotropic synthetic polymer scaffolds, which do not recapitulate the native anisotropy. In the original fibrin-based TEHV design, a suspension of nhdfs in fibrinogen and thrombin was injected into a tri-leaflet or bi-leaflet Teflon mold with semilunar valve geometry. After several weeks of *in vitro* culture, the nhdfs compacted and aligned the fibrin fibrils around the mold surfaces and replaced the initial fibrin gel with aligned collagen. The resulting TEHV had two or three leaflets extending from a cylindrical

root segment and was composed primarily of cell produced collagen. Due to the geometrical constraints of the mold, the collagen was aligned circumferentially in the root segment and from commissure to commissure in the leaflets, thus mimicking the collagen alignment in native semilunar valves.[18]

In the current approach, fibrin based engineered tissue tubes are formed, and after several weeks of *in vitro* culture, the tubes consist mainly of cell-produced collagen and have near native strength and stiffness. The tubes are allowed to shorten axially but are constrained by an inner mandrel in the radial direction; therefore, this collagen is primarily aligned in the circumferential direction. At this point, the tubular constructs are decellularized and placed over a three post frame as shown in Figure 1-2. Under back pressure, the tube collapses over the frame, forming a tri-leaflet valve that is capable of opening and closing in response to pressure gradients. When the tube is collapsed over the frame, the collagen alignment is from commissure to commissure, similar to the native heart valve.[31] This acellular engineered tissue is capable of being recellularized either *in vitro*, by seeded mesenchymal stem cells[30] or *in vivo* by host cell invasion after implantation.[32]

1.5. Mechanical Conditioning of Tissue Engineered Heart Valves

For most current TEHV designs, extensive *in vitro* culture is required to produce a valve with sufficient mechanical strength and stiffness for implantation.[15-20, 24, 31] This process is particularly important in fibrin-based TEHVs, which initially have low mechanical strength and stiffness.[18, 24] Often culture periods of several months are

required to achieve the desired properties, and this long term culture can be costly. With this in mind, several groups have developed bioreactors that provide mechanical stimuli to aid in tissue formation and accelerate TEHV maturation. A variety of mechanical stimulation modes including shear flow, transmural flow, static stretch, cyclic mechanical stretching, and flexure have been used to improve tissue formation and maturation.[16,19,20,22,24] A TEHV is a complex, three-dimensional structure, and fluid flow through a TEHV results in a combination of these stimulation modes. Due to the complexity of the system, the optimal mechanical conditioning protocol is still unknown.

Several research groups have developed pulse duplicator flow loop systems, designed to mimic *in vivo* conditions, and have seen improved mechanical properties in their TEHVs.[20,34] However, the loading in these systems is complex and difficult to control as the tissue remodels and TEHV properties change. Rather than attempting to replicate physiological conditions, some research groups have developed bioreactors to apply well-defined mechanical stimulation to TEHVs. Mol et al. developed a Diastolic Pulse Duplicator system in which pulsatile back pressure was applied to coapting leaflets, and they observed qualitative improvement in tissue formation using this simpler loading scheme.[16] Syedain et al. developed a pulse-stretch bioreactor in which the TEHV is placed inside a latex tube and cyclically distended by the injection and removal of culture medium from both ends of the device. This system facilitates the application of controlled cyclic stretching of the root and leaflets, as the distension is determined by the stiffer properties of the latex tube rather than the changing properties

of the developing tissue. By incrementally increasing the root distension from 5% to 15% over a three week conditioning period, they were able to increase the circumferential ultimate tensile strength (UTS) and Young's Modulus of the leaflets by 97% and 77%, respectively, compared to statically cultured controls.[24]

In our group's current approach, a modification of this pulse-stretch bioreactor is used to mechanically condition the tubular tissue constructs before they are decellularized and placed over the three-post frame. In this bioreactor, tubular fibrin-based tissues are placed on the outside of a latex support sleeve and attached to two custom end pieces. Cyclic stretching is achieved by the injection of culture medium into the lumen of the latex tubing.[31,35] A schematic of this bioreactor is shown in Figure 1-3. Advantages of this system include well-controlled cyclic stretching, simple assembly, and ease of sterilization between experiments.

Although a variety of cyclic stretching bioreactors have been developed to strengthen and reduce the culture time of TEHVs, the optimal stretching protocol for accelerated tissue formation has not been well characterized. While there has been some study of the effects of stretch magnitude and duration on the collagen production pathway in various fibroblast-like cells,[36-46] reported results have been highly variable, and a thorough investigation of cell response to cyclic stretching has not been performed. Additionally, several of the investigations into cyclic stretching induced collagen production have been performed in two-dimensional systems,[40,43] which may not necessarily translate to three-dimensional tissue-engineered constructs. Currently, seven to eight weeks of *in vitro* culture is required for fibrin-based TEHVs to reach near

physiological strength and stiffness. Long term *in vitro* culture is expensive, particularly for these large tubular tissue constructs, so a reduction in the required culture duration is highly desirable. The work presented here took steps to improve the effectiveness of bioreactor culture both by optimizing the cyclic stretching regimen and modifying the bioreactor to improve nutrient transport, ultimately aiming to accelerate collagen deposition and produce mechanically robust TEHVs more quickly and cost effectively.

1.6. Figures

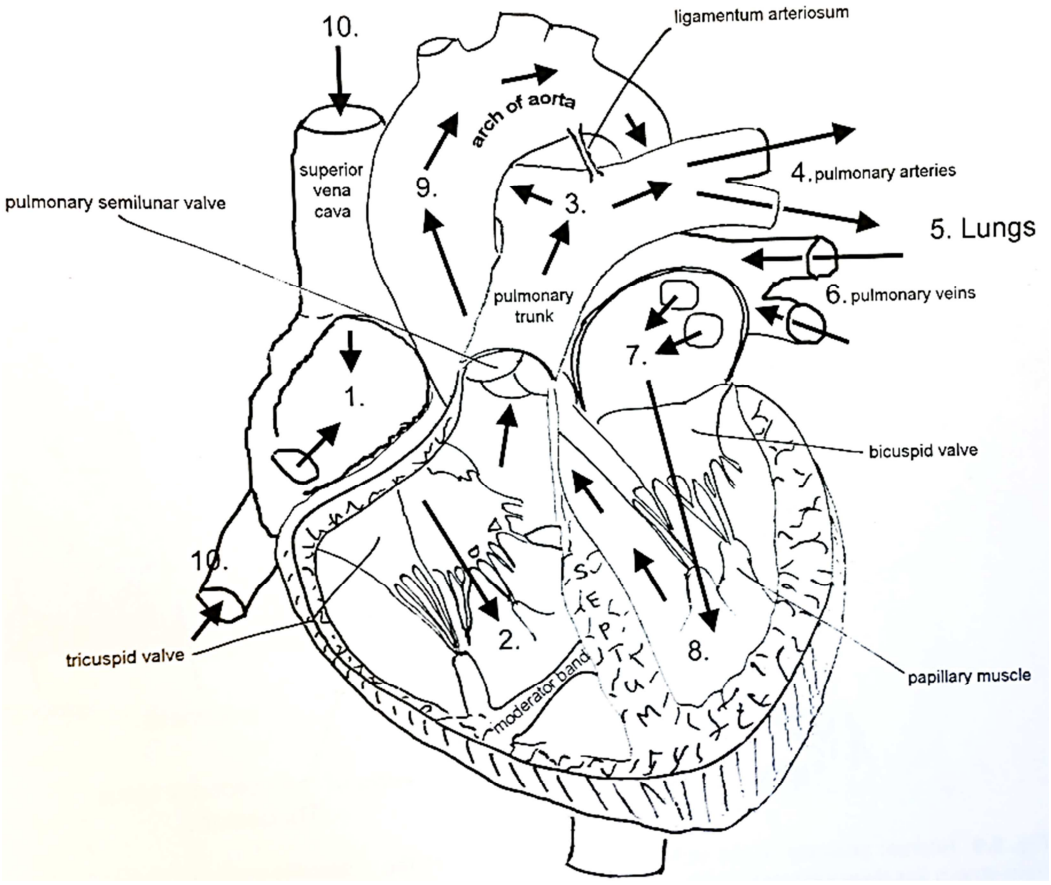

Figure 1-1.

Flow of blood through the human heart is regulated by the four heart valves, the tricuspid, pulmonary, bicuspid, and aortic valves. Adapted from [1].

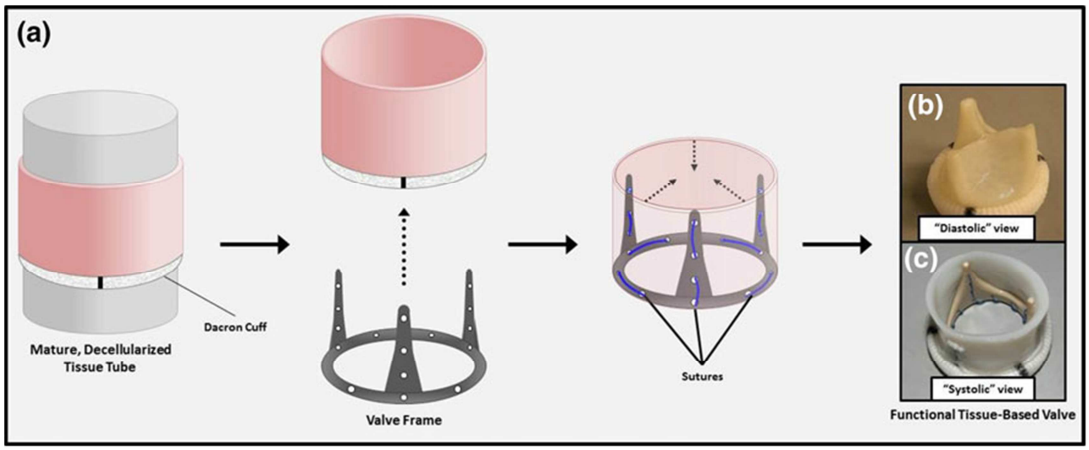

Figure 1-2.

(a) Schematic of tubular heart valve construction and images of the valve in the (b) closed and (c) open configurations. Adapted from [31]

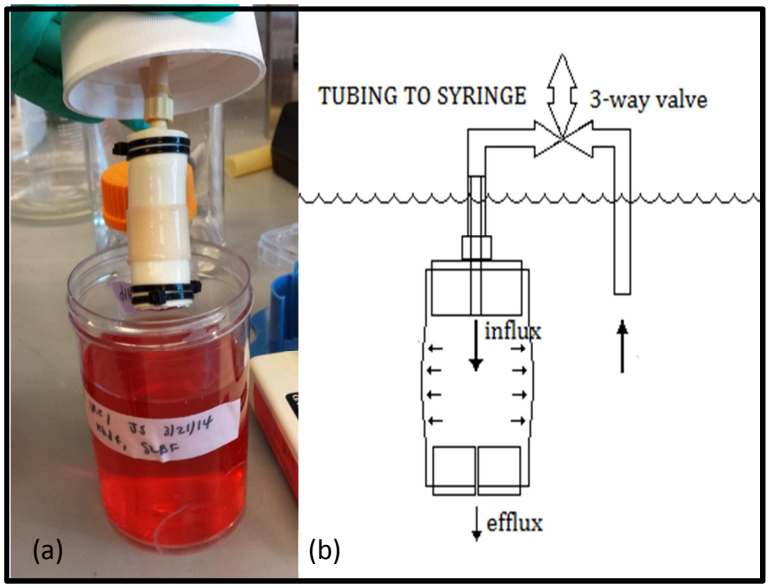

Figure 1-3.

Image (a) and schematic (b) of the current Tranquillo lab bioreactor for cyclically stretching large diameter tissue tubes. Medium is injected into the lumen of the latex by a reciprocating syringe pump causing cyclic distension of the latex sleeve and tissue construct. The syringe is refilled from the surrounding medium through a 3-way valve. Adapted from A. Weston.

Chapter 2. The Effects of Constant Amplitude, Intermittent, and Incrementally Increasing Strain Amplitude Cyclic Stretching on ERK1/2 and p38 Signaling in Dermal Fibroblasts

2.1. Introduction

Mechanical conditioning is a widely employed method for obtaining the desired properties and function in engineered tissues. In engineered heart valves, arteries, ligaments, and skeletal muscle, where high mechanical strength is a requirement, cyclic mechanical stretching regimens have been used to induce cells to increase their production and maturation of collagen.[16,19,24,35,36,41,42,45] Collagen is the major load bearing component in most native tissues, and increased collagen content is highly correlated with an increase in strength and stiffness in engineered tissues.[35,36,42,45,47,48]

While cyclic stretching regimens are a common step in many tissue engineering fabrication processes, much is still unknown about the mechanism through which stretching results in increased collagen content, and thus the optimal cyclic stretching protocol may not be employed. The need for optimized cyclic stretching protocols is particularly crucial in attaining suitable properties in engineered tissues based on a sacrificial fibrin gel scaffold. Fibrin is an attractive scaffold biomaterial, as it is completely biological, degradable, can be cast in various geometries, and can be aligned and remodeled by entrapped cells.[49] However, a fibrin gel has extremely low strength and stiffness compared to native collagenous tissues, and creating a fibrin-based tissue

with sufficient mechanical stiffness and strength for *in vivo* function absolutely requires stimulating an increase in the cellular production of collagen.

The success of constant amplitude cyclic stretching protocols in increasing cellular collagen production is limited by adaptation of the cells to the applied mechanical stimulus.[41,42] In order to combat the negative effects of adaptation, various stretching regimens have been employed including incrementally increasing strain amplitude approaches[42] as well as intermittent stretching, in which tissues are exposed to alternating periods of cyclic stretching and static culture.[36,41] These perturbations to constant amplitude cyclic stretching allow the cells to be re-stimulated by either subsequent applications of stretching after a rest period or an increment in the applied stretch amplitude. Previous studies have demonstrated that phosphorylation of extracellular signal-regulated kinase 1/2 (ERK1/2) occurs rapidly following the onset of cyclic stretching of cardiovascular fibroblasts, and that this activation is required for cyclic-stretching induced collagen transcription.[43] Similar signaling behavior has been observed for a variety of cell types in response to cyclic stretching, and it has been shown that the ERK1/2 activation response is transient, with peak activation occurring 5-20 minutes after the onset of cyclic stretching and return to baseline level by 1 hour.[41,43,50-52] Although this adaptation occurs rapidly, it has been shown that ERK1/2 can be reactivated following a rest period by a second onset of stretching.[41] This suggests that it may be possible to repeatedly activate ERK1/2 to maximize the benefit of cyclic stretching.

The aims of this study were (i) to characterize the transient signaling response of fibroblasts to constant amplitude cyclic stretching by monitoring phosphorylation of both ERK1/2 and p38, a known ERK1/2 inhibitor, and (ii) to determine the timing and nature of the perturbation to constant amplitude cyclic stretching that is required for ERK1/2 reactivation. This work provides insight into the signaling response of fibroblasts undergoing cyclic stretching and offers guidance in selecting a mechanical conditioning protocol to accelerate collagen production in fibrin-based engineered tissues.

2.2. Methods

2.2.1. Cell Culture

Neonatal human dermal fibroblasts (Lonza) were expanded in 50:50 DMEM:F12 with 15% fetal bovine serum (Hyclone), 100 µg/ml streptomycin, and 100 U/ml penicillin. Cells were grown to confluence and harvested for use at passage 7.

2.2.2. Fibrin-based Tissue Construct Fabrication and Culture

Fibrin gels with entrapped cells were created by suspending neonatal human dermal fibroblasts in DMEM and then mixing the cells with a 20 mM HEPES-buffered saline solution containing bovine fibrinogen (Sigma). In order to form a fibrin gel, a solution of bovine thrombin (Sigma) and $CaCl_2$ in DMEM was added to the fibrinogen/cell solution. The solution was injected into 6-well circular tissue-train plates

(Flexcell® International), which have a circular foam insert that anchors the gel around its circumference. The volume of gel in each well was 2 ml. The final composition of the gel was 6.7 mg/ml fibrinogen, 500,000 cells/ml, 0.8 U/ml thrombin, and 5 mM $CaCl_2$. The discs were allowed to gel for 6 minutes in the tissue culture hood at 20°C and an additional 24 minutes in a standard cell culture incubator at 37°C. After the solutions had gelled, DMEM supplemented with 10% fetal bovine serum, 100 µg/ml streptomycin, 100 U/ml penicillin, 0.25 µg/mL amphotericin B, 50 µg/ml ascorbic acid, and 2 µg/ml insulin was added (5 ml per well). Medium was replaced three times weekly. All constructs were cultured statically for one week before cyclic stretching regimens were applied.

2.2.3. Cyclic Stretching of Tissue Constructs

Uniaxial cyclic stretching was applied to the constructs using the FX-5000 Tension System and Arctangle® loading station (Flexcell® International). The 6-well tissue-train plates have a flexible silicone bottom which was uniaxially stretched by the application of vacuum beneath the wells (Figure 2-1,a-d). All cyclic stretching regimens were applied using a square waveform with a frequency of 0.5 Hz, and a duty cycle of 15%. The applied strain was validated for the fibrin constructs using digital image correlation as described by Raghupathy et al.[53] Relatively uniform uniaxial strain was applied to a central rectangular area approximately 13 mm by 17 mm, and this strain was consistently applied throughout the duration of the experiments. While there was some heterogeneity in the strain field in this region, the strain was primarily

uniaxial and, averaged over the region, was in good agreement with the set point. Four 6 mm biopsy punches were taken from this region for characterization (Figure 2-1,e). The constructs remained in a standard cell culture incubator for the duration of the stretching regimens.

2.2.4. Protein Extraction

At harvest, constructs were excised from the wells, rinsed in phosphate buffered saline (PBS), and frozen at -80°C. Samples were lysed by sonication in Bicine/CHAPs buffer with 1X Aqueous and DMSO Inhibitor Cocktails (ProteinSimple) and placed in an end over end mixer at 4°C for 30 minutes. The lysates were purified by centrifugation at 13,000 rpm for 15 minutes at 4°C. The protein concentrations were determined using a bicinchoninic acid assay (Pierce).

2.2.5. Nano-fluidic Proteomic Immunoassay for ERK1/2 Phosphorylation

Nano-fluidic immunoassay experiments were performed on the purified lysates using a Nanopro 1000 system (ProteinSimple, Mayo Proteomics Core Facility).[54] Lysates were used at a final concentration of 100 µg/ml. Briefly, this system separates proteins by isoelectric point within a small capillary, and fixes them to the inner surface of the capillary after separation. This sensitive separation allowed differentiation between the isoforms of the ERK1/2 protein. Separated proteins were incubated with a pan-ERK1/2 antibody at a dilution of 1:200 for 2 hours. This antibody binds to all isoforms of ERK1/2, so unphosphorylated, single phosphorylated, and double

phosphorylated ERK1 and ERK2 could be probed using a single antibody (Figure 2-2). Proteins were incubated in HRP-conjugated secondary antibody at 1:100 for 1 hour followed by chemiluminescence reagent. The emitted light was detected through the wall of the capillary with a 30 second exposure by a camera, outputting chemiluminescence intensity as a function of isoelectric point. Peak identification of the ERK1/2 isoforms was verified by registry with peaks from HeLa control samples and isoform specific antibodies. All antibodies and reagents were acquired from ProteinSimple. The results were quantified using Compass software (version 1.8.1) using the peak area function. Ratios of phosphorylated ERK1/2 (all phosphorylated isoforms) to total ERK1/2 (all isoforms) are reported and normalized as indicated in corresponding figure captions.

2.2.6. Western Blot for p38

Reducing SDS-PAGE was used to separate 20 µg of total protein per well. The proteins were transferred to a nitrocellulose membrane and blotted for phosphorylated p38 (Cell Signaling Technologies #9211) and total p38 (Cell Signaling Technologies #9212). The blots were blocked for 1 hour in 5% dry milk, 0.1% Tween-20 in PBS, and then incubated for 1 hour in primary antibody at 1:1000 in tris-buffered saline with 0.1% Tween-20 (TBS-T) and 5% bovine serum albumin. Blots were washed with TBS-T and incubated for 1 hour in secondary antibody (1:2000 anti-rabbit IgG, GE Healthcare) in the blocking solution. Finally blots were washed in TBS-T and TBS and developed using Luminata Classico enhanced chemiluminesence (EMD Millipore).

Films were scanned and digitized, and ImageJ (NIH) was used to quantify band density. The ratio of phosphorylated p38 to total p38 is reported and normalized as indicated in corresponding figure caption.

2.2.7. Statistics

All figures show mean ± standard deviation with at least n=3 per group. Significance was determined using Student's t-test for two groups and one-way ANOVA for more than two groups with the Tukey post-hoc test in GraphPad Prism software for Windows with $p<0.05$ reported as significant. Symbols or bars are used to indicate significant differences and explained in the corresponding figure captions.

2.3. Results

2.3.1. ERK1/2 and p38 MAPK phosphorylation time course: constant amplitude stretching

To determine the activation time course of ERK1/2 and p38 MAPK, samples were stretched continuously with 5% strain amplitude for 15 minutes, 1, 3, and 6 hours. At each time point stretched samples (n=3) and static controls (n=3) were harvested. Cyclic stretching resulted in peak phosphorylation of both ERK1/2 and p38 at 15 minutes (Figure 2-3a,b). By 1 hour, ERK1/2 phosphorylation was only slightly elevated above static levels, while p38 phosphorylation remained elevated until the 6 hour time

point. Original Western blots for phosphorylated and total p38 are shown in Figure 2-3c.

2.3.2. ERK1/2 pathway activation: strain amplitude dependence

In order to study the dependence of ERK1/2 phosphorylation on strain amplitude, samples were stretched with either 5% or 10% strain amplitude (n=3 per group). At 15 minutes stretched samples and static controls were harvested. Both 5% and 10% amplitude cyclic stretching resulted in ERK1/2 activation at 15 minutes, and there was no difference in the magnitude of activation between the two strain amplitudes (Figure 2-4). Note that each signaling experiment was carried out separately, so small discrepancies in the maximal ERK1/2 activation value are likely due to inter-experiment variation.

2.3.3. ERK 1/2 pathway reactivation: intermittent stretching

According to the determined ERK1/2 phosphorylation time course, peak phosphorylation was achieved at 15 minutes, after which point the cells were no longer responsive to the constant amplitude cyclic stretching. In order to determine how soon the pathway could be reactivated by a second onset of cyclic stretching, samples were stretched with 5% strain amplitude for 15 minutes and allowed to rest for 15 minutes, 3 hours, or 6 hours (n=3 per group). Following the rest period, the samples were stretched with 5% strain amplitude for an additional 15 minutes before harvest. ERK1/2 was unable to be reactivated fully after 15 minutes of rest, and there was a trend of

increasing reactivation up to the 6 hour time point where full reactivation was achieved (Figure 2-5a).

Next we tested various stretching durations within the 6 hour refractory period. Samples were stretched with 5% strain amplitude for 15 minutes, 1 hour, or 5 hours and then sat statically for the remainder of the 6 hour period (5 hours 45 minutes, 5 hours, and 1 hour, respectively). Then all samples were re-stimulated with 5% amplitude cyclic stretching for 15 additional minutes and harvested (n=3 per group). In all three groups, regardless of the stretch/rest durations within the 6 hour period, ERK1/2 was reactivated (Figure 2-5b).

2.3.4. ERK1/2 pathway reactivation: incrementally increasing strain amplitude stretching

Similarly, we sought to investigate the effects of an increase in strain amplitude on ERK1/2 phosphorylation. Samples were stretched with 5% amplitude for 1 or 6 hours, at which point the strain amplitude was increased to 10%. Samples were harvested (n=3 per group) immediately before and 15 minutes after the increment in strain amplitude. It was determined that stretching-induced ERK1/2 phosphorylation was only achieved by increasing the strain amplitude at 6 hours; the cells did not respond to the increment at the 1 hour time point (Figure 2-6). The experiment was repeated with an increment in strain amplitude of only 1% (5% to 6% at 6 hours), and full ERK1/2 activation was also achieved.

2.4. Discussion

In this model system for a fibrin-based engineered tissue, 5% strain amplitude cyclic stretching resulted in transient phosphorylation of both ERK1/2 and p38 MAPK with peak phosphorylation at 15 minutes for both. Phosphorylation of ERK1/2 returned to near-static levels by 1 hour, while p38 phosphorylation remained elevated for at least 3 hours. The magnitude of ERK1/2 activation at 15 minutes did not depend on the strain amplitude. Reactivation of ERK1/2 was achieved either by (i) the onset of an additional 5% amplitude stretching period after 6 hours of static culture, or (ii) an increment of 1% in the strain amplitude after 6 hours of constant amplitude cyclic stretching.

The transient ERK1/2 activation in response to 5% continuous stretching noted above has been observed on a similar time scale for a wide variety of cell types in both two-dimensional and three-dimensional culture.[41,43,50-52] In addition, our finding that the strain amplitude did not affect ERK1/2 activation has also been observed for Achilles tendon fibroblasts in an engineered tendon model subjected to strain amplitudes of 2.5%, 5%, and 10%.[41] As phosphorylation of ERK1/2 has been shown to be necessary for stretch-induced up-regulation of collagen transcription by cardiac fibroblasts,[43] it was hypothesized that some perturbation to constant amplitude cyclic stretching may be able to repeatedly activate ERK1/2 and increase collagen synthesis for the dermal fibroblasts in our fibrin-based engineered tissues.

It was determined that the dermal fibroblasts exhibited a 6 hour refractory period before ERK1/2 could be re-stimulated, either by the onset of an additional stretching period or an increment in the strain amplitude. Paxton et al. obtained a similar result in

their engineered tendon system in which rat Achilles tendon fibroblasts also exhibited a 6 hour refractory period before ERK1/2 could be reactivated by intermittent cyclic stretching.[41] In our system the durations of stretch and rest periods within the 6 hours did not affect ERK1/2 reactivation, so it appears that as long as the cells undergo a brief static period before a second onset of cyclic stretching, reactivation will be achieved. In addition, it was found that an increment in strain amplitude of only 1% was able to reactivate ERK1/2 after 6 hours of constant amplitude cyclic stretching.

In order to provide additional insight into ERK1/2 dynamics, we also characterized the time course of p38 phosphorylation in our system. p38 activation has been implicated in inhibiting ERK1/2 and thus having negative effects on stretch-induced collagen production. Papakrivopoulou et al. demonstrated that constitutively active p38 reduced promoter activity of procollagen1 α1, and that the combination of cyclic stretching and inhibition of p38 activation increased procollagen1 α1 transcription in cardiac fibroblasts.[43] In our same fibrin-based engineered tissue, we showed that drug inhibition of p38 activation (SB 203580) increased stretching-induced ERK1/2 phosphorylation and collagen deposition.[55] In the present study, p38 phosphorylation was maximal after 15 minutes of 5% amplitude stretching, but its phosphorylation duration was longer than that of ERK1/2, returning to static levels only at the 6 hour time point. Transient phosphorylation of p38 by cyclic stretching has been observed in other two-dimensional and three-dimensional systems as well.[41,43] It is proposed that the cell's refractory period for ERK1/2 activation may be caused by the

prolonged p38 phosphorylation and alleviated by the return of p38 to basal levels at 6 hours.

In summary, the nature ERK1/2 and p38 activation in response to cyclic stretching has been characterized for dermal fibroblasts in a fibrin-based engineered tissue. It was determined that ERK1/2 activation occurs within only the first hour of cyclic stretching, and the pathway can only be reactivated after a 6 hour refractory period. The ERK1/2 phosphorylation dynamics suggest that two optimized cyclic stretching regimens can be applied to fibrin-based engineered tissues: (i) an intermittent regimen in which cells are re-stimulated by cyclic stretching periods every 6 hours and (ii) an incremental regimen in which the strain amplitude is increased by 1% after no less than 6 hours of constant amplitude cyclic stretching. It is hypothesized that application of these regimens, which repeatedly activate ERK1/2, will accelerate collagen deposition by the fibroblasts in our engineered tissues. Long-term application of these cyclic stretching regimens is presented in Chapter 3.

2.5. Figures

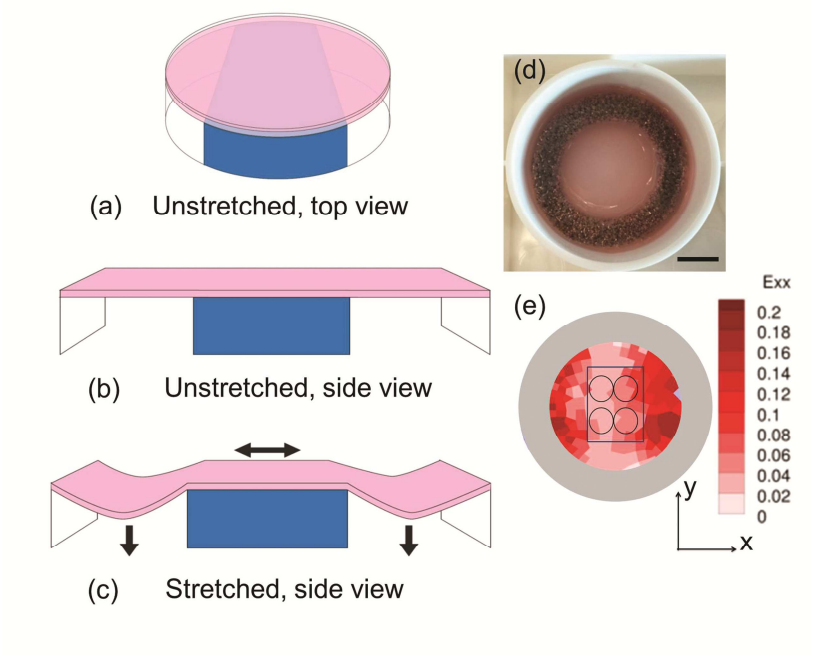

Figure 2-1.

Schematic of Flexcell® tension system for uniaxial cyclic stretching. (a) and (b) depict the unstretched top and side views, respectively, for a single well. The stretched configuration, produced by the application of vacuum beneath the well, is shown in (c). A sample fibrin-based tissue construct is shown in (d), secured to the perimeter of the silicone membrane by a foam ring with the black bar indicating 1 cm. The strain field is shown for 5% applied strain (e). For analysis, four 6 mm biopsy punches were taken from the uniaxially stretched region (blue rectangle).

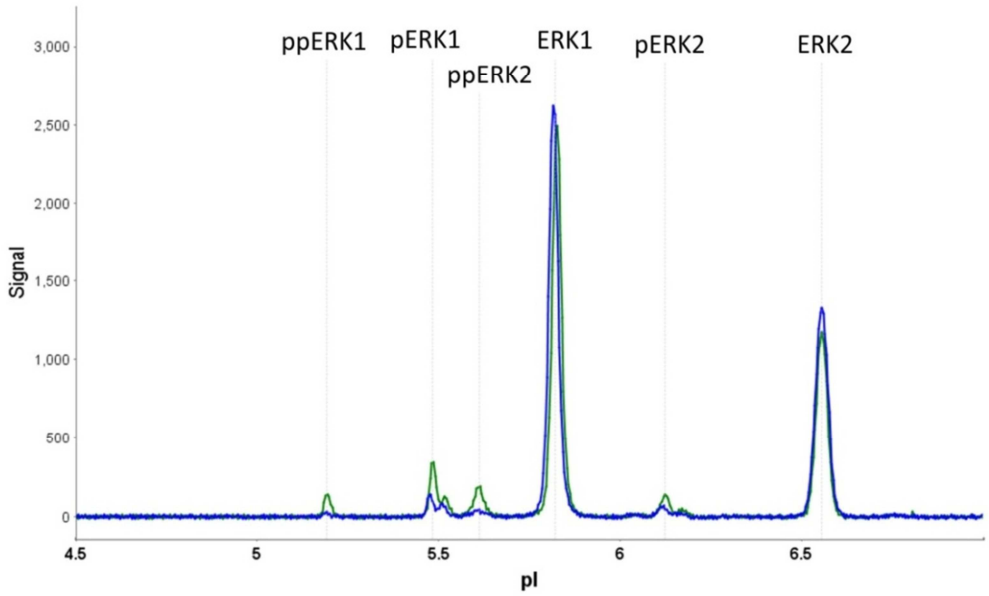

Figure 2-2.

Chemiluminescence intensity versus isoelectric point for static (blue) and 5% continuously stretched (green, with larger phosphorylated peaks) samples at 15 minutes. Peak identification was validated with HeLa control lysates and isoform specific antibodies.

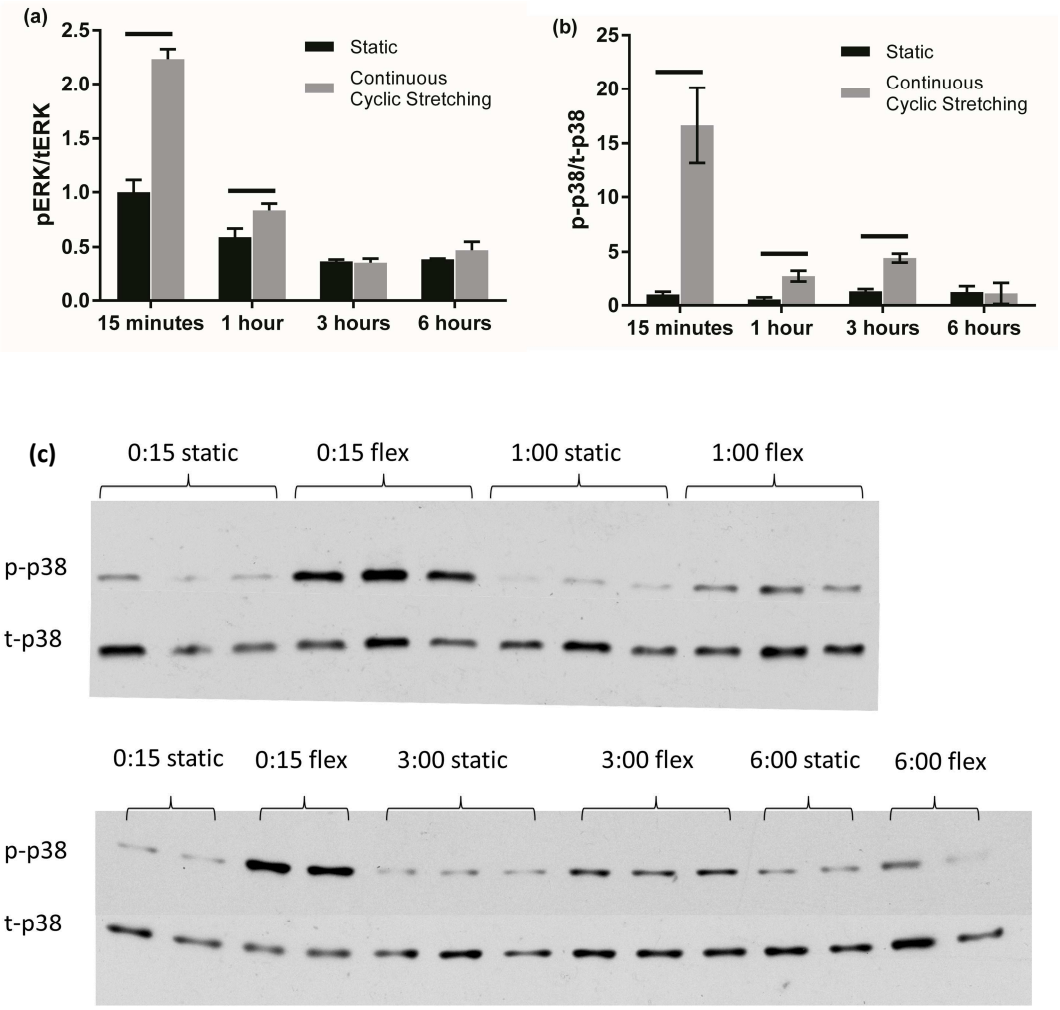

Figure 2-3.

(a) ERK1/2 and (b) p38 phosphorylation time courses during continuous cyclic stretching with 5% strain amplitude. All data are normalized to the 15 minute static value. Horizontal bars indicate differences ($p<0.05$) using Student's t-test between time-matched stretched and static samples (n=3 per group). (c) Representative Western blots for phosphorylated and total p38.

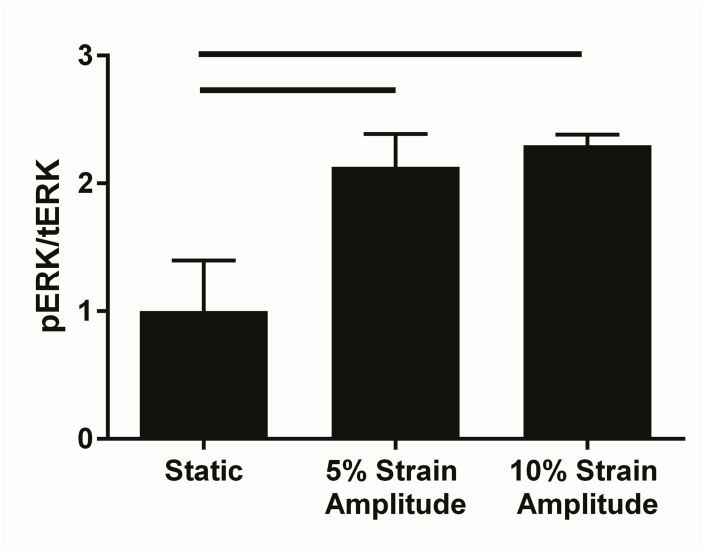

Figure 2-4.

ERK1/2 phosphorylation after 15 minutes of static culture, 5% constant amplitude cyclic stretching, or 10% constant amplitude cyclic stretching. All data are normalized to the 15 minute static value. Horizontal bars indicate differences ($p<0.05$) using one-way ANOVA with Tukey post hoc test (n=3 per group).

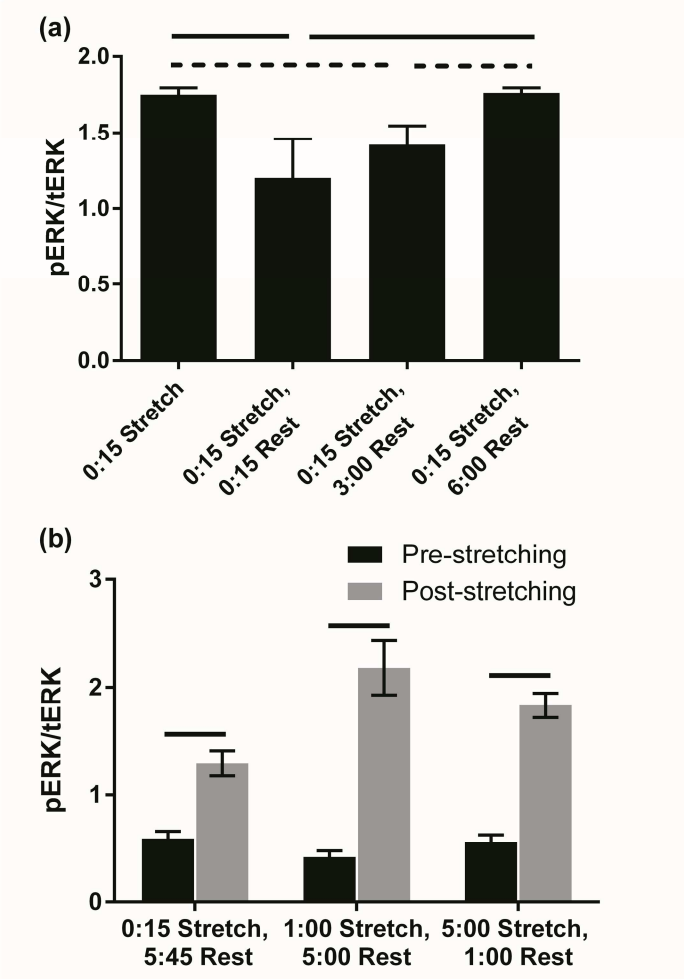

Figure 2-5.

(a) Reactivation of ERK1/2 15 minutes after onset of a second cyclic stretching period following rest durations of 15 minutes, 3 hours and 6 hours. ERK1/2 activation at the end of the initial 15 minute stretch is also shown. All data are normalized to the 15 minute static value. Solid horizontal bars indicate differences ($p<0.01$) and dashed horizontal bars indicate trends ($p<0.09$) using one-way ANOVA with Tukey post hoc test (n=3 per group). (b) Reactivation of ERK1/2 15 minutes after onset of a second cyclic stretching period following stretch/rest durations of 0:15/5:45, 1:00/5:00, and 5:00/1:00. All times are given in (hh:mm), and data are normalized to the 15 minute static value. Horizontal bars indicate differences ($p<0.05$) using Student's t-test between paired pre/post-stretching groups (n=3 per group).

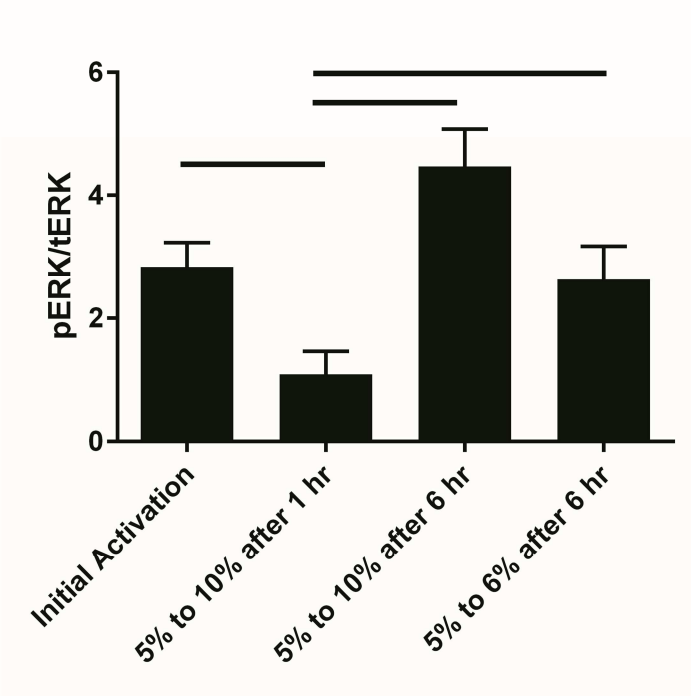

Figure 2-6.

Activation of ERK1/2 15 minutes following an increment in the strain amplitude. All data are normalized to the pre-perturbation value immediately prior to the strain increment. Horizontal bars indicate differences between groups ($p<0.01$) using one-way ANOVA with Tukey post hoc test (n=3 per group).

Chapter 3. The Effects of Optimized Intermittent and Incremental Cyclic Stretching Regimens on Collagen Deposition by Fibroblasts in an Engineered Tissue

3.1. Introduction

As discussed in Chapter 2, mechanical conditioning is a crucial step in the fabrication of engineered tissues where high mechanical strength and stiffness are required, such as heart valves, arteries, ligaments, and muscle. In the previous chapter, dermal fibroblasts' response to cyclic stretching at the cell signaling level was discussed, and several optimized regimens were proposed to maximize activation of ERK1/2, which has been implicated as an important early step in the collagen production pathway for fibroblasts undergoing cyclic stretching. While the cell signaling studies provided insight into cells' early response to cyclic stretching, the collagen production pathway is complex, involving many more components than just ERK1/2 and p38. Although it is hypothesized that maximizing ERK1/2 activation will lead to an increase in collagen transcription and ultimately collagen deposition, it is certainly not guaranteed, and the downstream responses must be thoroughly studied.

No single study has provided a comprehensive overview of cells' response to cyclic stretching from signaling to deposition. However, a variety of downstream responses have been investigated for fibroblast-like cells including transcription of genes involved in collagen synthesis, maturation, and remodeling,[38-40,43] deposition of insoluble collagen,[36-38,41,42] and collagen crosslinking.[36-38] Although these studies

certainly provide valuable information, the majority have focused on a single point in the collagen production pathway, so they do not provide a complete picture of the cellular response.

The aim of this study was to compare transcription and deposition of collagen in fibrin-based engineered tissues subjected to constant amplitude cyclic stretching and optimized intermittent and incrementally increasing strain amplitude regimens, which were chosen based on ERK1/2 activation dynamics. Both transcription of collagen types I and III, which are major components of native cardiovascular tissue, as well as total collagen deposition were studied. Combined with the signaling studies presented in Chapter 2, this study describes the effects of the three modes of cyclic stretching on fibroblasts in an engineered tissue environment throughout the entire collagen production process with the goals of understanding cyclic stretching-induced collagen production and accelerating collagen deposition in our engineered tissues.

3.2. Methods

3.2.1. Cell Culture

Neonatal human dermal fibroblasts (Lonza) were expanded in 50:50 DMEM:F12 with 15% fetal bovine serum (Hyclone), 100 µg/ml streptomycin, and 100 U/ml penicillin. Cells were grown to confluence and harvested for use at passage 7.

3.2.2. Fibrin-based Tissue Construct Fabrication and Culture

Fibrin gels with entrapped cells were created by suspending neonatal human dermal fibroblasts in DMEM and then mixing the cells with a 20 mM HEPES-buffered saline solution containing bovine fibrinogen (Sigma). In order to form a fibrin gel, a solution of bovine thrombin (Sigma) and $CaCl_2$ in DMEM was added to the fibrinogen/cell solution. The solution was injected into 6-well circular tissue-train plates (Flexcell® International), which have a circular foam insert that anchors the gel around its circumference. The volume of gel in each well was 2 ml. The final composition of the gel was 6.7 mg/ml fibrinogen, 500,000 cells/ml, 0.8 U/ml thrombin, and 5 mM $CaCl_2$. The discs were allowed to gel for 6 minutes in the tissue culture hood at 20°C and an additional 24 minutes in a standard cell culture incubator at 37°C. After the solutions had gelled, DMEM supplemented with 10% fetal bovine serum, 100 µg/ml streptomycin, 100 U/ml penicillin, 0.25 µg/mL amphotericin B, 50 µg/ml ascorbic acid, and 2 µg/ml insulin was added (5 ml per well). Medium was replaced three times weekly. All constructs were cultured statically for one week before cyclic stretching regimens were applied.

3.2.3. Cyclic Stretching of Tissue Constructs

Uniaxial cyclic stretching was applied to the constructs using the FX-5000 Tension System and Arctangle® loading station (Flexcell® International) as described in Section 2.2.3. The constructs remained in a standard cell culture incubator for the duration of the stretching regimens.

3.2.3.1. Experimental Design: Collagen Transcription

Collagen transcription was investigated for static control samples and three cyclic stretching regimens, shown in Figure 3-1. Constant strain amplitude ("constant") samples were stretched at 5% strain amplitude for 48 hours. Incrementally increasing strain amplitude ("incremental") samples were stretched at 5% amplitude for 24 hours followed by 6% amplitude for 24 hours. Intermittently stretched samples ("intermittent") were stretched at 5% amplitude for 15 minutes, followed by a 6 hour static period, and this regimen was repeated for the duration of the study. The intermittent samples were harvested at 49 hours, which was exactly 24 hours after the onset of a stimulation period. This was done for consistency with the incremental treatment group in which the samples were harvested 24 hours after the final increment.

3.2.3.2. Experimental Design: Collagen Deposition Experiment 1

Collagen deposition was measured after two weeks for static control samples and samples subjected to constant amplitude (5% or 13.5% strain amplitude), intermittent (15 min at 5%, 6 hours static, repeat), and incremental (5%-13.5%, increment by ~1% every 24 hours) cyclic stretching regimens (n=6 per group, pooled from two experimental repeats). Due to limitations of the stretching system, the target 1% increment in strain every 24 hours was not able to be achieved, and in the last several days of stretching, the increments decreased in magnitude. However, a measureable increase in strain was still applied every 24 hours.

3.2.3.3. Experimental Design: Collagen Deposition Experiment 2

In order to compare intermittent regimens with various combinations of stretch and rest durations, collagen deposition was measured for samples stretched for three weeks with three different intermittent cyclic stretching regimens: (i) 15 minutes at 5% strain followed by 6 hours of rest, (ii) 1 hour of 5% strain followed by 6 hours of rest, and (iii) 3 hours of 5% strain followed by 3 hours of rest. Control samples were stretched continuously with 5% constant amplitude for three weeks.

3.2.4. RNA Purification and cDNA Synthesis

Samples were harvested for real-time PCR 48 hours after beginning the selected stretching regimens. For consistency, all tissues were harvested 24 hours after a perturbation (onset of stretching or increment in amplitude). Tissues were excised from the wells and stored in RNAlater (QIAGEN) at 4°C. Samples were sonicated in RLT Plus, separated by centrifugation, and purified using the RNeasy Plus purification kit (QIAGEN) following the manufacturer's instructions. RNA concentration was measured by spectrometry (NanoDrop, University of Minnesota Biomedical Genomics Center). 275 ng of each RNA sample were reverse transcribed using SuperScript III reverse transcriptase (Invitrogen) and 100 ng of random hexamer primers. Controls without reverse transcriptase were also prepared for each sample.

3.2.5. Real-time PCR

Real-time PCR was performed using the 7900HT Fast Real-time PCR system (Applied Biosystems, University of Minnesota Lillehei Heart Institute) using the cDNA equivalent of 14 ng RNA, forward and reverse primers at a concentration of 600 nM, and 1X SYBR Green reagent (KiCqStart, Sigma) in a total volume of 12.5 µL. Primers were (5'-3'): fGAPDH(CGCATCTTCTTTTGCGTCGCCAG), rGAPDH(TGACAAGCTTCCCGTTCTCAGCC), fCOL1A1(GCCAAGACGAAGACATCCCACCA), rCOL1A1(CACGTCATCGCACAACACCTTGC), fCOL3A1(AACGGTCTCAGTGGAGAACG), and rCOL3A1(CCACTCTTGAGTTCAGGATGG).

Expression levels of collagen types I (COL1A1) and III (COL3A1) relative to static controls were determined by the comparative C_T method with GAPDH used as the reference gene.

3.2.6. Collagen and Cellularity Quantification

Collagen content was quantified using a hydroxyproline assay with a conversion factor of 7.46 mg of collagen for 1 mg 4-hydroxyproline.[56] A modified Hoescht assay was used to determine cellularity.[57]

3.2.7. Statistics

All figures show mean ± standard deviation with at least n=3 per group. Significance was determined using Student's t-test for two groups and one-way ANOVA for more than two groups with the Tukey post-hoc test in GraphPad Prism software for Windows with $p<0.05$ reported as significant. Symbols or bars are used to indicate significant differences and explained in the corresponding figure captions.

3.3. Results

3.3.1. Transcription of collagen types I and III in cyclically stretched samples

At 48 hours there were no differences in transcription of collagen I ($p=0.11$) or III ($p=0.15$) between the static, constant amplitude, intermittent, or incremental treatment groups (Figure 3-2) assessed using one-way ANOVA (n=5 per group, pooled from two experimental repeats).

3.3.2. Collagen Deposition Experiment 1: Comparison of Constant Amplitude, Intermittent, and Incremental Regimens

Total collagen per cell, based on cell number at harvest, was measured for tissues subjected to constant amplitude (5% or 13.5% amplitude), intermittent (15 min at 5%, 6 hours static, repeat), and incremental (5%-13.5%, increment by ~1% every 24 hours) cyclic stretching regimens. After two weeks, an increase in collagen per cell was measured in the 5% constant amplitude, intermittent, and incremental treatment groups

compared to static controls (Figure 3-3). The incremental treatment group showed the greatest increase in collagen per cell, 72% over static controls and 37% over the 5% constant amplitude samples. There was no difference in collagen per cell between the 5% constant amplitude and intermittent treatment groups.

3.3.3. Collagen Deposition Experiment 2: Intermittent Stretch/Rest Durations

After three weeks of intermittent stretching, collagen per cell was measured in samples subjected to three different intermittent regimens: 15 min stretch/6 hours rest, 1 hour stretch/6 hours rest, 3 hours stretch/3 hours rest (Figure 3-4). Data are shown normalized to continuously stretched controls. There were no differences in collagen per cell for the three regimens, and none of the intermittent regimens increased collagen deposition compared to continuously stretched controls.

3.4. Discussion

Based on the ERK1/2 data, intermittent and incremental regimens were selected to repeatedly activate ERK1/2 with the hypothesis that repeated activation would lead to increased collagen synthesis and deposition. After 48 hours there were no differences in mRNA expression of collagen type I or III between any of the treatment groups. After two weeks, incrementally stretched tissues had the most collagen per cell, while intermittent samples showed no improvement over their continuously stretched counterparts. In addition, there appeared to be no effect of intermittent stretch/rest duration on collagen production in the tissues. These data suggest that while ERK1/2

phosphorylation may be necessary for stretch-induced collagen transcription,[43] it is not a sufficient predictor of final collagen content in this system.

Based on the dynamics of ERK1/2 phosphorylation, intermittent and incremental regimens were designed to maximize ERK1/2 activation throughout the culture period. Intermittently stretched samples were subjected to repeated periods of 5% amplitude cyclic stretching for 15 minutes followed by 6 hours of static culture. The incrementally stretched samples were initially stretched with 5% strain amplitude, and the strain was increased by approximately 1% every 24 hours. While an increment every 6 hours would have been able to reactivate ERK1/2 more frequently, our goal was to apply the cyclic stretching regimen to long-term culture, and if the strain was incremented every 6 hours for several weeks, the amplitude would soon have exceeded the capabilities of the Flexcell® system and likely damaged the tissue. The chosen intermittent and incremental regimens are within the capabilities of both this model system as well as our bioreactors for larger engineered cardiovascular tissues.[31,35]

After 48 hours of static culture, 5% constant amplitude cyclic stretching, or the chosen intermittent and incremental regimens, there were no differences in mRNA expression of collagen types I and III. The 48 hour time point was chosen to allow differentiation between the regimens, and for consistency, intermittent and incremental samples were harvested 24 hours after a perturbation. In an engineered tissue strip made from polyglycolic acid seeded with vascular derived cells, Van Geemen et al. similarly observed only small differences in collagen type I and III mRNA after 24 hours of continuous stretching or 3 hours of stretching followed by 21 hours rest.[39] However, in

cyclic stretching studies where cells are simply adhered to the elastic substrate, significantly increased expression of collagen type I and/or III mRNA by fibroblasts has been observed on a similar time scale.[40,43] It is unknown whether this discrepancy is due to the nature of our system, wherein cells may not be experiencing the applied strain due to strain-shielding by the fibrin, or if the increase in collagen transcription is transient and we have not yet identified the peak time point.

The selected intermittent and incremental regimens were applied to fibrin-based tissues for two weeks along with 5% and 13.5% constant strain amplitude regimens and a static control. Incremental stretching was the most beneficial in our system, resulting in a 37-72% increase in collagen per cell over the other regimens. The benefits of incremental stretching have been demonstrated previously in our lab, as Syedain et al. found that incremental stretching (5% to 15% with a 2.5% increment every 3-4 days) increased collagen deposition and tissue strength and stiffness in tubular engineered tissues similarly prepared from dermal fibroblasts in a sacrificial fibrin gel.[42] The current study suggests that this stretching regimen can be improved further by employing smaller, more frequent increments in strain amplitude.

While intermittent stretching did increase collagen per cell compared to static culture, it did not result in further improvement over 5% constant amplitude stretching. In addition to the initial 15 minute stretch/6 hour rest regimen, two additional intermittent protocols (1 hour stretch/6 hour rest and 3 hour stretch/3 hour rest) were tested for three weeks, and none of them resulted in increased collagen per cell compared to continuously stretched controls. Rubbens et al. observed an increase in

collagen per cell at two weeks in their intermittently stretched samples (3 hours stretch, 3 hours static) compared to static controls; however, a continuously stretched treatment group was not included in this study for comparison.[36] In contrast to the present result, Paxton et al. found that intermittent stretching (10 minutes every 6 hours) increased the percentage of collagen in their fibrin-based "sinews" approximately 20% over continuously stretched samples.[41] However, there were several differences that may account for this discrepancy including the different cell type (tendon vs. dermal fibroblasts), fibrin gel composition, and strain amplitude (1% vs. 5%), as well as the sinew geometry in which the cells were allowed to compact the tissue strand, rather than being anchored on all sides in a circular well. Although the ERK1/2 dynamics appear to be favorable for the intermittent regimens in the present study, it may be that the prolonged static period has detrimental effects on collagen deposition in our system. Additionally, nutrient transport may be enhanced via convection during cyclic stretching of the highly hydrated fibrin gel and developing tissue,[58,59] so it is possible that the intermittent samples do not experience this nutrient and metabolite transport enhancement during the static periods, offsetting any benefit of repeated ERK1/2 activation.

Although ERK1/2 was being repeatedly activated in both intermittent and incremental stretching, only incremental stretching resulted in an increase in collagen per cell over both static samples and samples stretched with constant strain amplitude after two weeks. Clearly in our system, ERK1/2 phosphorylation alone is not a sufficient indicator of final collagen content. Additionally, transcription of collagen type

I and III after 48 hours does not seem to be predictive of collagen per cell at two weeks. It should be noted that the measured collagen content in a tissue is not only a function of collagen transcription, but also translation and the many intervening collagen processing and transport steps prior to incorporation into the extracellular matrix,[60] as well as collagen degradation,[61,62] all of which may also be affected by the different cyclic stretching regimens.

The present study represents data for a single isolation of dermal fibroblasts. At various points in the study, an additional isolation was used alongside the original isolation (data included in Appendix A), and while ERK1/2 and p38 phosphorylation results were similar for both isolations, the long-term collagen per cell results differed. Similar trends were observed for both isolations for the three stretching regimens; however, the magnitude of the improvement in collagen content was substantially lower. The additional isolation exhibited much higher basal collagen production, suggesting that the collagen synthesis pathway was already "saturated." A thorough investigation of this variability between isolations is outside the scope of this work but may provide insight into some of the largely unexplored portions of the collagen production pathway.

In summary, the transient nature of ERK1/2 and p38 phosphorylation was characterized in a fibrin-based engineered tissue model (Chapter 2), and the results were used to develop intermittent and incremental strain amplitude cyclic stretching regimens. While ERK1/2 was repeatedly activated in both regimens, incremental stretching resulted in a greater increase in collagen per cell, indicating that ERK1/2

phosphorylation alone is not a sufficient predictor of this long-term outcome of interest. The data suggest that an incremental stretching regimen with small, frequent increments is most beneficial for collagen production in this system and motivate the use of a similar regimen in our engineered cardiovascular tissue bioreactor systems.

3.5. Figures

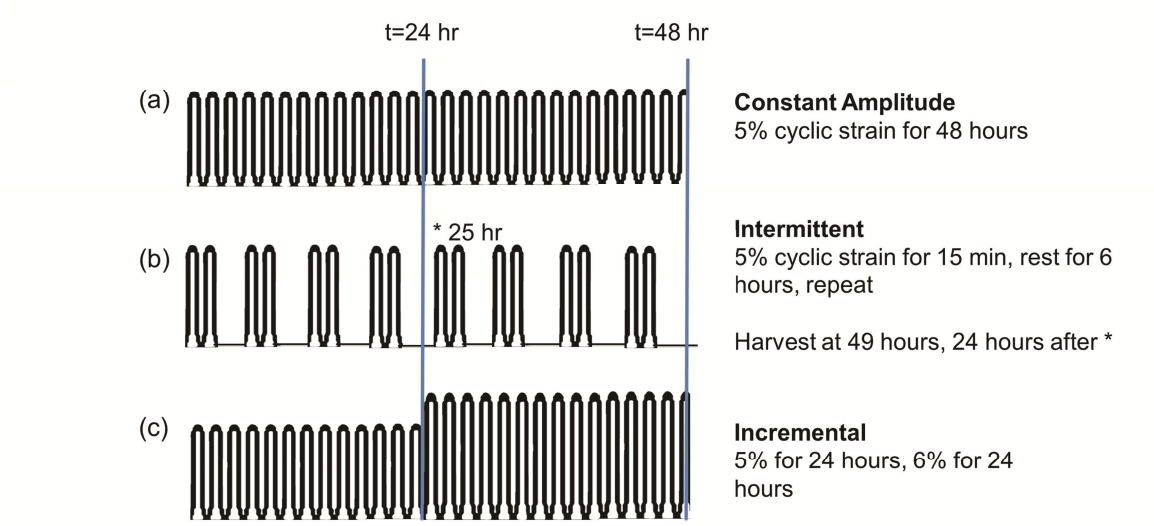

Figure 3-1.

Schematics of strain versus time for 48 hour (a) constant amplitude, (b) intermittent, and (c) incremental cyclic stretching regimens. 0.5Hz frequency and 15% duty cycle were used in all regimens.

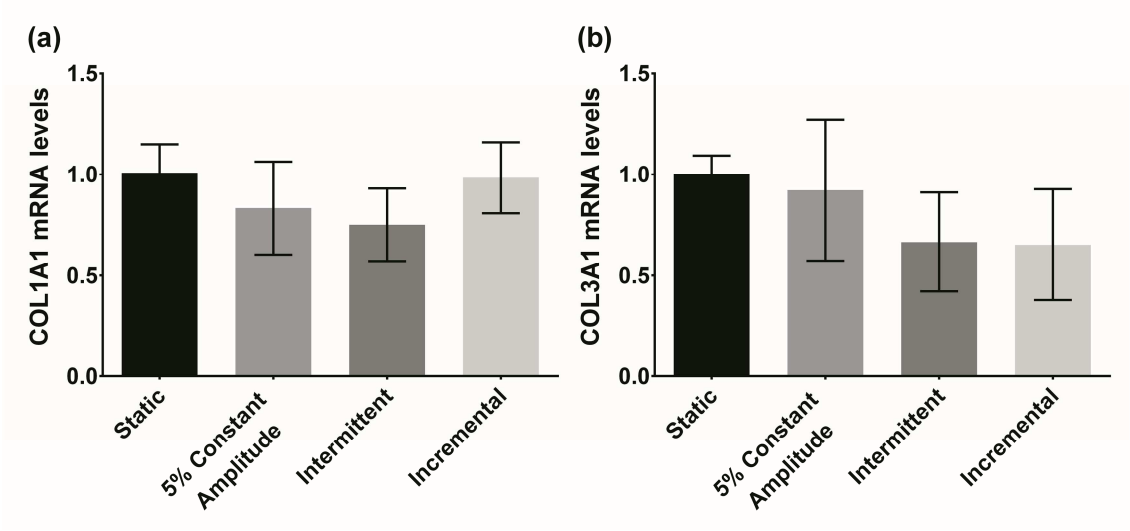

Figure 3-2.

(a) Collagen I,α1 and (b) collagen III,α1 mRNA levels at 48 hours in constant amplitude, intermittent, and incrementally stretched samples expressed relative to static control. GAPDH was used as the housekeeping gene. No significant differences were observed between groups (one-way ANOVA, n=5 per group, pooled from two experimental repeats).

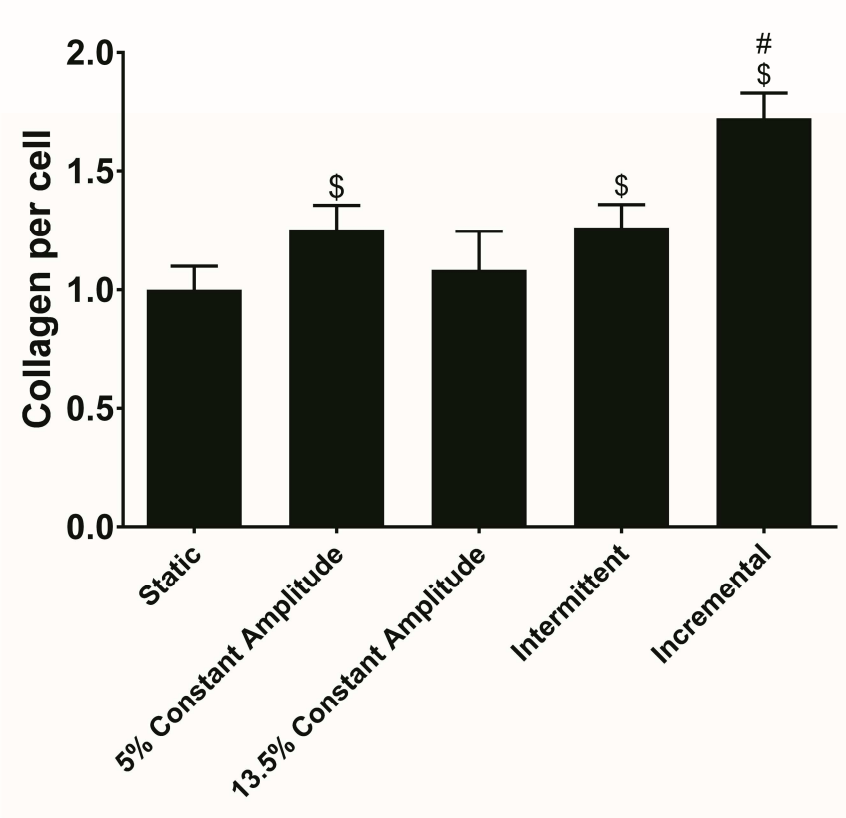

Figure 3-3.

Total collagen per cell at harvest for static, constant amplitude, intermittent, and incremental regimens after 2 weeks. Data were pooled from two experimental repeats and normalized to respective static controls. $=different from static control ($p<0.01$), #=different from all other stretched treatment groups ($p<0.01$) using one-way ANOVA with Tukey post hoc test (n=6 per group).

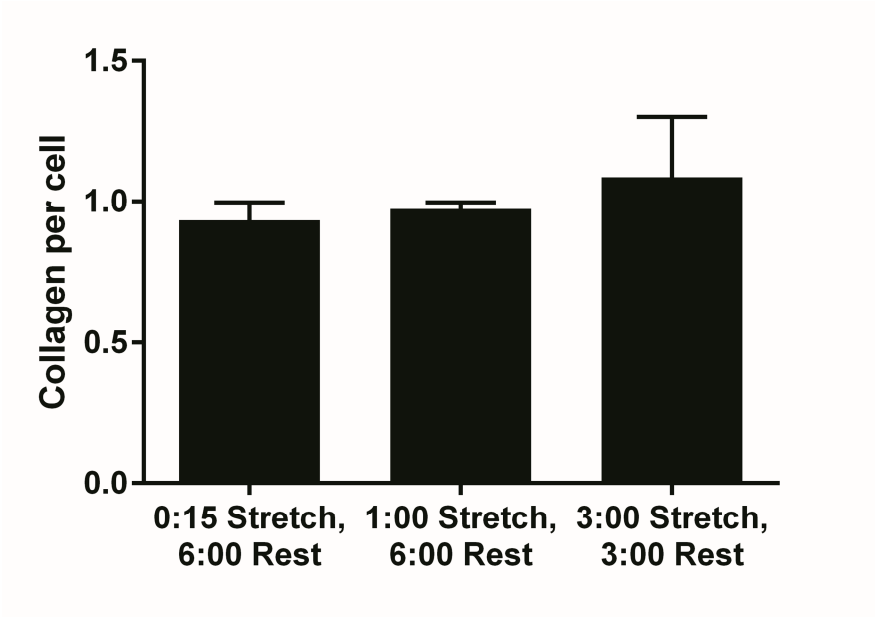

Figure 3-4.

Total collagen per cell at harvest for three intermittent regimens after 3 weeks. Data are normalized to continuously stretched controls. No significant differences were observed between groups (one-way ANOVA with n=3 per group).

Chapter 4. Computational Model of Solid Sleeve Cyclic Distension Bioreactor for Large Diameter Tubular Tissue Constructs

4.1. Introduction

A variety of systems for mechanically conditioning cells, tissues, and even whole organs are commercially available.[63-65] While these systems offer some advantages, including tight control of mechanical stimulation and continuous monitoring, they are often expensive and lack functional versatility. In our laboratory, a custom bioreactor was designed for culturing the large diameter tubular constructs used to create our tissue engineered heart valves. This system is a modification of the pulsed flow-stretch bioreactor, which was previously used successfully to create small diameter vascular grafts with sufficient burst pressure for implantation in preclinical small and large animal models.[35] The design is simple: after several weeks of static culture, the tubular tissue is placed over a latex support sleeve, and the sleeve is secured to two custom ULTEM end pieces with cable ties (Figure 4-1a). The sleeve, tissue, and end pieces are placed into a culture jar, and a reciprocating syringe pump is used to cyclically pump medium into the lumen of the latex tube, thus cyclically stretching the tissue (Figure 4-1b,c). The latex support sleeve is much stiffer than the engineered tissue, so the strain of the latex-tissue composite is dictated by the latex properties rather than by the changing properties of the developing tissue. Although the small diameter graft pulsed flow-stretch bioreactor did not require a latex support sleeve, this

component is necessary to ensure uniform strain and prevent tissue damage for the larger diameter (>16 mm) tissue tubes.

While the bioreactor does not permit feedback control of the applied strain, by calibrating the system for a range of syringe stroke volumes, predictable and consistent strain amplitudes can be applied to the large diameter tubular constructs. Benefits of this simple system include ease of set up, operation, and sterilization. In addition, as the materials for the bioreactor are relatively inexpensive, it is feasible to change parts and add features as needed. With this in mind, it is desirable to develop a computational model for the bioreactor, so the effects of changing a geometrical parameter or component on the applied strain amplitude can be investigated prior to purchasing or machining a new part. A fluid structure interaction (FSI) model of this bioreactor was developed using COMSOL Multiphysics® utilizing an arbitrary Lagrangian-Eulerian method approach with the goal of accurately predicting the strain amplitude for a given stroke volume in this bioreactor system. The model was validated by comparison with experimentally measured strain amplitudes over a range of relevant pump stroke volumes.

4.2. Methods

4.2.1. Model Geometry

The finite element method software, COMSOL Multiphysics (version 5, COMSOL, Inc.), was used to create a two-dimensional axisymmetric model of the large diameter tubular construct bioreactor. The geometry is shown in Figure 4-2. The upper

and lower ULTEM end pieces, latex support sleeve, and walls of the culture jar wall were all included in the model. The tubular tissue was not included in the model, as the applied strain was dictated primarily by the latex sleeve with the tissue stiffness being less than $1/10^{th}$ that of the latex. The geometric parameters are given in Table 4-1.

Table 4-1. Geometric parameters for the solid sleeve bioreactor model

Parameter	**Description**	**Value**	**Source**
L	Axial length of latex (between end pieces)	37.96 mm	Measured
R_i	Inner radius of latex	9.50 mm	Measured
Th	Thickness of latex	0.80 mm	Measured
R_{inlet}	Inlet radius	1.00 mm	Measured
R_{outlet}	Outlet radius	0.35 mm	Measured
H_{end}	Height of end cap	12.77 mm	Measured
H_{jar}	Height of jar	80 mm	Measured
R_{jar}	Radius of jar	30 mm	Measured

4.2.2. Material and fluid properties

Three materials were defined in the model: water at 20°C for the fluid domain, ULTEM for the two custom end pieces, and latex for the support sleeve. During bioreactor culture, the fluid domain typically consists of DMEM culture medium with 10% fetal bovine serum; however, the density and viscosity are nearly the same for culture medium and water,[66] so water was used to allow for easy visualization during experimental validation. As the experimental validation was performed on the bench top, the room temperature properties of water were used instead of properties at the

37°C incubator temperature. The necessary parameters for water,[67] ULTEM,[68] and latex[69] were determined from the literature. As the elastic modulus and Poisson's ratio of the latex were not specified by the manufacturer, these properties were measured experimentally by directed research student Alex Weston using a Bose Electroforce® 3200 tensile testing apparatus. The material and fluid properties are given below in Table 4-2,a-c. Both ULTEM and latex were treated as isotropic linear elastic materials.

Table 4-2a: Fluid Properties (Water at 20°C)

Parameter	**Value**	**Source**
Density	998.2 kg/m^3	[67]
Dynamic Viscosity	$1.00X10^{-3}$ kg/m*s	[67]

Table 4-2b. ULTEM Properties

Parameter	**Value**	**Source**
Elastic modulus	3600 MPa	[68]
Poisson's Ratio	0.3	[68]
Density	1270 kg/m^3	[68]

Table 4-2c: Latex properties

Parameter	**Value**	**Source**
Elastic modulus	1.2 MPa	Measured by Alex Weston for directed research, Fall 2014
Poisson's Ratio	0.35	Measured by Alex Weston for directed research, Fall 2014
Density	970 kg/m^3	[69]

4.2.3. Governing Equations and Boundary Conditions

4.2.3.1. Fluid domain

In the fluid domain, the fluid flow was governed by the incompressible Navier-Stokes equations in a moving coordinate system, neglecting contributions of gravity or any other volume forces:

$$\rho \frac{\partial \boldsymbol{u_{fluid}}}{\partial t} - \nabla \cdot \left[-P\mathbf{I} + \mu \left(\nabla \boldsymbol{u_{fluid}} + \left(\nabla \boldsymbol{u_{fluid}}\right)^{T}\right)\right] + \rho \left(\left(\boldsymbol{u_{fluid}}\right) \cdot \nabla\right) \boldsymbol{u_{fluid}} = 0$$

$$\nabla \cdot \boldsymbol{u_{fluid}} = 0$$

where ρ is the fluid density, $\boldsymbol{u_{fluid}}$ is the fluid velocity, P is the pressure, $\boldsymbol{I}$ is the identity matrix, and μ is the dynamic viscosity of the fluid. Axial symmetry was applied along the Z-axis (Figure 4-3, red line). All jar surfaces (Figure 4-3, blue lines) were treated as walls and the no-slip boundary condition was enforced. The top fluid surface was assigned an "open boundary" condition on which atmospheric pressure was applied. The opening at the top of the upper ULTEM end piece was defined as an inlet. Two different inlet boundary conditions were studied: cyclic normal inlet velocity and cyclic inlet pressure. The cyclic normal velocity boundary condition was defined by the piecewise function,

$$v_{in} = v_{max} \sin(\pi t), \qquad 0 < t \leq 1\ s$$

$$v_{in} = 0, \qquad 1\ s < t \leq 2\ s$$

where t is time and v_{max} is inflow velocity, calculated from the stroke volume of the syringe pump. The cyclic inlet pressure boundary condition was similarly defined by the piecewise function,

$$P_{in} = P_{max} \sin(\pi t)\,, \qquad 0 < t \leq 1\ s$$

$$P_{in} = 0, \qquad 1\ s < t \leq 2\ s$$

where P_{max} is the maximum inlet pressure, as measured by an in-line pressure transducer in the experimental validation. Continuous second derivative smoothing was used to achieve a gradual transition between the two halves of the functions. All boundaries between the fluid and latex or ULTEM were treated as moving walls, in which the fluid velocity must match the deformation rate (time derivative of displacement) of the solid boundary.

4.2.3.2. Solid domains

The stresses and structural deformations in the solid domains (latex and ULTEM) were determined by solving an equation for equilibrium, a constitutive equation relating stress and strain, and a kinematic equation relating displacements and strain:

$$\rho_{solid} \frac{\partial^2 \boldsymbol{u_{solid}}}{\partial t^2} - \boldsymbol{\nabla \cdot \sigma} = \boldsymbol{F_v}$$

$$\boldsymbol{\sigma} = \frac{1}{det(\boldsymbol{F})} \boldsymbol{F S F^T}$$

$$\boldsymbol{S} = \boldsymbol{C} : \boldsymbol{\epsilon}$$

$$\boldsymbol{\epsilon} = \frac{1}{2}[\boldsymbol{\nabla u_{solid}} + (\boldsymbol{\nabla u_{solid}})^T + (\boldsymbol{\nabla u_{solid}})^T \boldsymbol{\nabla u_{solid}}]$$

where ρ_{solid} is the density of the solid material, $\boldsymbol{u_{solid}}$ is the displacement of the solid domain, $\boldsymbol{\sigma}$ is the Cauchy stress, $\boldsymbol{F_v}$ is the body force per unit volume, $\boldsymbol{F}$ is the deformation gradient tensor, $\boldsymbol{S}$ is the second Piola-Kirchoff stress tensor, $\boldsymbol{C}$ is the

elasticity tensor, and $\boldsymbol{\epsilon}$ is the Green strain tensor. All materials were isotropic and linear elastic. As in the fluid domain, a boundary of axial symmetry was enforced along the Z-axis (Figure 4-3, red line). The top edge of the upper ULTEM end piece and latex sleeve (Figure 4-3, purple line) were constrained by a fixed constraint boundary condition, imposing zero displacement in both R and Z directions. The interfaces between the latex sleeve and the ULTEM end pieces were treated as if they were attached along their entire lengths, with continuity enforced across the boundaries between the materials. On all boundaries between the fluid domain and the latex or ULTEM, a boundary load was applied, representing the contributions of both pressure and viscous forces from the fluid. This load was given by:

$$\boldsymbol{F}_{boundary} = -\boldsymbol{n} \cdot \left(-P\boldsymbol{I} + \mu \left(\nabla \boldsymbol{u}_{\boldsymbol{fluid}} + \left(\nabla \boldsymbol{u}_{\boldsymbol{fluid}} \right)^{\boldsymbol{T}} \right) \right)$$

where $\boldsymbol{u}_{\boldsymbol{fluid}}$ is the fluid velocity field, P is the pressure, $\boldsymbol{I}$ is the identity matrix, μ is the dynamic viscosity for the fluid, and $\boldsymbol{n}$ is the normal vector to the boundary.

4.2.4. Moving Mesh and Solver Configuration

The governing equations for the fluid domain were solved on a moving deformed mesh, with mesh deformations computed using hyperelastic smoothing. The mesh deformation was prescribed to be zero in both R and Z directions along all exterior boundaries of the fluid domain. The mesh in the solid domains moved according to the deformations of the ULTEM and latex. A free triangular mesh was used and was refined until minimal change in the solution was detected. The system of

equations was solved using a PARDISO direct solver with a relative tolerance of 10^{-4} and a fully-coupled approach.

4.2.5. Experimental Validation of COMSOL Model

In order to validate the COMSOL model, experiments were carried out in which the pump stroke volume, inlet pressure, and resulting strain were monitored for a bioreactor with identical geometry to the model. Briefly, a latex tube was secured over the custom end pieces and placed in a glass container with flat sides to prevent optical distortion. Rather than cell culture medium, which is red in color, water was used during the validation experiments to allow better measurement of the latex deformation. A laser micrometer (Mitutoyo) was used to monitor the changing diameter of the latex through the jar during bioreactor operation. The micrometer beam was focused at the midpoint between the two ULTEM end pieces. Water was cyclically injected into the lumen of the latex tube, and the changing tube diameter was monitored. An in-line pressure transducer (Harvard Instruments) recorded the pressure at the inlet to the top ULTEM end piece. This procedure was repeated for three different latex sleeves at four different pump stroke volumes. The baseline and maximum diameter were recorded for each case, and the diametral strain, ε_D, was calculated as

$$\varepsilon_D = \frac{change\ in\ diameter}{initial\ diameter}.$$

The maximum diametral strain and peak pressure were averaged over six cyclic distension cycles for each trial.

4.3. Results

4.3.1.FSI Model Results

The FSI model was able to be solved for a range of reasonable inlet flows and pressures as well as perturbations to the bioreactor geometry. The deformation, von Mises stress, and velocity field predicted by the model for a pressure amplitude of 4.7 kPa are shown at t = 0.2, 0.5, 0.8, 1.2, and 1.6 seconds. (Figure 4-4a-e) Figure 4-4f shows the radial displacement of the latex at the midpoint between the two ULTEM end pieces as a function of time. As the pressure was increased toward P_{max}, the stress and deformation of the latex sleeve also increased with maximum radial displacement occurring just after the peak in the inlet pressure at t = 0.52 seconds. Figure 4-4g shows the radial displacement of the latex at t = 0.2, 0.5, and 0.8 seconds as a function of Z-coordinate along the length of the latex sleeve. The predicted radial displacement was uniform along the majority of the latex sleeve, tapering to zero at the attachment points to the end pieces.

4.3.2. Model Validation: Inlet Velocity Boundary Condition

The FSI model predictions were compared to experimental results using the inlet velocity boundary condition for four different pump stroke volumes. Experimental strain measurements were recorded for four different stroke volumes, and the COMSOL model was run for the inlet velocities corresponding to each stroke volume. For both the COMSOL model and the experiment, the maximum strain in the latex (measured at the

midpoint between the ULTEM end pieces) is plotted versus stroke volume (Figure 4-5). At the lower stroke volumes there was good agreement between the model and the experimental results; however, as the stroke volume was increased, the disparity between the model predications and experimentally measured strains increased. This was most pronounced at the 3.3 ml stroke volume with the model predicting a strain that was 33% higher than the average measured strain at that stroke volume.

4.3.3. Model Validation: Inlet Pressure Boundary Condition

Similarly, the experimentally measured and model predicted strains were compared with the cyclic inlet pressure boundary condition for the same four different pump stroke volumes. An in-line pressure transducer recorded the peak inlet pressure for each of the four stroke volumes, and this pressure was set as P_{max} for the inlet pressure boundary condition. The measured and predicted peak strains are plotted versus the peak inlet pressure (Figure 4-6). Good agreement exists between the experimental result and model predictions at all four stroke volumes.

4.4. Discussion

An FSI model of the solid sleeve bioreactor used for culturing large diameter tissue constructs has been developed in COMSOL using an arbitrary Lagrangian-Eulerian method. A time-dependent inflow or pressure was set at the bioreactor inlet, and the incompressible Navier-Stokes equations in a moving coordinate system and linear elastic structural deformations were solved for the fluid and solid domains,

respectively. The model was stable for a wide range of inlet conditions and geometries, encompassing the useful configurations for tubular construct culture. Two different inlet boundary conditions were studied: a cyclic inlet velocity, which was calculated from the pump stroke volume, and a cyclic inlet pressure, measured by an in-line pressure transducer. There was good quantitative agreement in maximum strain between the model predictions and experimental result for all stroke volumes when the inlet pressure boundary condition was used. When the inlet velocity boundary condition was used, the model predictions agreed with the experimental results at the smaller stroke volumes but over-estimated the strain for stroke volumes larger than 1.3 ml. This disparity increased with increasing stroke volume.

With the solver configuration, meshing scheme, and boundary conditions used in this study, the FSI model was able to be solved for a wide range of physically reasonable inlet conditions, geometries, and material parameters. Both cyclic inlet pressure and cyclic inlet velocity produced cyclic radial distension of the latex support sleeve, and this distension was fairly uniform along the entire length of the sleeve (Figure 4-4g) as was observed visually in the physical bioreactor set-up. Prior to experimental validation, an intuitive evaluation was performed during which parameters were varied and the outcomes were compared. Diametral strain increased with increasing inlet velocity and pressure amplitudes and decreased with an increase in the elastic modulus of the latex sleeve or outlet radius. As the model was found to behave in an intuitively reasonable manner, experimental validation was carried out for quantitative evaluation.

The primary goal in developing this model was to be able to input the pump stroke volume or corresponding inlet velocity amplitude and have the model accurately predict the strain amplitude in the latex support sleeve and thus the strain applied to a tissue construct. However, it was clear from the comparison between the FSI model predictions and experimental outcome that the model was not able to accurately predict the measured latex strain at all stroke volumes when the inlet velocity boundary condition was used (Figure 4-5). In an ideal system, all of the fluid injected by the reciprocating syringe pump must exit the lumen of the latex through the outlet in the lower end piece. However, in the real system the connection between the latex sleeve and the end pieces is not a perfect seal, and leaks through the cable tie attachment points do occur, especially at higher stroke volumes. This explains why the over-prediction of the model became worse with increasing stroke volume when the inlet velocity boundary condition was used. As the stroke volume and therefore the internal pressure increased, the leakage became more severe, and the idealized model failed to capture the behavior of the system.

In order to get around the issue of leakage, a cyclic pressure inlet boundary condition was employed using the inlet pressure amplitude that was recorded during experimental validation. In terms of the utility of the model, setting the inlet pressure is not as attractive as setting the inlet velocity because the pressure is not directly controllable in the experimental set-up, while the inlet velocity can be controlled directly by adjusting the pump stroke volume. However, in terms of validating the model, setting the inlet pressure based on the in-line measurement was useful as it

accounted for the leaking that occurred in the physical system. Any leakage of fluid from the lumen of the latex should have decreased this in-line pressure reading. As expected, when the inlet pressure boundary condition was employed, there was excellent agreement between the measured and predicted strain amplitudes at all stroke volumes (Figure 2-6). This further suggested that the previous disparities between the experimental results and model predictions at high stroke volumes were due to leakage, which resulted in lower than predicted internal pressures.

While the utility of the FSI model is limited by the leakage in the physical system, this study did serve to illuminate the substantial effect of leakage on the applied strain in the system and motivates improvement in the sealing mechanism if higher strain amplitudes are desired. If a better seal can be accomplished, the value of the model as a predictive tool will certainly be increased. Although the FSI model with the inlet velocity boundary condition cannot be used to accurately predict the outcome as geometrical and material parameters are varied at all stroke volumes, it is still a useful tool for making a semi-quantitative assessment of effects, particularly for bioreactor configurations with maximum internal pressures below 7 kPa.

In the present work, an FSI model of the solid sleeve bioreactor used to culture engineered tissue tubes for heart valve applications was developed in COMSOL. The model was validated experimentally, and it was determined that when a cyclic pressure inlet boundary condition was used the model-predicted and experimentally measured strain amplitudes were in excellent agreement. However, when the more physically relevant inlet velocity boundary condition was employed, the model failed to accurately

predict the outcome for large stroke volumes due to system leakage. While this discrepancy at high stroke volumes limits the utility of the FSI model, the model may still be a valuable tool for exploring different bioreactor geometries and materials at low stroke volumes.

4.5. Figures

Figure 4-1.

(a) Image of the solid sleeve bioreactor consisting of a latex support sleeve, ULTEM end pieces, tubular tissue, and culture jar. (b) and (c) images of the reciprocating syringe pump used to cyclically inject medium into the lumen of the latex tube.

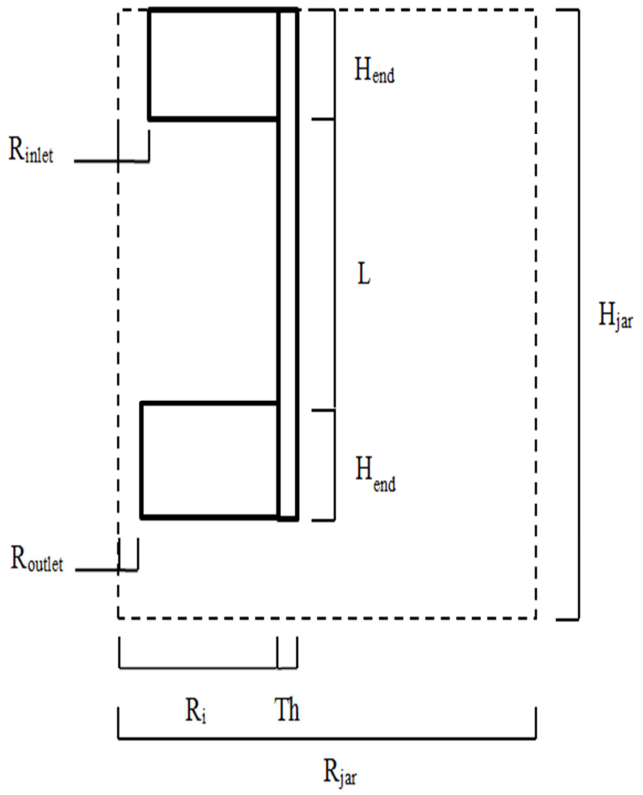

Figure 4-2.

2D axisymmetric bioreactor geometry with geometric parameters specified in Table 4-1. Adapted from A. Weston.

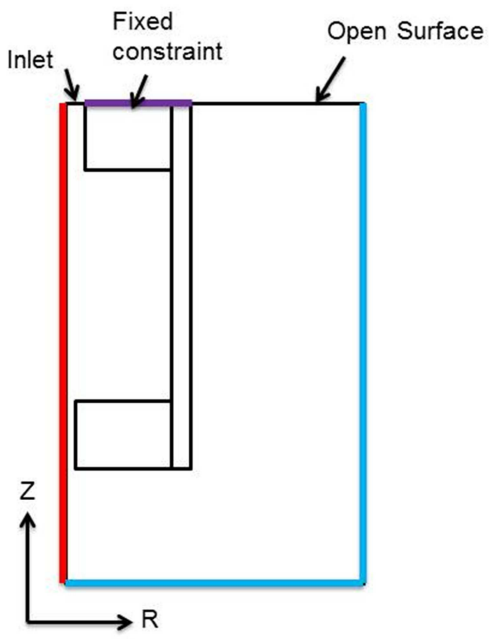

Figure 4-3.

Boundary conditions for COMSOL model. The vertical red line is the axis of rotational symmetry (left edge of fluid domain), blue lines indicate a wall boundary condition (bottom and right edges of fluid domain), and the purple line indicates a fixed constraint boundary condition on the solid domains (labeled with arrow).

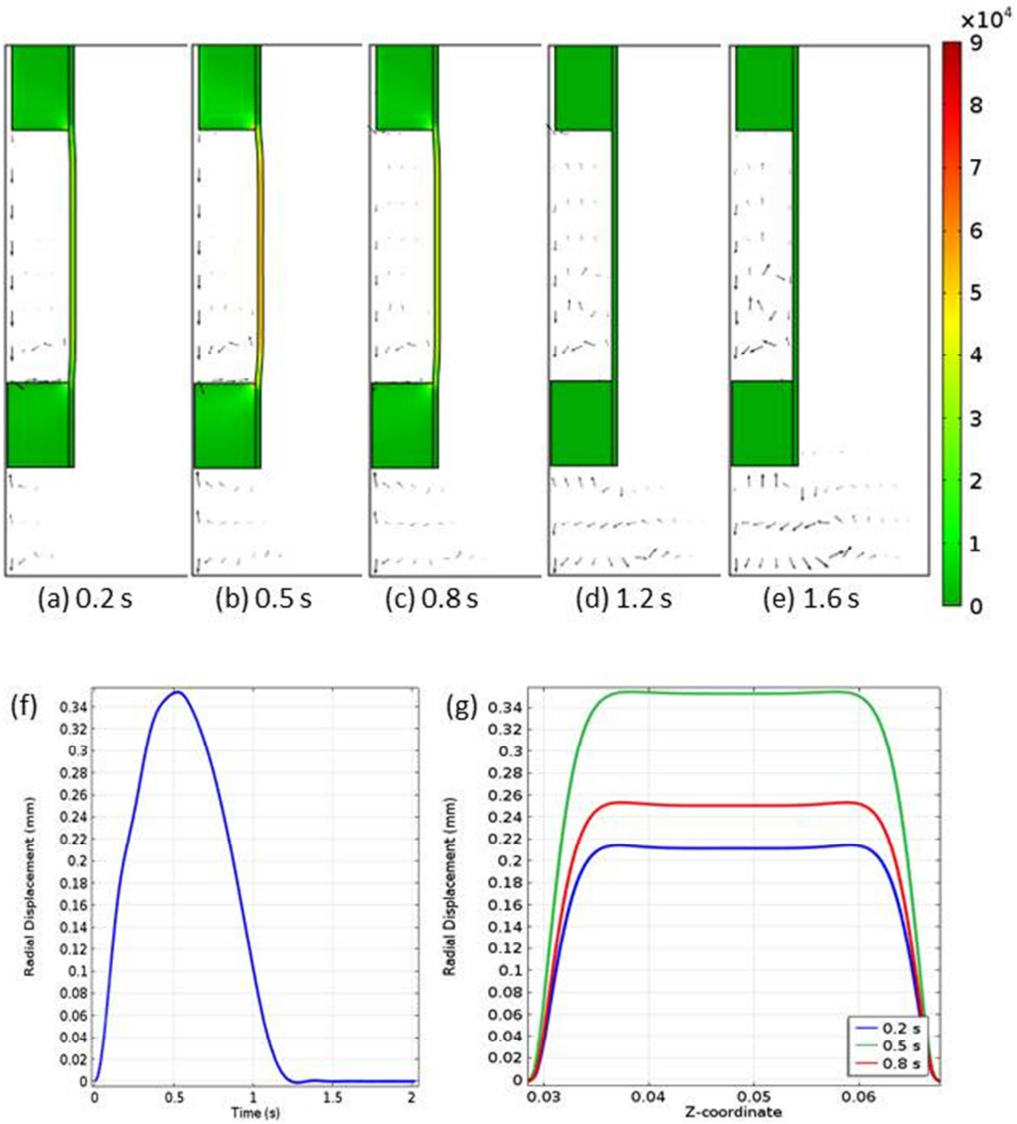

Figure 4-4.

COMSOL model results: (a-e) Deformation, von Mises stress, and arrows indicating relative velocity magnitude and direction at t = 0.2, 0.5, 0.8, 1.2, and 1.6 seconds for an inlet pressure amplitude of 4.7 kPa. Arrows are scaled in each image to better show the velocity field at each time point. (f) Radial displacement at the midpoint of the latex sleeve as a function of time and (g) radial displacement plotted versus z-coordinate along the latex sleeve at t = 0.2 (blue, bottom), 0.5 (green, top), 0.8 (red, middle) seconds.

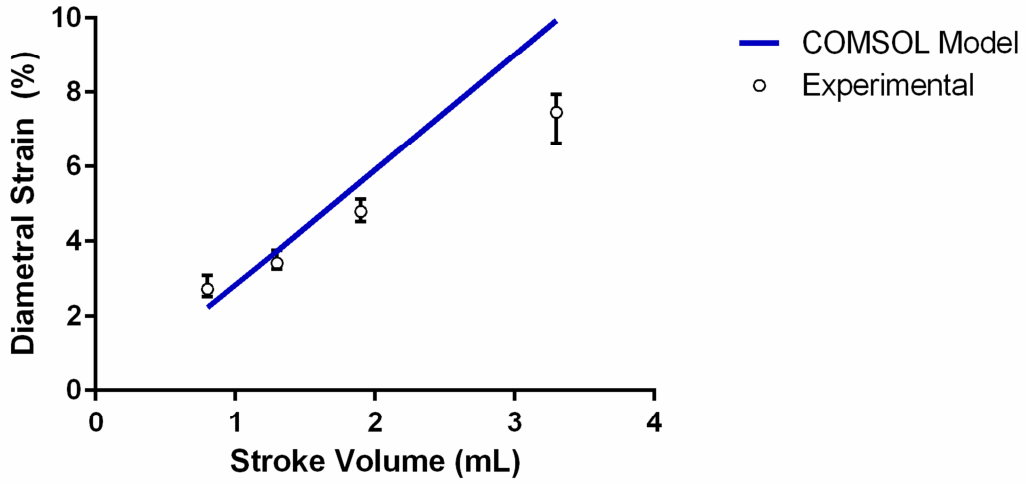

Figure 4-5.

Experimentally measured (open circle) and model predicted (line) maximum diametral strain versus pump stroke volume. At each stroke volume the mean and range of the three experimental repeats are plotted.

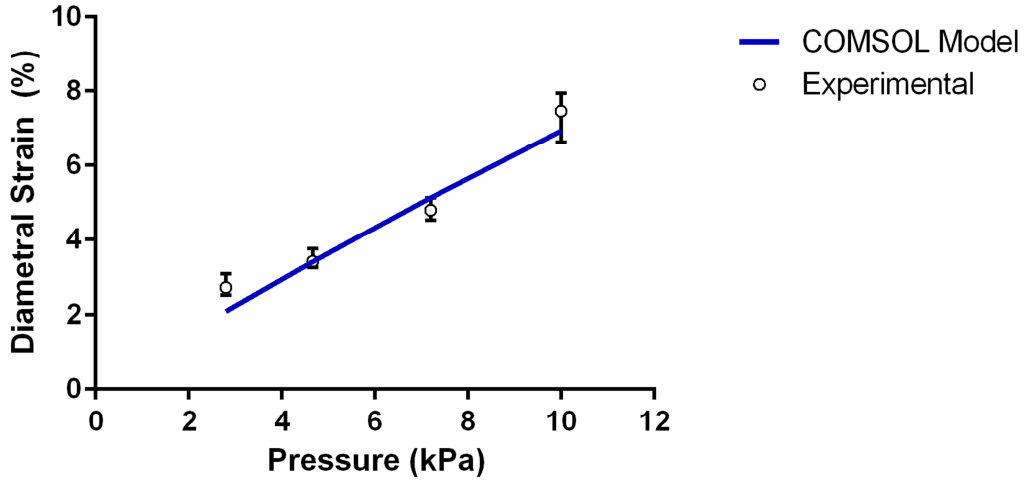

Figure 4-6.

Experimentally measured (open circle) and model predicted (line) maximum diametral strain versus peak inlet pressure. At each pressure the mean and range of the three experimental repeats are plotted.

Chapter 5. Design and Implementation of a Porated Sleeve Bioreactor for Enhanced Nutrient Transport in Large Diameter Tubular Constructs

5.1. Introduction

While there are many advantages to using fibrin as a scaffold for engineered cardiovascular tissue, one major drawback is fibrin's initially low strength and stiffness. As mentioned previously, a challenge that must be overcome when working with fibrin scaffolds is achieving sufficient strength and stiffness to withstand physiological loading. To reduce the cost of culturing a fibrin-based tissue-engineered heart valve (TEHV) for several months, it is desirable to achieve these properties as quickly as possible. In addition to optimizing the cyclic stretching regimen to increase cellular collagen production, another approach to reduce the culture time of fibrin-based tissues is to improve nutrient transport through the thickness of the tissue. In cardiovascular tissue engineering applications, relying on diffusion alone for transport of oxygen, growth factors, and other key nutrients often limits the thickness of viable, cellular tissue.[70] This transport limitation increases in severity as the cells within the engineered tissue proliferate and produce a dense extracellular matrix.

A variety of bioreactor systems have been developed that apply ablumenal[71] or lumenal[72,73] flow in an attempt to overcome this limitation and improve transport during the culture of engineered cardiovascular tissues. In addition, transmural flow, which provides forced convection of culture medium through the thickness of the tissue, has

shown promise as a means to increase cell viability and metabolism in the interior of thick tissues. Kitagawa et al. observed increased uniformity and proliferation of fibroblasts in a 2 mm thick synthetic polymer graft under radial perfusion.[74] Similarly, perfusion has been shown to increase the viability and metabolic activity of cardiomyoctes at the center of an engineered tissue 1.5 mm in thickness.[75]

It has been shown previously in our lab that a combination of lumenal, ablumenal and transmural flow and cyclic stretching was beneficial for small diameter (2-4 mm) tubular constructs, increasing both collagen content and burst pressure.[35] When scaling up this bioreactor to culture large diameter (16-22 mm) constructs, it was necessary to include a latex support sleeve to ensure uniform strain throughout the length of the tubular tissue and prevent necking. Cyclic stretching with a latex support sleeve has been used successfully to strengthen fibrin-based tissue tubes;[31,42] however, when the tissue is placed over a solid latex sleeve, only the ablumenal tissue surface is in contact with the medium, and both lumenal medium contact and transmural flow are not permitted. In the large diameter tubular constructs, the medium contacting surface shows more rapid remodeling of fibrin into collagen, likely due to increased nutrient concenrations.[31] The elastic support sleeve is required for the cyclic stretching aspect of bioreactor culture; however, it is desirable to redesign this sleeve to recover the beneficial effects of lumenal and transmural flow.

In this study a bioreactor with a porated latex support sleeve was designed to culture large diameter tissue tubes for TEHV applications, and a computational fluid dynamics (CFD) model was developed using COMSOL Multiphysics® to predict the

flow velocity field in and around the tissue. It was hypothesized that culture in the porated sleeve bioreactor would accelerate remodeling of the fibrin gel scaffold, particularly near the lumenal surface, due to increased nutrient diffusion permitted by lumenal medium contact as well as the introduction of convective nutrient transport resulting from the transmural flow and possible stimulatory effects of lumenal and interstitial shear stress. Acceleration of tissue remodeling will reduce the culture time required for the tubular constructs to reach sufficient strength and stiffness for use as TEHVs.

5.2. Methods

5.2.1. Cell Culture

Neonatal human dermal fibroblasts (Invitrogen) were expanded in 50:50 DMEM:F12 (Lonza) with 15% fetal bovine serum (Hyclone), 100 U/ml penicillin, and 100 µg/ml streptomycin. Passage 7 fibroblasts were harvested at confluence for use in tissue constructs.

5.2.2. Construct Fabrication and Culture

Tubular constructs were formed by casting a fibrin gel with entrapped dermal fibroblasts around a cylindrical mold. The mold consisted of a 22 mm diameter glass mandrel that was secured within a polycarbonate outer shell by tight fitting rubber stoppers. Prior to casting, the mandrels and outer shells were immersed in a solution of

5% Pluronic F-127 in distilled water for 2 to 4 hours and allowed to air dry. A well-mixed solution of fibroblasts, bovine fibrinogen (Sigma), bovine thrombin (Sigma), 20 mM HEPES-buffered saline, DMEM+HEPES, and $CaCl_2$ was injected into the negative space between the mandrel and outer casing and allowed to gel for 10 minutes at 20°C and an additional 30 minutes at 37°C. Final gel concentrations were 1 million/ml fibroblasts, 4 mg/ml fibrinogen, 0.8 U/ml thrombin, and 5 mM $CaCl_2$. After gelation the tubular constructs were ejected from the outer casing into jars containing 250 ml construct culture medium (DMEM with 10% fetal bovine serum, 1% antibiotic/antimycotic, 2 µg/ml insulin, and 50 µg/ml ascorbic acid). All constructs were housed in a standard cell culture incubator at 37°C. After five days to allow initial gel compaction, jars were placed on a rocker and rocked at a frequency of approximately 0.5 Hz. Medium was replaced three times per week.

5.2.3. Porated Sleeve Fabrication

Porated sleeves were created by laser cutting holes into latex tubing (Primeline Industries) using an Epilog laser (UMN CSE Machine Shop). The latex sleeve was placed over a mandrel and rotated such that either 8 or 16 columns of holes were cut around the circumference of the tube, as shown in Figure 5-1a. Pores were cut in the central 2.5 cm of the latex sleeve, based on the predicted axial length of the tissue tubes following cell-induced fibrin gel compaction during the initial static incubation. Pore diameter of 200 µm and axial spacing of 2.6 mm were used.

5.2.4. Bioreactor Conditioning

After three weeks of static culture to allow for gel compaction, tubular constructs were cyclically stretched in a custom built bioreactor.[31] Constructs were slid off their mandrels and placed over distensible sleeves which were either porated, as described above, or solid latex. Each tissue and supporting sleeve was fixed to ULTEM end pieces with cable ties and placed in a jar containing 200 ml of construct culture medium (Fig 5-1b). Cyclic distension was achieved by pulsatile flow of medium delivered by a reciprocating syringe pump. The pump injected medium through a 3-way valve into the lumen of the latex sleeve, and the back pressure produced by a small constriction point on the lower end piece caused the latex and tissue to cyclically distend. The syringe was refilled by drawing medium from the reservoir surrounding the tissue.

Constructs were conditioned for one or two weeks with cyclic distension at a frequency of 0.5 Hz and amplitude increasing incrementally over approximately 1-3% (1 week) or 1-6% (2 week) with increments of 1% every 2 days. In addition to the solid sleeve control, a second control group was included in which the lower end piece was removed from the porated sleeve bioreactor preventing pressurization of the tube lumen. This configuration provided pulsatile flow of medium through the lumen of the porated sleeve at the same volumetric injection rate but with no measureable distension (peak lumenal pressure less than 150 Pa).

Calibration of tube distension was performed using a laser micrometer (Mitutoyo) to measure the circumferential strain. Calibration was performed for solid

and porated latex sleeves with constructs that had been cultured statically for three weeks then placed over the sleeves. The culture jar was replaced with a square glass jar containing phosphate-buffered saline during calibration to minimize optical distortion. The laser micrometer was used to measure the circumferential strain of the latex-tissue composite as the stroke volume of the pump was varied.

5.2.5. Mechanical Testing

Uniaxial tensile tests were performed using an Instron testing system on strips cut from the tubular constructs in the circumferential direction (~2.5 mm by 12 mm). The tissue strips were placed in compressive grips and submerged in phosphate buffered saline throughout the test. Tissues were pre-stressed with a load of 0.008 N and six preconditioning cycles (0-10% strain) were performed. Tissues were stretched to failure at a rate of 3 mm/min as the force from the load cell was recorded. The engineering stress was calculated by dividing the force by the initial cross-sectional area of the tissue strip and the true strain was calculated from the instantaneous and initial lengths of the strip. The ultimate tensile strength (UTS) was the maximum stress achieved before failure, and the tangent modulus was calculated by performing regression on the linear portion of the stress-strain curve.

5.2.6. Histology and Immunostaining

Tissue strips cut from tubular constructs both circumferentially and axially were fixed in 4% paraformaldehyde, embedded in optimal cutting temperature compound

(OCT, Tissue-Tek), and frozen. For constructs cultured in the porated sleeve bioreactors, axial strips were taken both from regions along a column of pores and regions between columns of pores. 9 µm sections were stained with Lillie's trichrome and picrosirius red stains. Sections were also stained for collagen I, α1 (Novus, NB600-408). Samples were blocked in 5% normal donkey serum, incubated in primary antibody at a concentration of 1 µg/ml, and stained with Cy3-conjugated anti-rabbit secondary antibody (Jackson Immunoresearch). Hoechst 33342 (Invitrogen, H3570) was used to counterstain nuclei.

The cell distribution was quantified using a custom MATLAB® script.[76] Briefly, the user identifies the lumenal and ablumenal tissue surfaces, and the script determines the distance of the centroid of each cell from the lumenal surface. This quantification was performed on 4X images of Hoechst-stained axial sections. For each section a series of 4X images was pieced together to span the entire length of the axial section.

5.2.7. Collagen and Cellularity Quantification

Collagen content was quantified using a hydroxyproline assay with a conversion factor of 7.46 mg of collagen for 1 mg 4-hydroxyproline.[56] A modified Hoescht assay was used to determine cellularity.[57]

5.2.8. Measurement of Sleeve-Tissue Gap and Computational Fluid Dynamics (CFD) Model

In order to predict the flow field around and through the tissue tube, the dynamics of the tissue and sleeve distension were studied, and a basic CFD model was developed using COMSOL Multiphyics®. As the sleeve and tissue were distended by the pulsatile influx of medium, a gap formed between the tissue and the sleeve, and medium was able to flow both along the lumenal surface of the tissue as well as through the tissue thickness (transmural flow). The width of this gap was able to be approximated by monitoring the distension of the tissue/sleeve composite versus the sleeve alone under the same lumenal pressure amplitude using a laser micrometer. The peaks of the distension versus time profiles were aligned, and the gap width, *W*, was approximated at a set of discrete time points during a cycle as

$$W(t) = D_t(t) - D_s(t) - 2h \,,$$

where D_t was the outer diameter of the sleeve/tissue composite, D_s was the outer diameter of the sleeve alone, and h was the thickness of the tissue. As the strains utilized were small, it was assumed that the tissue thickness was constant throughout the distension cycle.

A CFD model was developed for the tissue at the onset of bioreactor culture using the measured tissue properties, lumenal pressure waveform, and gap width dynamics for the initial strain amplitude of 1%. The lumenal pressure and gap width were both set manually for different points in the cycle, and the flow of medium through and around the tissue was solved at steady state for each pressure/gap width pair. There was no physical coupling between fluid flow and tissue deformation

included in this basic model. Both the maximum and time-averaged pressure/gap width pairs are considered here.

An approximation of the full porated sleeve bioreactor geometry neglecting curvature was used (Fig. 5-2a), in which an axial segment including one column of pores bounded by symmetry conditions on the lateral faces defined the total domain. As the diameter of the sleeve and tissue were much greater than the thicknesses, this was a reasonable approximation of the full geometry and decreased the required time for computation. The model included discrete inlets (representing the pores in the sleeve), a gap domain in which fluid was able to flow freely, and a tissue domain represented by a homogeneous, isotropic porous material. The gap width was assumed to be constant in the axial direction, as the experimentally measured gap width was fairly uniform, decreasing slightly (<10%) at the top and bottom tissue edges. The parameters used in this model are included in Table 5-1.

Parameter	**Description**	**Value**	**Source**
L	½ axial length of porated sleeve/tissue	13.7 mm	Measured
D_{pore}	Pore diameter	200 µm	Measured
H	Tissue thickness	1 mm	Measured
d	Axial pore spacing	2.6 mm	Measured
W	Gap width	0.4 mm, maximum 0.25 mm, time averaged	Measured
P	Lumenal pressure	500 Pa (peak) 318 Pa (time averaged)	Measured

Table 5.1: Input parameters for porated sleeve bioreactor model

The COMSOL Multiphysics® module for free and porous media flow was used to seamlessly couple flow in the gap region with flow through the porous tissue. At each pore in the latex sleeve, an inlet boundary condition was specified using the measured lumenal pressure, and on all exterior surfaces (Figure 5-2b, purple lines) an outlet pressure of 0 Pa was specified. Along the solid portions of the latex sleeve (Figure 5-2b, green lines) a no-slip boundary condition was utilized. Fluid flow in the gap region was governed by the steady-state Navier-Stokes equations:

$$-\nabla \cdot [-P\mathbf{I} + \mu(\nabla \boldsymbol{u} + (\nabla \boldsymbol{u})^T)] + \rho\big((\boldsymbol{u}) \cdot \nabla\big)\boldsymbol{u} = 0$$

$$\nabla \cdot \boldsymbol{u} = 0$$

and flow in the porous material was governed by the Brinkman equations:

$$-\nabla \cdot \left[-P\mathbf{I} + \frac{\mu}{\varepsilon}(\nabla \boldsymbol{u} + (\nabla \boldsymbol{u})^T)\right] + \frac{\mu}{\kappa}\boldsymbol{u} = 0$$

$$\nabla \cdot \boldsymbol{u} = 0$$

where $\boldsymbol{u}$ is the velocity, P is the pressure, $\mathbf{I}$ is the identity matrix, μ is the dynamic viscosity of the fluid, ρ is the fluid density, and ε and κ are the porosity and permeability of the porous material, respectively. Continuity of stress and continuity of velocity were enforced across the interface between the gap and tissue domains. The properties of water at 37°C were used for the fluid, and previously measured values for the permeability and porosity of fibrin-based tissue constructs were used for the porous material. These properties are given in Table 5-2.

Parameter	Value	Source
Density	992 kg/m^3	[67]
Dynamic Viscosity	$6.9X10^{-4}$ kg/m*s	[67]
Tissue Permeability	10^{-15} m^2	[77]
Tissue Porosity	0.4	Measured by Muaz Nik Rushdi, directed research Spring 2012

Table 5-2: Fluid and tissue properties used in porated sleeve bioreactor model

A free tetrahedral mesh was used for both domains and was refined until minimal change in the solution was detected. The system of equations was solved using a generalized minimal residual (GMRES) iterative solver with relative tolerance of 10^{-6}.

5.2.9. Statistics

All figures show mean ± standard deviation with at least n = 3 per group. Significance was determined using Student's t-test for two groups and one-way ANOVA with a Tukey-Kramer post hoc test for more than two groups with $p<0.05$ reported as significant. All experiments were repeated at least twice and porated sleeve data were normalized to solid sleeve control values for each experiment to account for variation between castings.

5.3. Results

5.3.1. Lumenal collagen deposition after one week of bioreactor conditioning

Tubular constructs were cyclically stretched for one week with either solid support sleeves (control) or porated sleeves with eight columns of pores around the circumference of the sleeve. Lumenal collagen deposition was not observed in samples cultured on solid latex sleeves (Figure 5-3a,c). Regions of lumenal collagen deposition were observed in the tissues conditioned on the porated sleeves (Figure 5-3b,d), as indicated by the green straining in Lillie's trichrome on circumferential sections. However, this thin collagen layer was not present across the entire lumenal surface of the tissue, and appeared to be concentrated in patches that were 300-500 μm in width as viewed in circumferential sections. There were no differences in cellularity, collagen per cell, UTS, or modulus between the porated sleeve samples and the solid sleeve controls (Figure 5-3e-h).

5.3.2. Localization of collagen layer to porated regions

In order to investigate the regions of lumenal collagen deposition observed in the porated sleeve samples, a two-week experiment was performed in which tissues were cyclically stretched on porated sleeves with the same pore array (8 circumferential columns of pores). At harvest, axial strips were taken between columns of pores (Figure 5-4a, red box) and along columns of pores (Figure 5-4a, blue box). Lumenal collagen deposition was not observed in sections that were taken from areas between columns of pores (Figure 5-4b,d). However, along a column of pores, a layer containing cells and collagen was present on the lumenal tissue surface (Figure 5-4c,e).

5.3.3. Lumenal remodeling increased with increased pore density and culture duration

In an attempt to increase the uniformity of lumenal collagen deposition, sleeves with 16 columns of pores were fabricated, and tissues were cultured for two weeks on these porated sleeves alongside solid sleeve controls. Figure 5-5 shows trichrome-stained axial and circumferential sections from tissues cyclically stretched on solid and porated sleeves as well as porated sleeve controls lacking the bottom end piece. All porated sleeve sections shown in Figure 5-5 were taken along rows or columns of pores. A highly cellular region was present on the lumenal surface of the cyclically stretched porated sleeve samples (Figure 5-5b,e,h,k), and a thin layer of collagen was present in this region. Serial sectioning revealed that 1 mm wide axial strips with high cell density were centered on each pore column. The cell nuclei in this layer appeared elongated in the circumferential sections (Figure 5-5h) and punctate in the axial sections (Figure 5-5k) indicating that the cells were aligned circumferentially. In the solid sleeve controls "dead zones," areas with few cells and little remodeling, were present on the lumenal surface as indicated by the black arrows in Figure 5-5a,d,j. In the porated sleeve control samples with the lower end piece removed, there was no evidence of lumenal collagen layer (Figure 5-5c,f,i,l). These controls had a thickness of 0.90±0.09 mm and were thinner than both the cyclically stretched porated sleeve samples (1.36±0.06 mm) and solid sleeve controls (1.24±0.11 mm).

Sections stained for type I collagen (Figure 5-6) clearly showed that the lumenal layer in the cyclically stretched porated sleeve samples consisted of densely packed cells surrounded by collagen. Picrosirius red staining also highlighted the lumenal layer

of collagen present in tissues cyclically stretched on these porated sleeves (Figure 5-7). This layer was not present in solid sleeve control samples. Despite these apparent localized differences, in terms of bulk properties there were no differences in cellularity, collagen per cell, UTS, or modulus between the porated sleeve samples and the solid sleeve controls (Figure 5-7e-h).

5.3.4. Porated sleeve culture increases cell density near lumenal surface

The distribution of cells was quantified in sections from tissues cyclically stretched for two weeks on solid sleeves or porated sleeves with 16 columns of pores. For samples cultured on porated sleeves, the cell distribution was quantified for axial sections taken along columns of pores and between columns of pores. The dense cell layer present in the porated sleeve samples was ignored in this count, and the "lumenal surface" was defined just inside this layer. Cell nuclei were counted in three different zones, 25-100 µm, 100-175 µm, and 175-250 µm from the surface, and data are reported as cells/4x image. Nuclei within 25 µm of the surface were not counted to avoid including cells that were part of the dense lumenal layer present in the porated sleeve samples. In sections taken along a column of pores, the cell density was increased in the 25-100 µm region compared to solid sleeve controls (Fig. 5-8). In contrast, in sections taken between columns of pores there was no increase in cell density compared to solid sleeve controls. There were no differences in cell density among any of the groups in the regions that were more distant from the lumenal surface (>100 µm).

5.3.5. CFD model predictions for flow field

For both the time-averaged and maximum inlet pressure/gap width conditions, the CFD model predicted flow of medium that was primarily lumenal, with less than 0.01% of the flow volume entering the tissue. Figure 5-9 shows the CFD model predictions for the time-averaged boundary pressure/width condition. The normal velocity at the lumenal surface (Fig. 5-9a) of the tissue was highest directly across the gap from the discrete pores, and away from the pores the normal velocity was several orders of magnitude smaller. The transmural velocity decreased sharply within ~300 μm upon entering the tissue (Fig. 5-9b) with much of the flow recirculating back into the gap as indicated by the negative sign of the normal velocity in regions surrounding each pore (Fig 5-9a). The transmural velocity magnitude and flow streamlines are shown in Figure 5-9c, clearly highlighting the flow pattern. The lumenal shear stress (Fig. 5-9d) was also elevated within ~0.5 mm of each discrete pore.

While peak transmural flow velocity approached 150 μm/s, the average velocity over the entire tissue volume was 0.3 μm/s for both maximum and time-averaged lumenal pressures. This volume-averaged transmural velocity translates to a Peclet number (Pe) of 0.2 for dissolved oxygen and ~2 for growth factors such as epidermal growth factor, using diffusion coefficients measured in fibrin gels.[78,79] After 3 weeks of static culture, our tissue tubes were substantially denser at ~100 mg/ml protein than a typical 3 mg/ml fibrin gel, so the above Peclet numbers provide a conservative estimate.

The average lumenal shear stress was computed for both the tissue as a whole and the region where improved remodeling was observed, approximated by a

rectangular prism centered on the column of pores with a width of 1 mm and depth of 100 µm into the tissue. The shear stress magnitude imposed on the cells by the interstitial flow was also estimated based on the computed interstitial velocity using the theory of Wang and Tarbell.[80] These values are summarized in Table 5-3.

CFD model prediction	**Time-averaged lumenal pressure**	**Maximum lumenal pressure**
Average transmural (radial) velocity – whole tissue	0.3 µm/s	0.3 µm/s
Average interstitial shear stress magnitude – whole tissue	0.06 dyn/cm^2	0.06 dyne/cm^2
Average interstitial shear stress magnitude – improved region	0.2 dyn/cm^2	0.4 dyn/cm^2
Average lumenal shear stress magnitude – whole tissue	8 dyn/cm^2	14 dyn/cm^2
Average lumenal shear stress magnitude – improved region	13 dyn/cm^2	32 dyn/cm^2

Table 5-3. CFD model predictions for flow in and around tissue tube

Averaged over the full tissue volume, the time-averaged lumenal and interstitial shear stresses were 8 dyn/cm^2 and 0.06 dyn/cm^2, respectively. In the improved region, shear stress magnitudes were approximately twice the volume-averaged values with magnitudes of 13 dyn/cm^2 and 0.2 dyn/cm^2 for the lumenal and interstitial shear stresses, respectively.

5.4. Discussion

In the previously employed bioreactor used to culture tissue tubes for heart valve applications,[31] lumenal and transmural flow were prevented by the presence of a solid support sleeve used to ensure uniform tissue strains. While the solid sleeve bioreactor applied well-controlled cyclic strain to the tissue, it was desirable to combine this mechanical stimulation with the enhanced nutrient transport and possible shear stress stimulation that lumenal and transmural flow provide.[35,66,72-74,77,81] After one week of bioreactor culture on porated support sleeves, there were no differences in the bulk properties of the tissues compared to solid sleeve controls; however, there was evidence of lumenal remodeling of the fibrin gel scaffold into cell-produced collagen in the proximity of the pores (Fig. 5-3b,d). Due to the relatively low pore density of the sleeve with just 8 columns of pores and the short culture duration, it was not surprising that differences were not observed in the overall tissue composition, strength, or stiffness. The regions of lumenal remodeling were small compared to the overall tissue volume; therefore, they did not substantially influence the tissue properties. In order to examine the location of the regions of lumenal remodeling, a two-week experiment was performed in which tissues were cultured on the same porated sleeves, and axial sections were taken from areas both between and along columns of pores (Fig. 5-4). The localization of lumenal remodeling to the columns of pores in the support sleeve verified that the observed effects were a direct consequence of the pores, and confirmed the hypothesized benefit of lumenal and transmural flow.

In an effort to improve the uniformity of remodeling across the lumenal surface of the tissue, the density of pores in the support sleeve was doubled and two-week experiments were conducted. A dense layer of circumferentially oriented cells surrounded by collagen was present along columns of pores, extending at least 1 mm in width. This layer was similar in appearance to the ablumenal surface of the tissue, which was in contact with the recirculating medium (Figures 5-5-5-7). The collagen-rich layer at the ablumenal surface was ~3 times as thick as the lumenal layer; however, the ablumenal surface of the tissue was in contact with culture medium for the 3 weeks of static culture before the tissues were mounted into the bioreactor while the lumenal surface was in contact with the glass mandrel. The lumenal remodeling was not observed in any of the solid sleeve control samples nor in the non-distending porated sleeve controls with the lower end piece removed. It was noted that there were “dead zones” with few cells and very little collagen production at the lumenal surface of many of the solid sleeve control samples. It is hypothesized that these dead zones were a result of insufficient nutrient transport though the tissue or related shear stimulation.

In samples cyclically stretched on porated sleeves, the cell density within 100 µm of the lumenal surface along a column of pores was double that of the solid sleeve controls. This indicated that there was enhanced cell survival and/or proliferation in this region. While in the solid sleeve samples and between columns of pores the cell density was lower at the lumenal surface and reached a plateau around 175-250 µm, along pore columns the cells were distributed uniformly throughout the tissue tube wall (Figure 5-8). In a perfusion bioreactor, Kitagawa et al. found that by applying transmural flow to

synthetic polymer scaffolds seeded with NIH/3T3 cells they were able to achieve a uniform distribution of live cells throughout the thickness of the engineered tissue compared to samples cultured without flow.[74] Perfusion-enhanced cell viability, proliferation, and metabolic activity have also been observed for a variety of other cell types.[75,81-83]

As lumenal medium contact, lumenal flow, and transmural flow occurred simultaneously with porated sleeves in this bioreactor, the mechanism behind the increased remodeling and cellularity is unclear. While the contact of culture medium certainly enhanced transport at the lumenal surface via diffusion, there was also the possibility of convective transport due to transmural flow through the porous tissue as well as shear-induced cell stimulation due to lumenal and transmural flow. A CFD model was developed to predict the flow field around and through tissue tubes in the porated sleeve bioreactor. The model was developed using the tissue properties and pump settings at the onset of bioreactor culture, and while additional work must be done to investigate transmural flow velocities as the tissue matures, the model predicted the transmural flow magnitude and lumenal flow at early time points.

In line with experimental observations, the CFD model predicted that the effects of the porated sleeve were localized to regions near the discrete pores in the sleeve (Fig. 5-9). Averaged over the entire tissue, the transmural flow velocity was only 0.3 μm/s, which is substantially smaller than the transmural flow velocity (21 μm/s) in the pulsed flow-stretch bioreactor employed to culture small diameter vascular grafts without an elastic support sleeve.[35] Although the volume-averaged transmural velocity was small,

the corresponding Peclet numbers of ~0.2-2 for key nutrients suggest that both diffusion and transmural convection may have contributed to the increased cellularity and remodeling observed along columns of pores, at least at early time points. In addition, the transmural flow velocity was substantially higher near the discrete pores (Fig. 5-9c), and convective transport was likely dominant in these regions.

In the region of increased cellularity and remodeling around the pores, both the lumenal and interstitial shear stresses were elevated. Shear-induced alterations in gene expression and motility have been observed for fibroblasts in both 2D and 3D culture, although the effects have not been studied as extensively as for endothelial cells.[84] Increased proliferation and differentiation of dermal fibroblasts in a perfused collagen gel has been reported with interstitial shear stresses ranging from 0.15 to 0.33 dyn/cm^2,[81] which are similar in magnitude to the predicted interstitial shear stresses in the regions of improved remodeling in our system (0.2-0.4 dyn/cm^2).

While differences were visible in the histological sections, there were no measured differences in the overall cellularity, collagen per cell, UTS, or modulus between the solid sleeve and porated samples. Although this appears to conflict with the finding of increased cell and collagen density near the lumenal surface in the porated sleeve samples, it should be noted that this region comprised only a small fraction of the tissue (~2.5%). In addition, the bulk properties of the tissue were assessed for circumferential strips spanning three columns of pores, so it is likely that the localized differences were masked when averaged over the large volume.

There were several limitations to the basic CFD model, including the assumption of constant gap width around the circumference of the bioreactor. As the tissue did not slide off the sleeve during culture, the gap width must have been variable around the circumference, with points of contact between the tissue and sleeve between columns of pores. This variable gap width would generate asymmetry in the lumenal flow with increased flow along columns of pores where the gap was widest. In addition, fluid-structure interaction was not included in the current model, as the available pressure and gap width data made it possible to obtain predictions for the flow field in a less computationally intensive manner. While a full fluid-structure interaction model may be able to predict the gap width asymmetry and more accurately describe the flow field, the development of this complex model is unnecessary to approximate the flow field and associated shear stresses.

These results suggest that with optimization of the porated sleeve design and extended culture duration, the porated sleeve bioreactor can be used to increase cell density and accelerate fibrin remodeling into a collagenous matrix at the lumenal surface of large diameter engineered tissue tubes. It is clear that increased pore density is required to achieve uniform remodeling, as currently the remodeling was limited to a quarter of the lumenal surface. As pore density is increased, care must be taken to avoid applying detrimental magnitudes of lumenal or transmural flow, as high flow rates may damage the tissue or wash out newly synthesized matrix components.[77] Based on the CFD model predictions, the current transmural flow velocities are at least an order of magnitude lower than those employed in our sleeve-less small diameter vascular graft

bioreactor,[35] suggesting that a moderate increase in transmural flow will not have damaging effects.

In the present work, a porated sleeve bioreactor was developed to culture large diameter engineered tissue tubes for tubular heart valve applications with the ultimate goals of accelerating tissue formation and reducing the required culture duration. Preliminary studies with this bioreactor support this approach, highlighting the beneficial effects of combined lumenal medium contact and lumenal and transmural flow on cellularity and collagen deposition. While the enhanced remodeling was localized to regions near pores in the elastic support sleeve, these short-term results motivate long-term implementation of this bioreactor and optimization of the porated sleeve design for improved tissue uniformity.

5.5. Figures

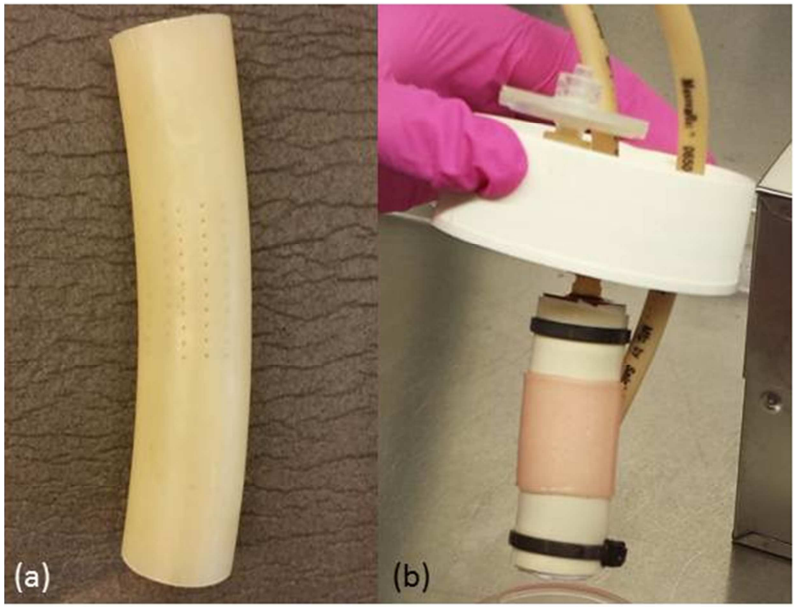

Figure 5-1.

(a) Porated latex sleeve with 16 columns of pores and (b) porated sleeve bioreactor with a 22 mm diameter tissue tube mounted over the central porated region.

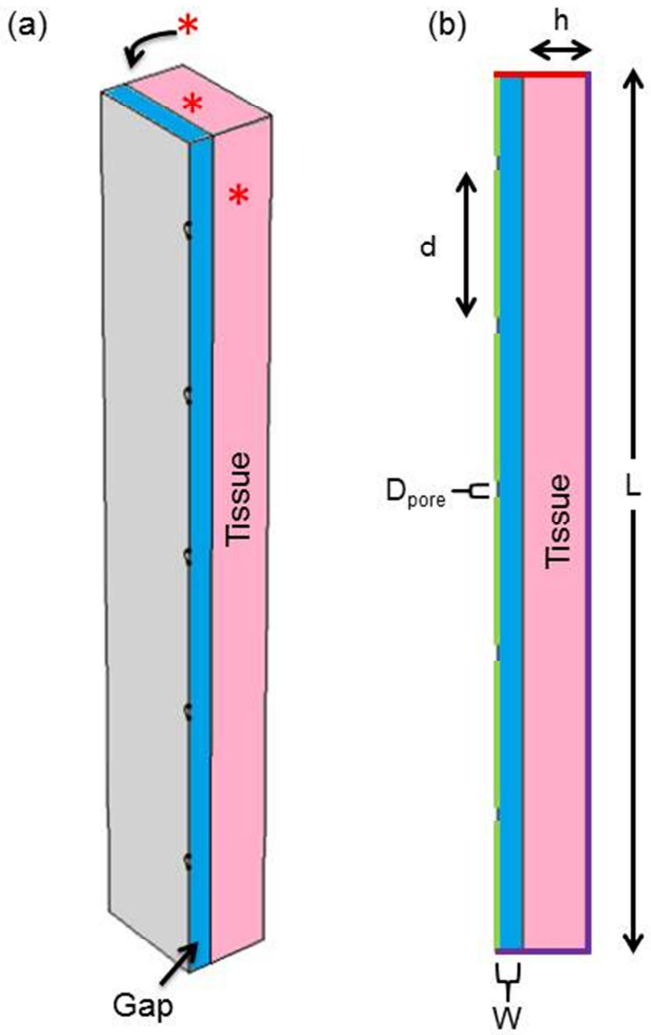

Figure 5-2.

(a) Three-dimensional schematic of model geometry showing the porated sleeve, fluid domain, and tissue domain. The symmetry faces are indicated with an asterisk. (b) Cross-section of model geometry showing boundary conditions and geometric parameters. No-slip (green lines, left edge of geometry) was enforced along the solid portions of the sleeve, an outlet pressure of 0 Pa was applied on exterior surfaces of the domain (purple lines, bottom and right edges of geometry), and symmetry was enforced (red line, top edge of geometry) on the top surface to generate the full axial length of the gap/tissue. The inlet pressure was set at the five pores in the sleeve.

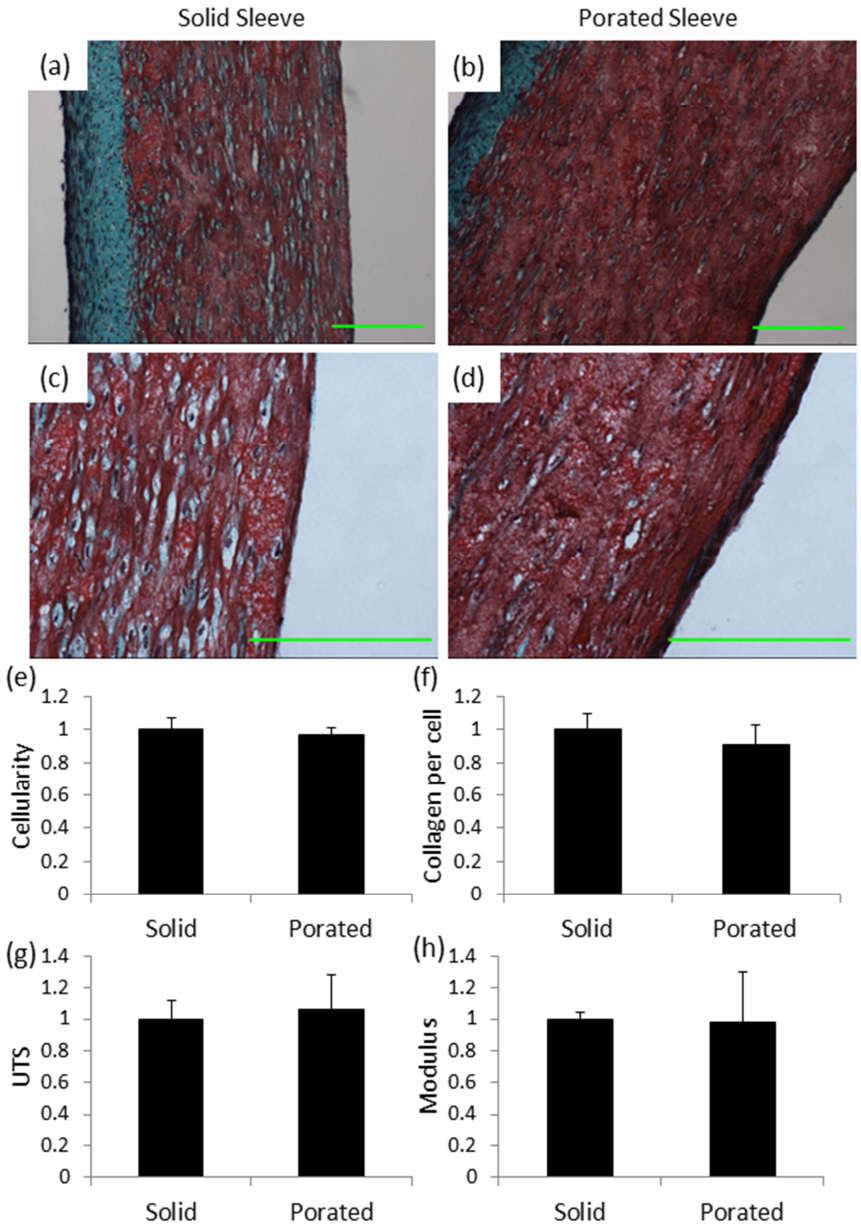

Figure 5-3.

1-week study results. 10x (a,b) and 20x (c,d) images of trichrome-stained circumferential sections from tissues cyclically stretched on solid sleeves (left) and porated sleeves (right) for 1 week. The lumenal surface of the tissue is on the right. Red staining indicates non-collagenous protein, green indicates collagen, and nuclei are stained dark purple/black. All scale bars are 200 µm. (e) Cell number per volume, (f) collagen per cell, (g) UTS, and (h) modulus for solid sleeve and porated sleeve samples. Data represent two experimental repeats, and all values are normalized to solid sleeve controls (n=3-4 per group).

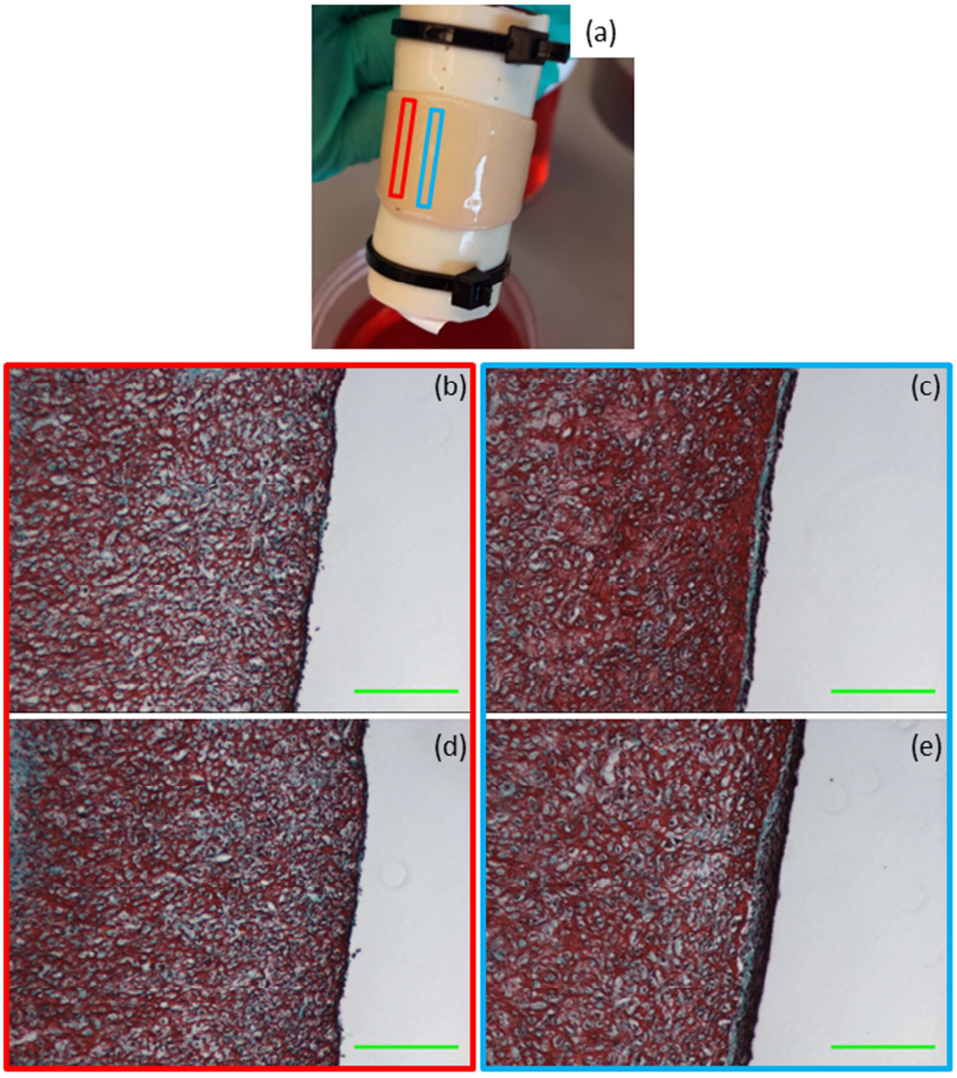

Figure 5-4.

Localization of collagen deposition to columns of pores. (a) Locations of axial sections taken from areas between columns of pores (red box, left) and along a column of pores (blue box, right) after two weeks of bioreactor culture. 10x trichrome stained sections of areas (b,d) between columns of pores and (c,e) along columns of pores. The lumenal surface is on the right in all images, and scale bars are 200 µm.

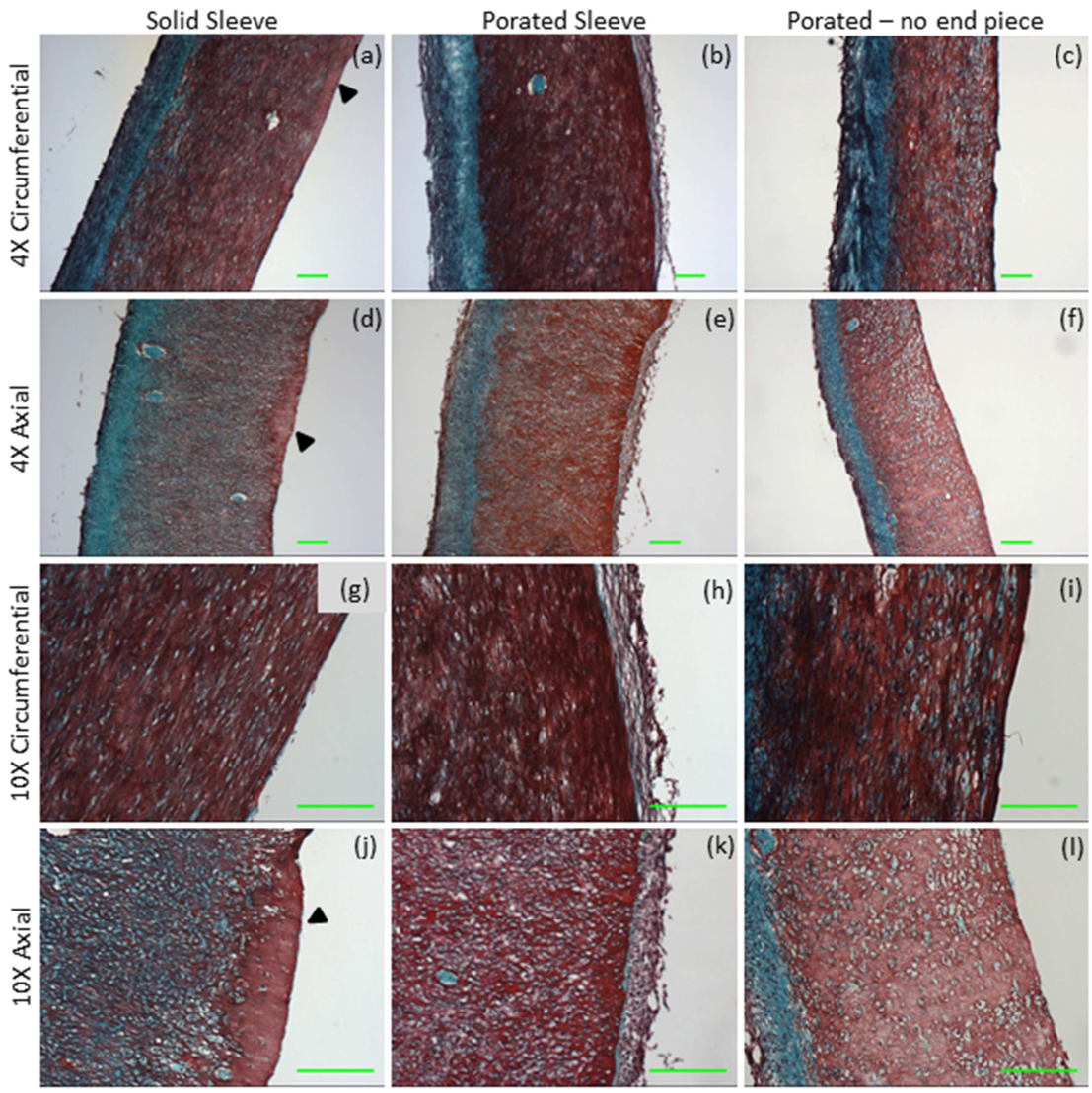

Figure 5-5.

Trichrome-stained 4x (a,b,c) and 10x (g,h,i) circumferential sections and 4x (d,e,f) and 10x (j,k,l) axial sections of tissues cultured on solid sleeves (left), porated sleeves (center), or porated sleeves with the lower bioreactor end piece removed (right) for two weeks. Black arrows indicate “dead zones” present on the lumenal surface of solid sleeve control tissues. All porated sleeve sections shown here were taken along columns of pores. The lumenal surface of the tissue is on the right. All scale bars are 200 µm.

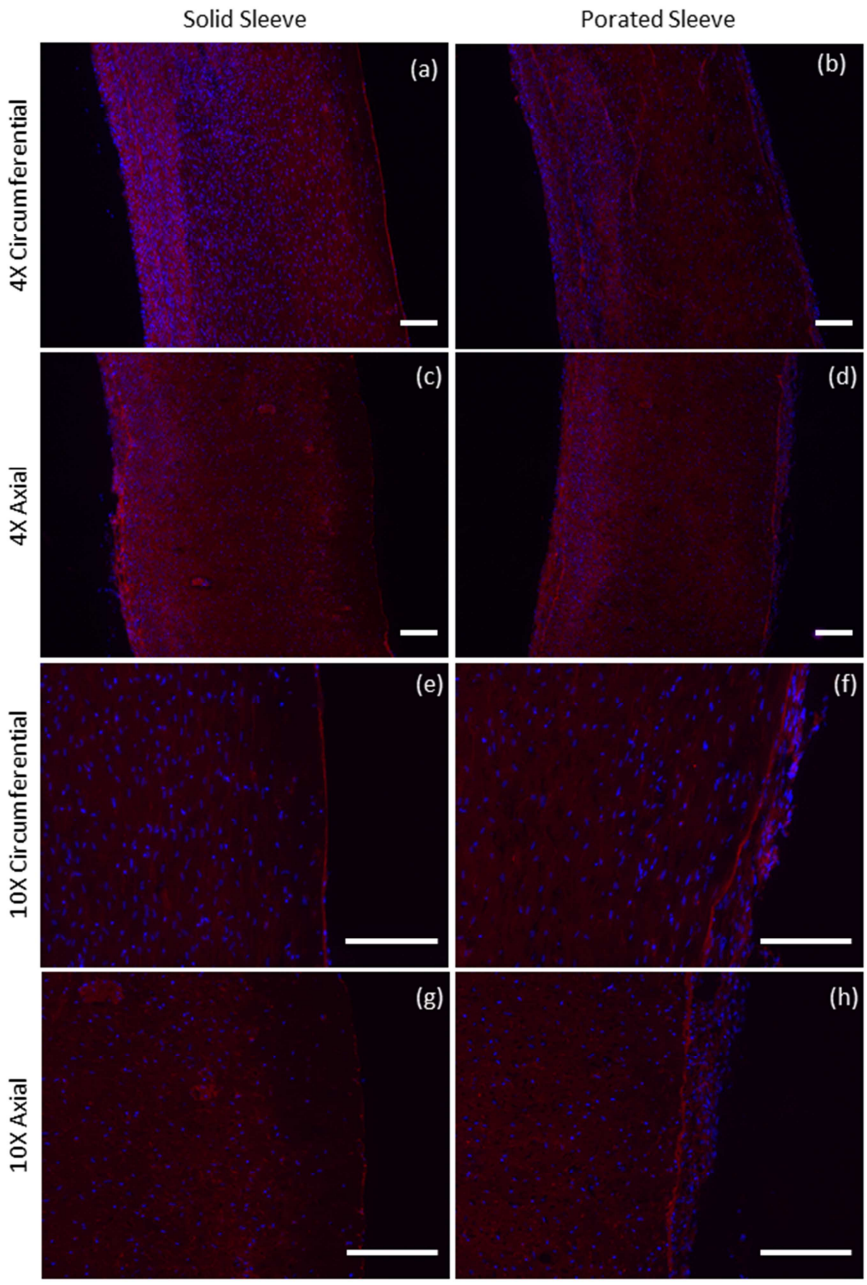

Figure 5-6.

4x (a,b) and 10x (e,f) circumferential sections and 4x (c,d) and 10x (g,h) axial sections stained for type I collagen (red) and counterstained with Hoechst dye (blue). Tissues were cyclically stretched on solid sleeves (left) or porated sleeves with 16 columns of pores (right) for two weeks. All porated sleeve sections shown here were taken along columns of pores. The lumenal surface of the tissue is on the right. All scale bars are 200 μm.

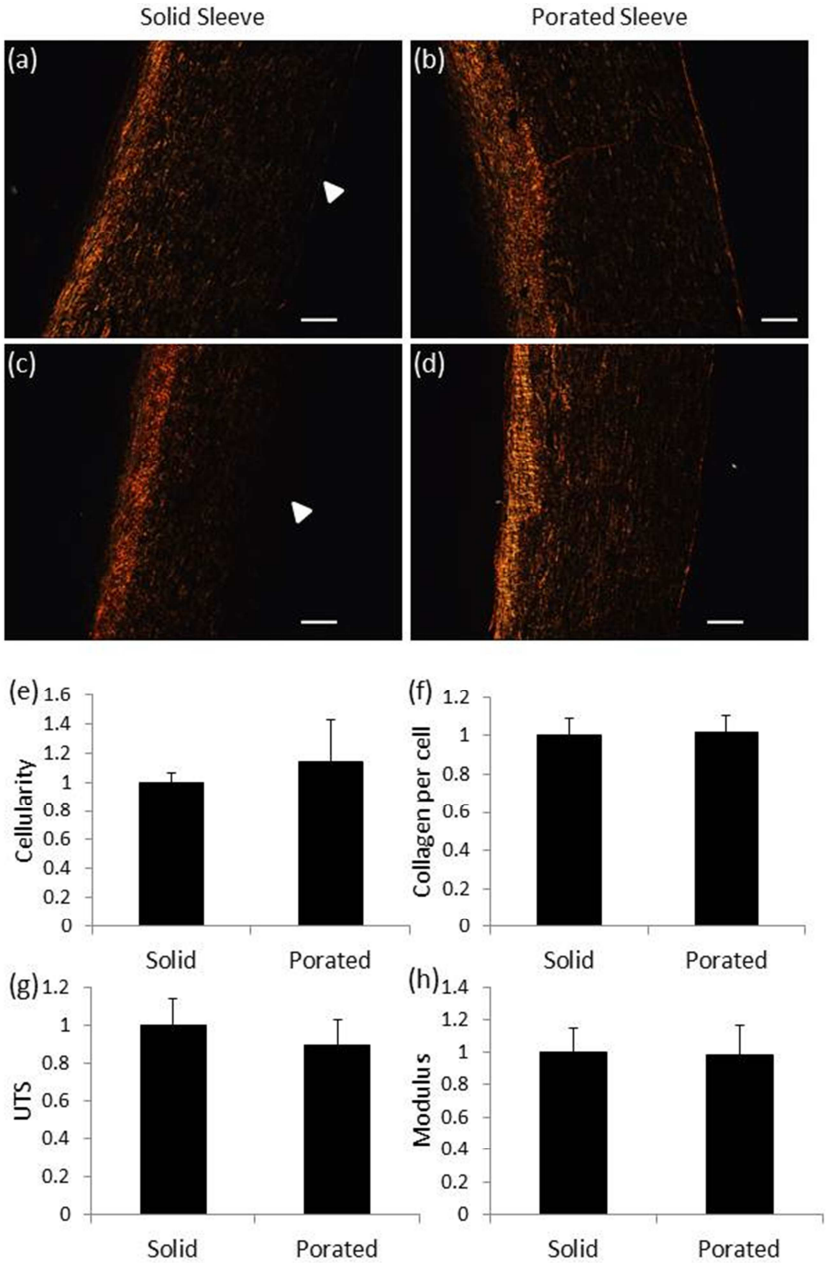

Figure 5-7.

4x images of picrosirius red-stained circumferential sections from tissues cyclically stretched on solid sleeves (a,c) and porated sleeves with 16 columns of pores (b,d) for two weeks. In all images the lumenal surface of the tissue is on the right. White arrows in (a) and (c) indicate the lumenal surface of the tissue. All scale bars are 200 μm. (e) Cell number per volume, (f) collagen per cell, (g) UTS, and (h) modulus for solid sleeve and porated sleeve samples. Data represent three experimental repeats, and all values are normalized to solid sleeve controls (n=3 per group).

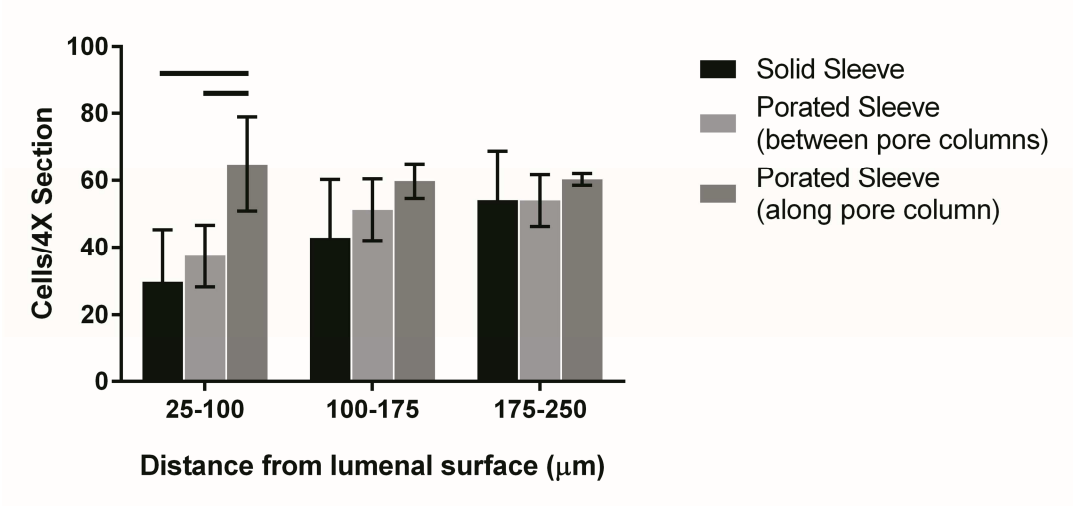

Figure 5-8.

Cell count per 4X image in zones 25-100 µm, 100-175 µm, and 175-250 µm from the lumenal tissue surface for samples cyclically stretched on solid sleeves or porated sleeves (both along and between columns of pores) for two weeks. Horizontal bars indicate differences in cell number ($p<0.05$) using one-way ANOVA with Tukey-Kramer post hoc test (n=3-4 per group)

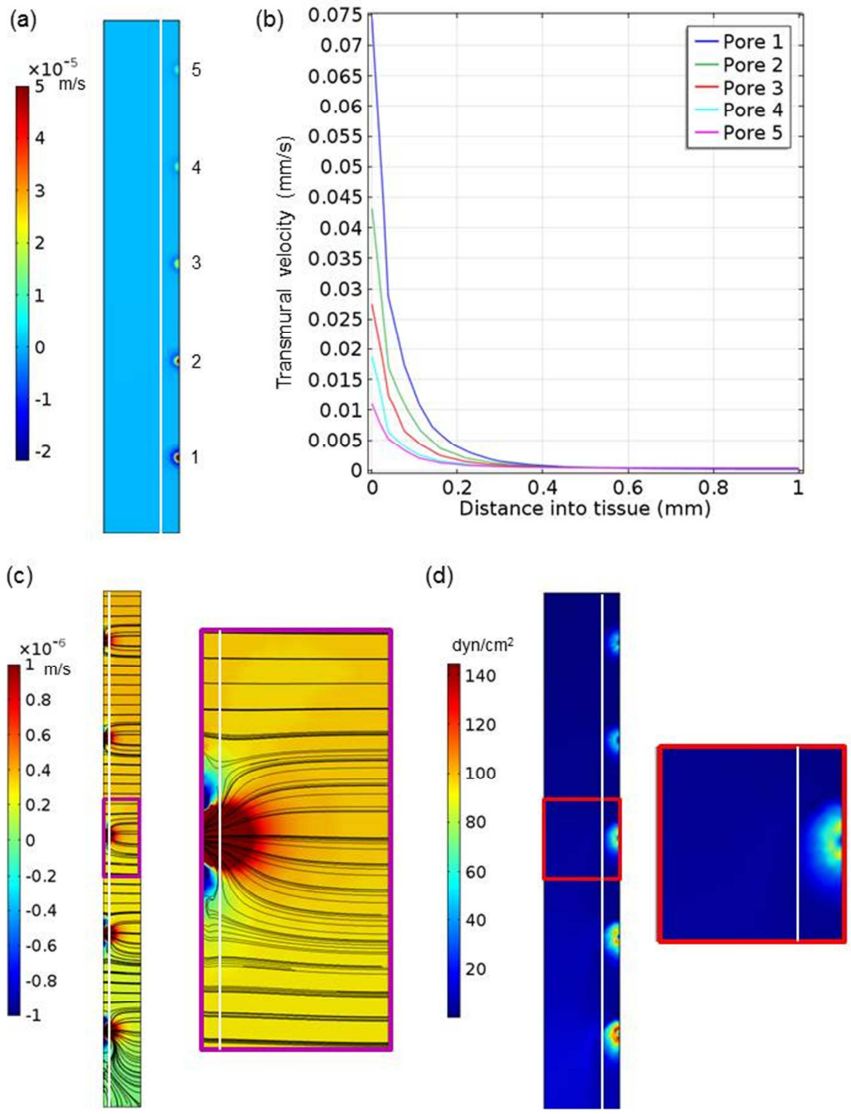

Figure 5-9.

CFD model results for the time-averaged pressure/gap width condition. (a) A plot of the normal velocity (m/s) at the lumenal tissue surface (en-face view). (b) The transmural (radial) velocity is plotted versus distance into the tissue along a horizontal line centered at each of the five pores with pore 1 being closest to the outlet boundary and pore 5 nearest the symmetry surface. (c) A side view of the transmural (radial velocity) magnitude (m/s) and velocity streamlines through the thickness of the tissue. A magnified view of the flow near a pore is indicated by the purple box. (d) A plot of the shear stress magnitude (dyn/cm^2) at the lumenal tissue surface (en-face view). A magnified view of the shear stress near a pore is indicated by the red box. All surface plots (a,b,d) are oriented such that the bottom pore is the one closest to the gap outlet and the top pore is nearest the symmetry surface. The vertical white line indicates the boundary of the 1 mm by 100 µm "improved" region.

Chapter 6. Conclusions and Future Directions

6.1. Major Contributions

The present work has contributed substantially to the fields of mechanotransduction and cardiovascular tissue engineering. These contributions were communicated through oral and poster presentations at both local and national conferences, and three manuscripts have been published or are in preparation. A synopsis of the major contributions of this work to the field is included in the following sections.

6.1.1. Overcoming adaptation to cyclic stretching: ERK1/2 and p38 activation

The basic research utilizing the Flexcell® tension system described in Chapter 2 provided insight into the interaction between the ERK1/2 and p38 pathways in cyclically stretched fibroblasts. While it has been documented that cells adapt to constant amplitude cyclic stretching, the underlying cell signaling producing this phenomenon had not been well characterized prior to the present work. The cells' six hour refractory period before possible ERK1/2 reactivation coincided with the return of p38 phosphorylation to basal levels, suggesting that the transient activation of p38 serves to keep ERK1/2 activation in check. In addition, it was determined that both an additional onset of cyclic stretching as well as small increments (>1%) in strain amplitude can fully reactivate ERK1/2 once p38 activation has subsided. As ERK1/2 activation has been shown to be required for cyclic-stretching induced collagen

deposition, this research provided the basis for the development of optimized cyclic stretching regimens for tissues where high mechanical strength and stiffness are required.

6.1.2. ERK1/2 activation alone is not sufficient to induce increased collagen deposition

Chapter 3 describes the long-term application of regimens selected based on ERK1/2 phosphorylation dynamics with the goal of increasing collagen deposition by fibroblasts in a fibrin gel. It was determined that while both intermittent and incrementally increasing strain amplitude cyclic stretching regimens reactivated ERK1/2, only incremental cyclic stretching increased cellular collagen deposition compared to continuously stretched controls. This indicates that contrary to prior hypotheses, ERK1/2 activation alone is not a sufficient predictor of final collagen content. In our fibrin gel system, an incremental regimen with daily increments in strain amplitude of 1% was able to increase collagen per cell 34% compared to controls stretched with constant amplitude after only two weeks, and this improvement may shorten the required culture time in our engineered cardiovascular tissues.

6.1.3. Development of a fluid-structure interaction model for solid sleeve tubular tissue bioreactor

The development of a fluid-structure interaction model for the currently employed tubular tissue bioreactor is described in Chapter 4. The COMSOL Multiphysics model predicts the fluid flow and structural deformation of the solid

support sleeve given the pump stroke volume or inlet pressure and the geometry and properties of the support sleeve. This model showed excellent agreement with experimental measurements at low stroke volumes. It is expected that the model will serve as a useful tool for exploring alterations in bioreactor geometry and materials prior to purchasing or machining a new part or material. In addition, the model provides the framework to ensure that adequate cell culture medium mixing occurs as parameters or materials are altered.

6.1.4. Design of a porated sleeve bioreactor improved lumenal remodeling in large diameter tissue tubes

A porated sleeve bioreactor was designed to enhance nutrient transport in large diameter engineered tissue tubes for heart valve applications. Proof-of-concept studies using this new bioreactor design demonstrated that bioreactor culture utilizing a porated support sleeve resulted in the presence of a dense layer of cells and collagen at the lumenal surface as well as increased cell density extending 100 μm into the tissue from this layer. In addition to the experimental bioreactor implementation, a COMSOL model was developed to predict the flow velocity field in and around the tissue. While medium contact certainly enhanced nutrient diffusion at the lumenal surface, model predictions suggested that localized convective effects and shear stimulation may have contributed to the increased lumenal remodeling observed along columns of pores. These studies highlight the beneficial effects of lumenal and transmural flow and motivate long term implementation of this system as well as optimization of porated

sleeve parameters. Furthermore, this bioreactor configuration may find additional applications in construct decellularization and/or recellularization prior to construct implantation.

6.2. Future Directions

6.2.1. Further Characterization of Cyclic Stretching-Induced Collagen Production Pathway

Studies of ERK1/2 and p38 signaling, collagen transcription, and collagen deposition provided considerable insight into the response of fibroblasts to cyclic stretching in a three-dimensional engineered tissue environment highlighting the complexity of the cell signaling response and downstream effects. It was determined that ERK1/2 signaling alone is not a sufficient indicator of collagen production. In addition, preliminary investigations into lot-to-lot variability presented in Appendix A suggest that similar ERK1/2 activation in two different lots of fibroblasts may result in different collagen deposition outcomes.

As the intermediate steps between ERK1/2 activation and collagen deposition are largely uncharacterized,[41] further study of the cyclic stretching-induced collagen production pathway is necessary to better understand the system dynamics and predict the long-term collagen deposition outcome. While ERK1/2 signaling and p38 inhibition have been implicated as key players in the collagen production pathway, complex crosstalk occurs between the mitogen activated protein kinase (MAPK) cascades, and it

is important to consider individual cascades within the greater context of the full MAPK network.[85,86] Additionally, now that the methods are in place to characterize MAPK phosphorylation with the Nanopro Immunoassay system, it is possible to obtain detailed information about isoform specific phosphorylation rather than simply considering each cascade as an on/off switch. It is possible that by studying the MAPK network as a whole, differences in in the "reactivation" due to intermittent versus incremental cyclic stretching and/or lot-to-lot variation in signaling dynamics will become apparent.

In addition to a detailed study of the MAPK network, there is still much work to be done in characterizing the downstream effects of cyclic stretching. Study of intermediate steps in the collagen production pathway such as transcription factor activation[86] and binding[86,87] and gene promoter activity[43,87] can help to provide a valuable link between MAPK signaling and gene expression. Finally, while the bulk of the current research has focused on collagen production, it is equally important to consider the effects of cyclic stretching on matrix metalloproteinase (MMP) profiles, collagen degradation, and collagen maturation.[60-62] Future work investigating the comprehensive effects of cyclic stretching on cell signaling as well as matrix deposition, degradation, and remodeling may aid in the further optimization of bioreactor conditioning regimens for accelerated tissue formation.

6.2.2. Optimization of Porated Sleeve Parameters

Culture in the porated sleeve bioreactor resulted in the presence of a dense lumenal layer of cells and cell-produced collagen. However, this layer was not present

across the entire lumenal surface of the tissue but was localized along lines of discrete pores in the sleeve. When pore density was doubled from 8 to 16 columns of pores around the sleeve circumference, there were still areas in the porated sleeve samples that were lacking this lumenal cell layer and remodeling. Future work focusing on the porated sleeve design is required in order to achieve uniform remodeling of the entire engineered tissue tube, and iterative optimization will be required to assess the tissue properties and uniformity as the pore array is altered. While it is expected that further increasing pore density will result in more uniform remodeling of the lumenal surface, negative effects such as medium pooling and tissue damage may be associated with the increased flow. These trade-offs will have to be balanced, and it is expected that the COMSOL model will be a valuable tool for predicting the flow through and around the tissue as sleeve parameters are changed.

It may be possible to fabricate a porated sleeve that promotes uniform lumenal tissue remodeling using the current method of laser cutting discrete pores into solid latex tubing. However, the pore diameter and array options are limited by the power and precision of the laser cutting system, and as increased pore densities are sought, it may be necessary to seek out an alternative method for producing the porated support sleeves. With the increasing prevalence of 3D printing and electrospinning technologies, it may be possible to fabricate elastic sleeves with more uniform porosity for use in the bioreactor system. As several elastic materials are available for use with 3D printers and electrospinners, it may now be feasible to print or spin a porous, elastic structure for use as a support sleeve.[88-90] These technologies show promise as affordable

and flexible options for optimizing sleeve design for accelerated, uniform tissue remodeling.

6.2.3 Fluid Structure Interaction Model of Porated Sleeve Bioreactor

In Chapter 5 a CFD model describing flow through and around the tissue in the porated sleeve bioreactor was presented. This model was useful for predicting the lumenal and transmural flow velocities; however, many simplifications were made in the creation of this model. The cyclic motion of the sleeve and tissue were ignored, and the tissue was treated as a stationary porous object rather than a deforming poroelastic material. In order to better understand the applied strain and flow patterns, a full FSI model must be developed. Implementing arbitrary Lagrangian Eulerian techniques as presented in Chapter 4 for the solid sleeve bioreactor is less straightforward when a poroelastic material is included in the model.

At present, COMSOL does not have built-in functionality allowing coupling of the Navier-Stokes equations employed in the free flow domain with the Biot poroelasticity formulation used for the tissue domain. However, there has been extensive study of the appropriate coupling conditions for these two domains, and it may be possible to implement these constraints in a custom designed interface condition. Badia et al. provide a comprehensive overview of the conditions and methods used to couple these two domains, and they present a well-posed problem with enforcement of continuity of velocities and stresses at the interface.[91] Calo et al. employed a simplified Biot formulation written in terms of the pore pressure and

structural velocity only; however, the use of this simplified form requires the application of artificial boundary conditions at the interface.[92]

Future work should consider how best to implement proper interface conditions in COMSOL or if an alternate software package is better equipped to solve this problem. In addition to developing the computational framework for this system, a thorough study of the properties of the developing engineered tissue will add increased accuracy to the model. The tissue thickness, permeability, porosity, and poroelastic constitutive constants change as the tissue matures, and the time dependent tissue properties must be characterized for the model to be relevant throughout the course of bioreactor culture. The development of a fully coupled FSI model of the porated sleeve bioreactor with well-defined parameters is highly desirable as it will permit us to better predict the strain magnitude and flow velocities experienced by the developing tissue construct. In addition, it may be possible to couple the fluid flow results with kinetic data to predict concentrations of key nutrients within the tissue or investigate use of a similar system for the detergent decellularization of tubular constructs.[31]

6.2.4. Long-term Application of Optimized Cyclic Stretching in Porated Sleeve Bioreactor

Optimized cyclic stretching and enhanced nutrient transport have been investigated in parallel for accelerating the remodeling of the fibrin gel scaffold into cell-produced collagen. The next step in improving bioreactor culture for the large diameter engineered tissue tubes would be to implement this optimized cyclic stretching

(1% daily increments in strain amplitude) in the porated sleeve bioreactor for long term culture. While this follows the logical progression of iterative bioreactor improvement, in practice this combination poses several challenges. Unlike the previously employed solid sleeve bioreactor, in the porated sleeve bioreactor the applied strain is affected to some extent by the properties of the developing tissue. Variability in tissue properties has been observed both between castings and even between tissues within the same casting. In the solid sleeve system, this variability is not a major issue, because the strain is largely dictated by the stiffness of the latex sleeve. In contrast, in the porated sleeve system, some sort of feedback control will be required to apply precise strain amplitudes (less than 1% variation between samples). This may be as simple as periodically measuring the strain with the laser micrometer and adjusting the pump accordingly; although automated control may be desired in future systems.

The current porated sleeve bioreactor studies have been limited to two weeks in duration and 6% strain amplitude. As the durations of future experiments are extended toward the standard culture periods of four to five weeks, additional studies must be performed to investigate the effects of lumenal and transmural flow in more mature tissues subjected to larger strain amplitudes. As high transmural flow velocities may have negative consequences on collagen deposition,[74.77] care must be taken to balance the desired strain amplitude with a flow velocity that is conducive to tissue formation. However, with these practical challenges overcome, it is hypothesized that implementing optimized cyclic stretching in a bioreactor system that allows for lumenal

medium contact and transmural flow will further accelerate collagen production in the engineered tissues.

References

1. A. J. Weinhaus, K. P. Roberts, in *Handbook of Cardiac Anatomy, Physiology, and Devices*, P. A. Iaizzo, Ed. (Springer Science+Business Media, New York, 2009), pp. 59-85.
2. R. B. Hinton, K. E. Yutzey, Heart valve structure and function in development and disease. *Annu Rev Physiol* **73**, 29-46 (2011).
3. P. M. Taylor, P. Batten, N. J. Brand, P. S. Thomas, M. H. Yacoub, The cardiac valve interstitial cell. *Int J Biochem Cell Biol* **35**, 113-118 (2003).
4. P. A. Iaizzo, in *Handbook of Cardiac Anatomy, Physiology, and Devices*, P. A. Iaizzo, Ed. (Springer Science+Business Media, New York, 2009), pp. 3-12.
5. P. Stradins, R. Lacis, I. Ozolanta, B. Purina, V. Ose, L. Feldmane, V. Kasyanov, Comparison of biomechanical and structural properties between human aortic and pulmonary valve. *Eur J Cardiothorac Surg* **26**, 634-639 (2004).
6. D. Mavrilas, Y. Missirlis, An approach to the optimization of preparation of bioprosthetic heart valves. *J Biomech* **24**, 331-339 (1991).
7. D. Lo, I. Vesely, Biaxial strain analysis of the porcine aortic valve. *Ann Thorac Surg* **60**, S374-378 (1995).
8. J. A. Stella, J. Liao, M. S. Sacks, Time-dependent biaxial mechanical behavior of the aortic heart valve leaflet. *J Biomech* **40**, 3169-3177 (2007).
9. M. Thubrikar, *The Aortic Valve*. (CRC Press, Inc., Boca Raton, 1990), pp. 104-106.
10. A. S. Go, D. Mozaffarian, V. L. Roger, E. J. Benjamin, J. D. Berry, M. J. Blaha, S. Dai, E. S. Ford, C. S. Fox, S. Franco, H. J. Fullerton, C. Gillespie, S. M. Hailpern, J. A. Heit, V. J. Howard, M. D. Huffman, S. E. Judd, B. M. Kissela, S. J. Kittner, D. T. Lackland, J. H. Lichtman, L. D. Lisabeth, R. H. Mackey, D. J. Magid, G. M. Marcus, A. Marelli, D. B. Matchar, D. K. McGuire, E. R. Mohler, 3rd, C. S. Moy, M. E. Mussolino, R. W. Neumar, G. Nichol, D. K. Pandey, N. P. Paynter, M. J. Reeves, P. D. Sorlie, J. Stein, A. Towfighi, T. N. Turan, S. S. Virani, N. D. Wong, D. Woo, M. B. Turner, Heart disease and stroke statistics--2014 update: a report from the American Heart Association. *Circulation* **129**, e28-e292 (Jan 21, 2014).
11. R. Bryant, in *Heart Valves: From Design to Clinical Implantation*, P. A. Iaizzo, R. W. Bianco, A. J. Hill, J. D. St. Louis, Eds. (Springer Science+Business Media, New York, 2013), pp. 45-72.
12. C. M. Martin, in *Heart Valves: From Design to Clinical Implantation*, P. A. Iaizzo, R. W. Bianco, A. J. Hill, J. D. St. Louis, Eds. (Springer Science+Business Media, New York, 2013), pp. 72-81.

13. R. John, K. Liao, in *Heart Valves: From Design to Clinical Implantation*, P. A. Iaizzo, R. W. Bianco, A. J. Hill, J. D. St. Louis, Eds. (Springer Science+Business Media, New York, 2013), pp. 121-158.
14. T. Shinoka, C. K. Breuer, R. E. Tanel, G. Zund, T. Miura, P. X. Ma, R. Langer, J. P. Vacanti, J. J. E. Mayer, Tissue engineering heart valves: Valve leaflet replacement study in a lamb model. *Ann Thorac Surg* **60**, S513-S516 (1995).
15. S. P. Hoerstrup, R. Sodian, S. Daebritz, J. Wang, E. A. Bacha, D. P. Martin, A. M. Moran, K. J. Guleserian, J. S. Sperling, S. Kaushal, J. P. Vacanti, F. J. Schoen, J. E. Mayer, Jr., Functional living trileaflet heart valves grown in vitro. *Circulation* **102**, III44-49 (2000).
16. A. Mol, N. J. B. Driessen, M. C. M. Rutten, S. P. Hoerstrup, C. V. C. Bouten, F. P. T. Baaijens, Tissue engineering of human heart valve leaflets: A novel bioreactor for a strain-based conditioning approach. *Ann Biomed Eng* **33**, 1778-1788 (2005).
17. M. R. Neidert, R. T. Tranquillo, Tissue-Engineered Valves with Commissural Alignment. *Tissue Eng Part A* **12**, 891-903 (2006).
18. P. S. Robinson, S. L. Johnson, M. C. Evans, V. H. Barocas, R. T. Tranquillo, Functional Tissue-Engineered Valves from Cell-Remodeled Fibrin with Commissural Alignment of Cell-Produced Collagen. *Tissue Eng Part A* **14**, 83-95 (2008).
19. T. C. Flanagan, C. Cornelissen, S. Koch, B. Tschoeke, J. S. Sachweh, T. Schmitz-Rode, S. Jockenhoevel, The in vitro development of autologous fibrin-based tissue-engineered heart valves through optimised dynamic conditioning. *Biomaterials* **28**, 3388-3397 (2007).
20. S. P. Hoerstrup, R. Sodian, J. S. Sperling, J. P. Vacanti, J. E. Mayer, Jr., New pulsatile bioreactor for in vitro formation of tissue engineered heart valves. *Tissue Eng* **6**, 75-79 (2000).
21. C. Williams, S. L. Johnson, P. S. Robinson, R. T. Tranquillo, Cell sourcing and culture conditions for fibrin-based valve constructs. *Tissue Eng* **12**, 1489-1502 (2006).
22. G. C. Engelmayr, Jr., V. L. Sales, J. E. Mayer, Jr., M. S. Sacks, Cyclic flexure and laminar flow synergistically accelerate mesenchymal stem cell-mediated engineered tissue formation: Implications for engineered heart valve tissues. *Biomaterials* **27**, 6083-6095 (2006).
23. A. Balguid, A. Mol, M. A. A. van Vlimmeren, F. P. T. Baaijens, C. V. C. Bouten, Hypoxia Induces Near-Native Mechanical Properties in Engineered Heart Valve Tissue. *Circulation* **119**, 290-297 (2009).

24. Z. H. Syedain, R. T. Tranquillo, Controlled Cyclic Stretch Bioreactor for Tissue-Engineered Heart Valves. *Biomaterials* **30**, 4078-4084 (2009).
25. Z. Syedain, M. Lahti, S. Johnson, P. Robinson, G. Ruth, R. Bianco, R. Tranquillo, Implantation of a Tissue-engineered Heart Valve from Human Fibroblasts Exhibiting Short Term Function in the Sheep Pulmonary Artery. *Cardiovasc Eng Technol* **2**, 101-112 (2011).
26. T. C. Flanagan, J. S. Sachweh, J. Frese, H. Schnoring, N. Gronloh, S. Koch, R. H. Tolba, T. Schmitz-Rode, S. Jockenhoevel, In Vivo Remodeling and Structural Characterization of Fibrin-Based Tissue-Engineered Heart Valves in the Adult Sheep Model. *Tissue Eng Part A* **15**, 2965-2976 (2009).
27. D. Schmidt, P. E. Dijkman, A. Driessen-Mol, R. Stenger, C. Mariani, A. Puolakka, M. Rissanen, T. Deichmann, B. Odermatt, B. Weber, M. Y. Emmert, G. Zund, F. P. Baaijens, S. P. Hoerstrup, Minimally-invasive implantation of living tissue engineered heart valves: a comprehensive approach from autologous vascular cells to stem cells. *J Am Coll Cardiol* **56**, 510-520 (2010).
28. B. Weber, P. E. Dijkman, J. Scherman, B. Sanders, M. Y. Emmert, J. Grünenfelder, R. Verbeek, M. Bracher, M. Black, T. Franz, J. Kortsmit, P. Modregger, S. Peter, M. Stampanoni, J. Robert, D. Kehl, M. van Doeselaar, M. Schweiger, C. E. Brokopp, T. Wälchli, V. Falk, P. Zilla, A. Driessen-Mol, F. P. T. Baaijens, S. P. Hoerstrup, Off-the-shelf human decellularized tissue-engineered heart valves in a non-human primate model. *Biomaterials* **34**, 7269-7280 (2013).
29. B. Weber, M. Y. Emmert, L. Behr, R. Schoenauer, C. Brokopp, C. Drögemüller, P. Modregger, M. Stampanoni, D. Vats, M. Rudin, W. Bürzle, M. Farine, E. Mazza, T. Frauenfelder, A. C. Zannettino, G. Zünd, O. Kretschmar, V. Falk, S. P. Hoerstrup, Prenatally engineered autologous amniotic fluid stem cell-based heart valves in the fetal circulation. *Biomaterials* **33**, 4031-4043 (2012).
30. Z. H. Syedain, A. R. Bradee, S. Kren, D. A. Taylor, R. T. Tranquillo, Decellularized Tissue-Engineered Heart Valve Leaflets with Recellularization Potential. *Tissue Eng Part A* (2012).
31. Z. Syedain, L. Meier, J. Reimer, R. Tranquillo, Tubular Heart Valves from Decellularized Engineered Tissue. *Ann Biomed Eng* **41**, 2645-2654 (2013).
32. Z. Syedain, L. A. Meier, M. T. Lahti, S. Johnson, R. T. Tranquillo, Implantation of Completely Biological Engineered Grafts Following Decellularization into the Sheep Femoral Artery. *Tissue Eng Part A* (2014).
33. P. E. Dijkman, A. Driessen-Mol, L. Frese, S. P. Hoerstrup, F. P. Baaijens, Decellularized homologous tissue-engineered heart valves as off-the-shelf alternatives to xeno- and homografts. *Biomaterials* **33**, 4545-4554 (2012).

34. D. K. Hildebrand, Z. J. Wu, J. E. Mayer, Jr., M. S. Sacks, Design and hydrodynamic evaluation of a novel pulsatile bioreactor for biologically active heart valves. *Ann Biomed Eng* **32**, 1039-1049 (2004).
35. Z. H. Syedain, L. A. Meier, J. W. Bjork, A. Lee, R. T. Tranquillo, Implantable arterial grafts from human fibroblasts and fibrin using a multi-graft pulsed flow-stretch bioreactor with noninvasive strength monitoring. *Biomaterials* **32**, 714-722 (2011).
36. M. P. Rubbens, A. Mol, R. A. Boerboom, R. A. Bank, F. P. Baaijens, C. V. Bouten, Intermittent straining accelerates the development of tissue properties in engineered heart valve tissue. *Tissue Eng Part A* **15**, 999-1008 (2009).
37. R. A. Boerboom, M. P. Rubbens, N. J. Driessen, C. V. Bouten, F. P. Baaijens, Effect of strain magnitude on the tissue properties of engineered cardiovascular constructs. *Ann Biomed Eng* **36**, 244-253 (2008).
38. M. P. Rubbens, A. Mol, M. H. van Marion, R. Hanemaaijer, R. A. Bank, F. P. T. Baaijens, C. V. C. Bouten, Straining mode-dependent collagen remodeling in engineered cardiovascular tissue. *Tissue Eng Part A* **15**, 841-849 (2009).
39. D. Van Geemen, A. Driessen-Mol, F. P. T. Baaigens, C. Bouten, Understanding strain-induced collagen matrix development in engineered cardiovascular tissues from gene expression profiles. *Cell Tissue Res* **352**, 727-737 (2013).
40. S. G. Kim, T. Akaike, T. Sasagaw, Y. Atomi, H. Kurosawa, Gene expression of type I and type III collagen by mechanical stretch in anterior cruciate ligament cells. *Cell Struct Funct* **27**, 139-144 (2002).
41. J. Z. Paxton, P. Hagerty, J. J. Andrick, K. Baar, Optimizing an intermittent stretch paradigm using ERK1/2 phosphorylation results in increased collagen synthesis in engineered ligaments. *Tissue Eng Part A* **18**, 277-284 (2012).
42. Z. H. Syedain, J. S. Weinberg, R. T. Tranquillo, Cyclic distension of fibrin-based tissue constructs: Evidence of adaptation during growth of engineered connective tissue. *Proc Natl Acad Sci U S A* **105**, 6537-6542 (2008).
43. J. Papakrivopoulou, G. E. Lindahl, J. E. Bishop, G. J. Laurent, Differential roles of extracellular signal-regulated kinase 1/2 and p38MAPK in mechanical load-induced procollagen alpha1(I) gene expression in cardiac fibroblasts. *Cardiovasc Res* **61**, 736-744 (2004).
44. B. C. Isenberg, R. T. Tranquillo, Long-Term Cyclic Distention Enhances the Mechanical Properties of Collagen-Based Media-Equivalents. *Ann Biomed Eng* **31**, 937-949 (2003).
45. A. Solan, S. L. Dahl, L. E. Niklason, Effects of mechanical stretch on collagen and cross-linking in engineered blood vessels. *Cell Transplant* **18**, 915-921 (2009).

46. J. L. Balestrini, K. L. Billiar, Equibiaxial cyclic stretch stimulates fibroblasts to rapidly remodel fibrin. *J Biomech* **39**, 2983-2990 (2006).
47. M. R. Neidert, E. S. Lee, T. R. Oegema, R. T. Tranquillo, Enhanced fibrin remodeling in vitro with TGF-beta 1, insulin and plasmin for improved tissue-equivalents. *Biomaterials* **23**, 3717-3731 (2002).
48. M. Stekelenburg, M. C. Rutten, L. H. Snoeckx, F. P. Baaijens, Dynamic straining combined with fibrin gel cell seeding improves strength of tissue-engineered small-diameter vascular grafts. *Tissue Eng Part A* **15**, 1081-1089 (2009).
49. E. D. Grassl, T. R. Oegema, R. T. Tranquillo, A fibrin-based arterial media equivalent. *J Biomed Mater Res* **66A**, 550-561 (2003).
50. K. Nishimura, P. Blume, S. Ohgi, B. E. Sumpio, Effect of different frequencies of tensile strain on human dermal fibroblast proliferation and survival. *Wound Repair Regen* **15**, 646-656 (2007).
51. J. Rubin, T. C. Murphy, X. Fan, M. Goldschmidt, W. R. Taylor, Activation of extracellular signal-regulated kinase is involved in mechanical strain inhibition of RANKL expression in bone stromal cells. *J Bone Miner Res* **17**, 1452-1460 (2002).
52. J. H. Jansen, F. A. Weyts, I. Westbroek, H. Jahr, H. Chiba, H. A. Pols, J. A. Verhaar, J. P. van Leeuwen, H. Weinans, Stretch-induced phosphorylation of ERK1/2 depends on differentiation stage of osteoblasts. *J Cell Biochem* **93**, 542-551 (2004).
53. R. Raghupathy, C. Witzenburg, S. P. Lake, E. A. Sander, V. H. Barocas, Identification of Regional Mechanical Anisotropy in Soft Tissue Analogs. *J Biomech Eng* **133**, (2011).
54. R. A. O'Neill, A. Bhamidipati, X. Bi, D. Deb-Basu, L. Cahill, J. Ferrante, E. Gentalen, M. Glazer, J. Gossett, K. Hacker, C. Kirby, J. Knittle, R. Loder, C. Mastroieni, M. Maclaren, T. Mills, U. Nguyen, N. Parker, A. Rice, D. Roach, D. Suich, D. Voehringer, K. Voss, J. Yang, T. Yang, P. B. Vander Horn, Isoelectric focusing technology quantifies protein signaling in 25 cells. *Proc Natl Acad Sci U S A* **103**, 16153-16158 (2006).
55. J. Weinbaum, J. Schmidt, R. Tranquillo, Combating Adaptation to Cyclic Stretching by Prolonging Activation of Extracellular Signal-Regulated Kinase. *Cel Mol Bioeng* **6**, 279-286 (2013).
56. H. Stegemann, K. Stalder, Determination of hydroxyproline. *Clin Chim Acta* **18**, 267-273 (1967).

57. C. Williams, S. L. Johnson, P. S. Robinson, R. T. Tranquillo, Cell sourcing and culture conditions for fibrin-based valve constructs. *Tissue Eng* **12**, 1489-1502 (2006).
58. N. O. Chahine, M. B. Albro, E. G. Lima, V. I. Wei, C. R. Dubois, C. T. Hung, G. A. Ateshian, Effect of Dynamic Loading on the Transport of Solutes into Agarose Hydrogels. *Biophys J* **97**, 968-975 (2009).
59. M. B. Albro, N. O. Chahine, R. Li, K. Yeager, C. T. Hung, G. A. Ateshian, Dynamic loading of deformable porous media can induce active solute transport. *J Biomech* **41**, 3152-3157 (2008).
60. E. G. Canty, K. E. Kadler, Procollagen trafficking, processing and fibrillogenesis. *J Cell Sci* **118**, 1341-1353 (2005).
61. C. C. Berry, J. C. Shelton, D. L. Bader, D. A. Lee, Influence of external uniaxial cyclic strain on oriented fibroblast-seeded collagen gels. *Tissue Eng* **9**, 613-624 (2003).
62. J. W. Ruberti, N. J. Hallab, Strain-controlled enzymatic cleavage of collagen in loaded matrix. *Biochem Bioph Res Co* **336**, 483-489 (2005).
63. "Tissue Train Tension System." *Flexcell International Corporation*. 2011. Web. <http://www.flexcellint.com/slideshow4.htm>.
64. "Hollow Organ Bioreactors." *Harvard Apparatus.* 2014. Web. <http://www.harvardapparatusregen.com/media/pdf/Hollow%20Organ%20Bioreactor%20Brochure.pdf>.
65. "Electroforce® 5200 Biodynamic® Test Instruments." *Bose*. 2015. Web. <http://worldwide.bose.com/electroforce/en_us/web/5200_products/page.html>.
66. M. A. Swartz, M. E. Fleury, Interstitial flow and its effects in soft tissues. *Annu Rev Biomed Eng* **9**, 229-256 (2007).
67. "Physical Characteristics of Water." *Therm Excel.* 2014. Web. <http://www.thermexcel.com/english/tables/eau_atm.htm>.
68. "Sabic Innovative Plastics Ultem 1000 Pei." *MatWeb*. 2015. Web. <http://www.matweb.com/search/datasheet.aspx?matguid=88212c8b2c264bfb9d2dd419c2d8172b>.
69. "Primeline Specification Sheet." *Primeline Industries.* 2013. Web. <http://www.primelineindustries.com/latex-tubing-specsht.htm>.
70. J. Malda, T. J. Klein, Z. Upton, The roles of hypoxia in the in vitro engineering of tissues. *Tissue Eng* **13**, 2153-2162 (2007).
71. D. Seliktar, R. Black, R. Vito, R. Nerem, Dynamic Mechanical Conditioning of Collagen-Gel Blood Vessel Constructs Induces Remodeling In Vitro. *Ann Biomed Eng* **28**, 351-362 (2000).

72. B. Tschoeke, T. C. Flanagan, S. Koch, M. S. Harwoko, T. Deichmann, V. Ella, J. S. Sachweh, M. Kellomaki, T. Gries, T. Schmitz-Rode, S. Jockenhoevel, Tissue-Engineered Small-Caliber Vascular Graft Based on a Novel Biodegradable Composite Fibrin-Polylactide Scaffold. *Tissue Eng Part A* **15**, 1909-1918 (2009).
73. S. P. Hoerstrup, G. Zünd, R. Sodian, A. M. Schnell, J. Grünenfelder, M. I. Turina, Tissue engineering of small caliber vascular grafts. *Eur J Cardio-Thorac* **20**, 164-169 (2001).
74. T. Kitagawa, T. Yamaoka, R. Iwase, A. Murakami, Three-dimensional cell seeding and growth in radial-flow perfusion bioreactor for in vitro tissue reconstruction. *Biotechnol Bioeng* **93**, 947-954 (2006).
75. M. Radisic, L. Yang, J. Boublik, R. J. Cohen, R. Langer, L. E. Freed, G. Vunjak-Novakovic, Medium perfusion enables engineering of compact and contractile cardiac tissue. *Am J Physiol Heart Circ Physiol* **286**, H507-516 (2004).
76. N. K. Weidenhamer, D. L. Moore, F. L. Lobo, N. T. Klair, R. T. Tranquillo, Influence of culture conditions and extracellular matrix alignment on human mesenchymal stem cells invasion into decellularized engineered tissues. *J Tissue Eng Regen Med* **9**, 605-618 (2015).
77. J. W. Bjork, R. T. Tranquillo, Transmural flow bioreactor for vascular tissue engineering. *Biotechnol Bioeng* **104**, 1197-1206 (2009).
78. S. M. Ehsan, S. C. George, Nonsteady state oxygen transport in engineered tissue: implications for design. *Tissue Eng Part A* **19**, 1433-1442 (2013).
79. J. V. Nauman, P. G. Campbell, F. Lanni, J. L. Anderson, Diffusion of Insulin-Like Growth Factor-I and Ribonuclease through Fibrin Gels. *Biophys J* **92**, 4444-4450 (2007).
80. D. M. Wang, J. M. Tarbell, Modeling interstitial flow in an artery wall allows estimation of wall shear stress on smooth muscle cells. *J Biomech Eng* **117**, 358-363 (1995).
81. C. P. Ng, B. Hinz, M. A. Swartz, Interstitial fluid flow induces myofibroblast differentiation and collagen alignment in vitro. *J Cell Sci* **118**, 4731-4739 (2005).
82. J. van den Dolder, G. N. Bancroft, V. I. Sikavitsas, P. H. M. Spauwen, J. A. Jansen, A. G. Mikos, Flow perfusion culture of marrow stromal osteoblasts in titanium fiber mesh. *J Biomed Mater Res A* **64A**, 235-241 (2003).
83. D. Pazzano, K. A. Mercier, J. M. Moran, S. S. Fong, D. D. DiBiasio, J. X. Rulfs, S. S. Kohles, L. J. Bonassar, Comparison of Chondrogensis in Static and Perfused Bioreactor Culture. *Biotechnol Prog* **16**, 893-896 (2000).

84. Z. D. Shi, J. M. Tarbell, Fluid flow mechanotransduction in vascular smooth muscle cells and fibroblasts. *Ann Biomed Eng* **39**, 1608-1619 (2011).
85. D. Fey, D. R. Croucher, W. Kolch, B. N. Kholodenko, Crosstalk and signaling switches in mitogen-activated protein kinase cascades. *Front Physiol* **3**, 355 (2012).
86. J. H. Wang, B. P. Thampatty, J. S. Lin, H. J. Im, Mechanoregulation of gene expression in fibroblasts. *Gene* **391**, 1-15 (2007).
87. B. Saitta, S. Gaidarova, L. Cicchillitti, S. A. Jimenez, CCAAT binding transcription factor binds and regulates human COL1A1 promoter activity in human dermal fibroblasts: demonstration of increased binding in systemic sclerosis fibroblasts. *Arthritis Rheum* **43**, 2219-2229 (2000).
88. "Rubber-Like." *Stratasys*. 2015. Web. <http://www.stratasys.com/materials/polyjet/rubber-like>.
89. "Materials: Rubber-Like." *i.materialise.* 2015. Web. <http://i.materialise.com/materials/rubber-like/technical-specifications>.
90. P. Gibson, H. Schreuder-Gibson, D. Rivin, Transport properties of porous membranes based on electrospun nanofibers. *Colloids Surf A Physicochem Eng Asp* **187–188**, 469-481 (2001).
91. S. Badia, A. Quaini, A. Quarteroni, Coupling Biot and Navier-Stokes equations for modelling fluid-poroelastic media interaction. *J Comput Phys* **228**, 7986-8014 (2009).
92. V. M. Calo, N. F. Brasher, Y. Bazilevs, T. J. R. Hughes, Multiphysics model for blood flow and drug transport with application to patient-specific coronary artery flow. *Comput Mech* **43**, 161-177 (2008).
93. B. C. Isenberg, R. T. Tranquillo, Long-Term Cyclic Distention Enhances the Mechanical Properties of Collagen-Based Media-Equivalents. *Ann Biomed Eng* **31**, 937-949 (2003).

Appendix A. Comparison of Collagen Production in Two Lots of Dermal Fibroblasts

A.1. Motivation

Chapters 1 and 2 present data for a single lot of neonatal human dermal fibroblasts (lot #0000232777, Lonza). During the course of these experiments, a second lot of neonatal human dermal fibroblasts was purchased (lot #1165554, Invitrogen), and this lot was used alongside the original fibroblasts. These lots are referenced using the last three digits of the lot numbers (777 and 554) throughout this section. Almost immediately, differences were noted in the collagen deposition by these two lots of cells, both in the Flexcell disc format as well as qualitatively in the larger tubular valve constructs. In order to provide insight into these differences, a side-by-side comparison of both the basal (static) collagen production as well as the cyclic stretching-induced response was performed in the Flexcell system format. All procedures were performed according to the methods described in Chapters 1 and 2.

A.2. Comparison of ERK1/2 Activation

First, ERK1/2 phosphorylation was measured for both cell lots after 15 minutes of 5% constant amplitude cyclic stretching. Cells were entrapped in fibrin gel scaffolds as described in Chapters 1 and 2. As shown in Figure A-1, there was increased ERK1/2 phosphorylation in both cell lots due to cyclic stretching, 3.7-fold and 5.4-fold by the 777 and 554 cells, respectively. While it appears that the 554 cells achieved higher

ERK1/2 activation levels than the 777 cells, additional experiments would be required to definitively confirm this difference. After only 15 minutes of cyclic stretching ERK1/2 phosphorylation levels are changing rapidly, so this difference may be an artifact of the order in which the plates were removed from the system and harvested. What is known is that ERK1/2 was activated by cyclic stretching on the same order of magnitude in both cell lots.

A.3. Collagen Deposition by 554 and 777 Fibroblasts

Next, collagen deposition by cells from the two lots was compared. Fibrin discs with either 777 or 554 cells entrapped were cultured statically for one week, at which point they were cyclically stretched with strain amplitude of 5% for one or two weeks. Samples that remained in static culture for the additional one or two weeks were maintained as static controls. The results of this study are shown in Figure A-2. In static culture alone, the 554 cells produced more than twice the amount of collagen at both time points. After one week of cyclic stretching (Fig A-2a), both 554 and 777 cells exhibited increased collagen deposition per cell; however, the effect was greater for the 777 cells. After two weeks of cyclic stretching (Fig A-2b), only the 777 cells had increased collagen per cell due to cyclic stretching. There was no difference between stretched samples and static controls for the 554 cells at this time point.

A.4. Discussion and Conclusions

These results indicated that the 554 cells, which had a higher level of basal collagen deposition, were not as responsive to cyclic stretching, in terms of collagen deposition. This suggests that the collagen production pathway may have been saturated in the 554 cells, and cyclic stretching was unable to stimulate the cells further. Interestingly, as discussed above, the ERK1/2 pathway was activated to the same extent, if not more, in the 554 cells compared to the 777 cells. Along with the data presented in Chapter 2, this further confirmed that ERK1/2 activation alone was not a sufficient predictor of final collagen content in our fibrin-based engineered tissues.

This comparison highlights an interesting phenomenon that had not been previously explored in our lab. While the 554 cells were not nearly as responsive to cyclic stretching, they produced more collagen in static culture than the cyclically stretched 777 cells. While these effects have not been fully characterized in the large diameter tubular tissue constructs, it may be that the use of the 554 cells in static culture conditions will result in tissues with sufficient mechanical strength and stiffness without the need for bioreactor conditioning. However, it should be noted that the present study was only concerned with collagen deposition. Other cyclic stretching induced effects such as collagen maturation, crosslinking, and alignment may still require cyclic stretching even when the 554 cells are used.

A.5. Figures

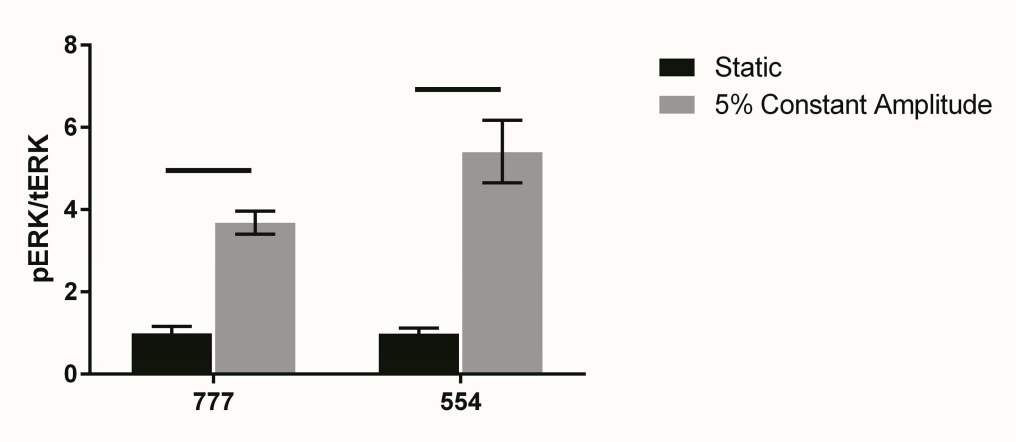

Figure A-1.

Ratio of phosphorylated to total ERK1/2 for 777 and 554 fibroblasts, normalized to respective static control. Samples were harvested after 15 minutes of 5% constant amplitude cyclic stretching. Horizontal bars indicate difference between static/5% stretching groups using Students t-test (n=3 per group).

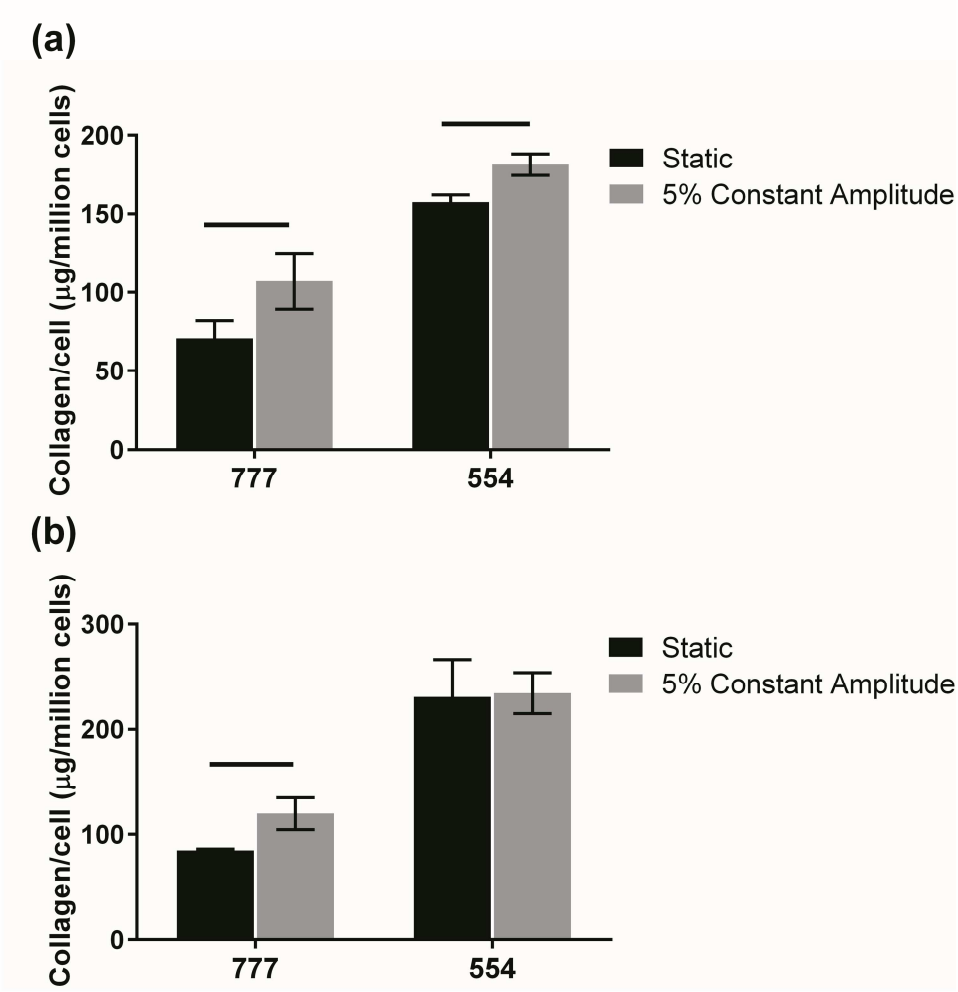

Figure A-2.

Collagen per cell in constructs after (a) one and (b) two weeks of 5% constant amplitude cyclic stretching for 777 and 554 lots of fibroblasts. Horizontal bars indicate difference between static/5% stretching groups using Students t-test (n=3 per group).

Appendix B. The Effect of Pulse Frequency on Tissue Properties in the Porated Sleeve Bioreactor

B.1. Motivation

Chapter 5 presented a porated sleeve bioreactor designed to culture large diameter fibrin-based tissue tubes for heart valve applications. As discussed, this bioreactor accelerated lumenal remodeling in regions within approximately 1 mm of the discrete columns of pores. In the previously described studies, the syringe pump frequency was set to 0.5 Hz resulting in an influx of medium every two seconds. As this lumenal and transmural flow appeared to be beneficial for tissue formation, it was hypothesized that it may be possible to further enhance this effect by increasing the pump frequency, thus increasing the influx of fresh culture medium at the lumenal surface of the tissue. We chose to change the pump frequency rather than the stroke volume, because this allowed us to alter the amount of medium delivered to the tissue without changing the applied strain amplitude. A study of the effects of two different pump frequencies, 0.5 Hz and 0.75 Hz, is presented here. All procedures were performed according to the methods described in Chapter 5 using porated support sleeves with 16 columns of pores for two weeks of bioreactor culture.

B.2. Effect of Frequency on Collagen and Cellularity

After two weeks there were no differences in the cellularity (Figure B-2a) or collagen per cell (Figure B-2b) between tissues stimulated with 0.5 Hz or 0.75 Hz pulse

frequencies. With the current porated sleeve geometry and culture duration it appeared that there was no measurable augmentation in collagen production or cellularity with the increased frequency.

B.3. Effect of Frequency of Lumenal Remodeling

Histological sections revealed poor fixation in these samples, and the majority of the lumenal collagen layer was not well preserved. Prior to this study, all experiments had been only one week in duration, and tissue thickness was approximately 0.5-0.6 mm. In this two week experiment, the harvested tissues were much thicker and more remodeled, so it was hypothesized that the volume of fixative was insufficient. The volume of 4% paraformaldehyde per sample was increased in subsequent studies (including all histological sections shown for two week studies in Chapter 5) from ~2 mL to ~4 mL to achieve better fixation and avoid loss of the lumenal remodeling layer. Additionally, after this study great care was taken to minimize contact with and manipulation of the lumenal tissue surface to better preserve this region.

Although it was difficult to make out the lumenal layer of collagen and cells, as most of this region did not survive fixation and sectioning, it appeared that samples stimulated with both frequencies had remnants of lumenal collagen deposition as shown by trichrome staining (Figure B-2).

B.4. Discussion and Conclusions

There were no observable differences in bulk properties or lumenal collagen remodeling between samples cultured in the porated sleeve bioreactor with pump frequency of 0.5 Hz or 0.75 Hz. An increase in pump frequency did not result in increased collagen content or cellularity of the tissue as a whole, and the tissues appeared qualitatively similar when visualized with a trichrome stain. It should be noted that the sample size for this study was small (n=2 per group), and because it was the first attempt at fixing the thicker tissues, it was difficult to compare the poorly fixed samples. However, as substantial improvement in tissue formation was not immediately apparent at the higher pump frequency, a frequency of 0.5 Hz was utilized in all subsequent studies.

Pump frequency was selected as the variable parameter in this experiment, as it allowed us to increase the influx of culture medium at the lumenal surface without changing the applied strain, assuming the sleeve and tissue were able to fully relax back to the initial state between each pulse. While this was the case for frequencies less than ~1 Hz, as pump frequency increased further, the sleeve and tissue tended to balloon out. The injected medium did not have sufficient time to flow out of the pores and end cap outlet before another pulse of medium arrived. This is obviously not desirable and limits the maximum frequency that can be applied in this system without altering the geometry of the ULTEM end piece. In addition, cycling at a higher frequency took a toll on the plastic syringes used to inject the medium, causing them to break daily rather than lasting the two day period between media changes.

By changing the pump frequency rather than the stroke volume, we were able to apply the same strain amplitude to all of the tissues. Chapters 1 and 2 highlight the effects of cyclic strain amplitude on collagen production in engineered tissues; however, all of these studies were performed at a single frequency (0.5 Hz), and it is unknown what effect the changing cyclic strain frequency may have on the fibroblasts in our system. Isenberg et al. found no effect of stretch frequency on the mechanical properties of vascular grafts consisting of smooth muscle cells in a collagen gel scaffold, although the pump duty cycle (held constant in the present work) did appear to have an effect.[93]

Although there was no apparent difference between tissues cultured with the two different stimulation frequencies in this study, as the porated support sleeve and bioreactor culture conditions are further refined, it may be worthwhile to consider the effect of pulse frequency once again. This small-scale study considered only two frequencies and one porated sleeve geometry, so it does not completely rule out the possibility of a frequency effect in porated sleeve bioreactor culture.

B.5. Figures

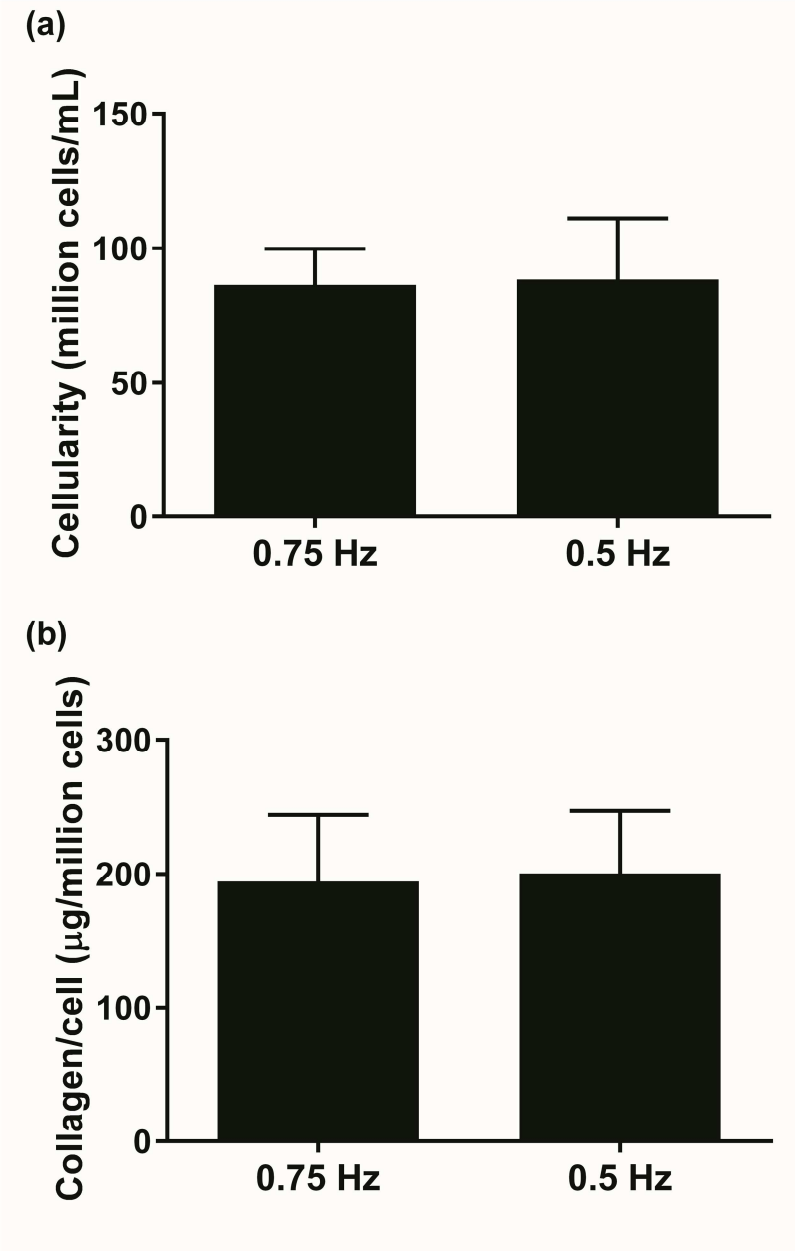

Figure B-1.

(a) Cellularity and (b) collagen per cell in samples stimulated at 0.5 and 0.75 Hz frequencies (n=2 per group).

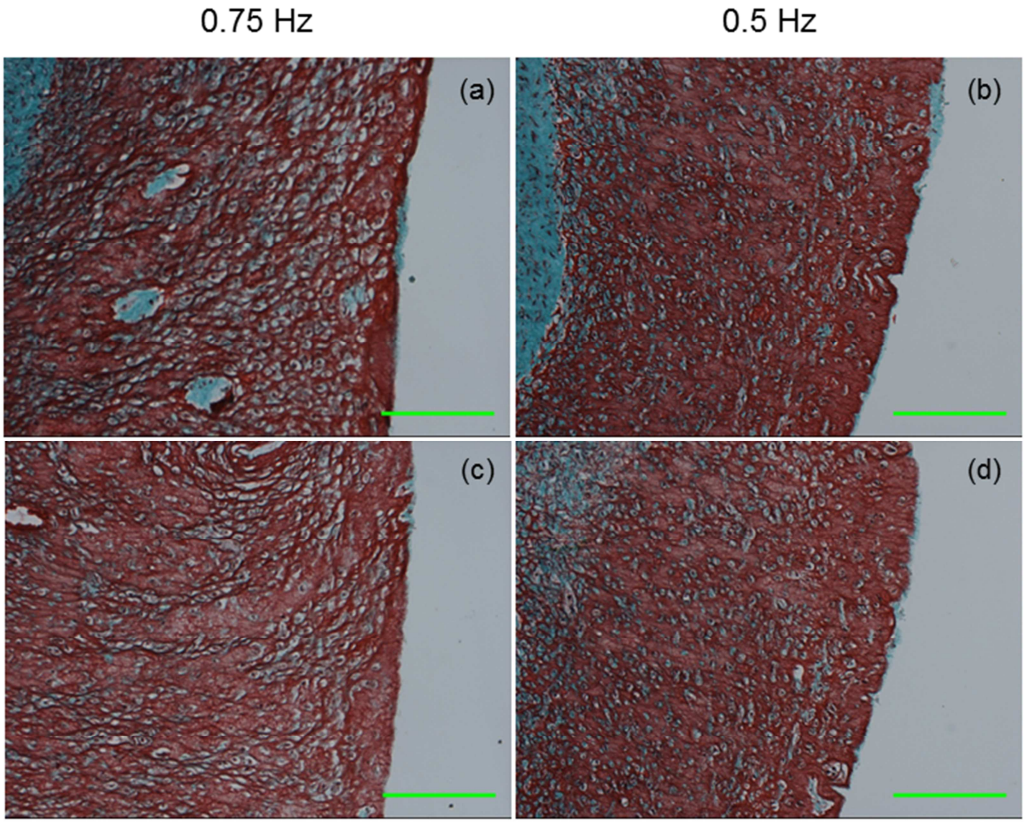

Figure B-2.

10X trichrome-stained sections of samples stimulated with (a,c) 0.75 Hz and (b,d) 0.5 Hz. Remnants of the cell and collagen layer are visible in patches on the lumenal surface. The lumenal surface is on the right in all images, and scale bars are 200 µm.

Appendix C. Protocols

C.1. Casting Flexcell Plates (3D)

NOTE: This should all be done sterilely, in the hood

1. Prepare solutions (13 mL per plate, which gives you 1 mL extra)

    For 1 plate

    Fibrinogen: 2.8 mL lot 021M fibrinogen stock (at 30 mg/mL) + 5.8 mL of 20mM HEPES

        in saline solution

    Thrombin: 0.433 mL thrombin stock + 1.7 mL DMEM+HEPES + 32.5 uL 2M $CaCl_2$

    Cells: 2.2 mL of passage 7 nhdfs at 3 million/mL concentration

2. Mix solutions 4:1:1 by volume (Fibrinogen:Thrombin:Cells)

    First at cells to fibrinogen and mix well, then add thrombin and mix again

3. Pipette 2 mL into the center of each well of a Flexcell Tissue Train plate

4. Quickly tilt the plate around to get the solution to cover the entire foam ring before gelation

5. Let sit in the hood for 6 minutes

6. Place in incubator for 24 minutes to continue gelation

7. Add 5 mL of medium (DMEM+10% FBS + 1% anti/anti+2 ug/mL insulin + 50 ug/ml ascorbic acid) to each well

8. Culture in incubator (37°C, 5% CO_2, 95% humidity)

Equipment and Reagents:

Name	Company	Product Number
Fibrinogen, lot 021M	Sigma	Lot 021M
1M HEPES solution	Corning	25-060-CI
0.9% Saline Solution	Hospira	RL-2099
Thrombin (25U/mL in 20mM HEPES)	Sigma	
DMEM+HEPES	Gibco by Life Technologies	10564-011
Calcium Chloride	Sigma	383147-100G
Neonatal human dermal fibroblasts (Lot 777)	Lonza	Lot #0000232777
Flexcell Tissue Train Plate, circular foam, untreated	Flexcell International	TTCF-4001U
Incubator	Nuaire	5500
DMEM	Gibco by Life Technologies	11995-065
FBS (fetal bovine serum)	Hyclone	Lot AXK51176
Antibiotic/Antimycotic	Gibco	15240-062
Insulin	Sigma	I9278
Ascorbic Acid	Sigma	A5960-100G

C.2. Tissue Harvest, Lysis, and Protein Extraction for Western Blot or Nanopro Immunoassay

1. Rinse tissue in cold Dulbecco's phosphate buffered saline (DPBS)
2. Place tissue in 1.2 mL microcentrifuge tube and snap freeze by submerging in liquid nitrogen for >1 min
3. Store frozen samples at -80°C until you are ready to lyse them and extract the protein.
4. Prepare lysis buffer on ice (all reagents from Protein Simple) – I use 350 ul per flexcell tissue or 100 ul for a 6mm biopsy punch of tissue

    Lysis buffer components: Bicine/CHAPs lysis buffer + 1X Aqueous Inhibitor Mix + 1X DMSO inhibitor mix

5. Add lysis buffer to the microcentrifuge tube with the sample in it – keep on ice
6. Lyse by sonication – 60% power for 30 seconds

    Clean the probe between samples with 0.1% Tween 20 in ddH20

7. Place tubes in the cold room on the end-over-end mixer for 30 minutes
8. Spin tubes at 13000rpm for 15 minutes at 4°C
9. Remove supernatant into new microcentrifuge tube, discard the pellet
10. Store lysates at -80°C.
11. Quantify protein concentration using BCA Protein Assay Kit

Equipment and Reagents:

Name	Company	Product Number
1.2 mL Microcentrifuge tubes	USA Scientific	
Dulbecco's Phosphate Buffered Saline (DPBS)	Gibco by Life Technologies	14190-144
Liquid Nitrogen	NA	NA
Bicine/CHAPs Buffer	Protein Simple	CODE: 040-764
Aqueous Inhibitor Mix (25X)	Protein Simple	CODE: 040-482
DMSO Inhibitor Mix (50X)	Protein Simple	CODE: 040-510
125 Volt Sonicator System	QSonica LLC	Q125
End-over-end mixer	Labnet	
Refrigerated microcentrifuge (Alford Lab)	Thermo Scientific	
Tween 20	Sigma Aldrich	P1379
Pierce BCA Protein Assay Kit	Thermo Scientific	23227

C.3. Western Blot

Run Gel

1. Thaw lysates on ice
2. Prepare 2X Laemmli sample buffer by adding DTT to a final concentration of 50mM (100mM) in 2X solution
3. Dilute lysates to same concentration (according to BCA assay results) and add equal volume lysate and Laemmli sample buffer
4. Boil samples for 5 minutes using the high setting on the heat block
5. Briefly spin samples to collect in the bottom of the tube
6. Prepare gels and gel box

    Remove comb and tape from 4-20% gradient gels

    Assemble gel box, making sure there is no leakage
7. Mix 85 mL 10X Tris/Glycine/SDS Buffer with 765 mL water (from distilled water tap)
8. Fill space between gels with 1X SDS buffer and fill outside area in gel box to fill line for 2 gels
9. Starting with dual color protein standard in the first well, use long pipette tips to pipette samples into the wells
10. Run gels at 200V for 1 hour

Transfer Gel

1. Mix 80 mL 10X CAPS buffer (recipe below), 80 mL methanol, and 640 mL ddH20

    CAPS Buffer: 22g CAPS [3-(cyclohexylamino)-1-propane sulfonic acid] in 1 L ddH20,

    pH to 11
2. Prepare transfer sandwich by soaking all components in 1X CAPS buffer

    Per gel: 2 pieces of filter paper, 2 sponges, 1 piece of nitrocellulose cut to size
3. Remove gel from between the two plates by cracking at the 4 arrows
4. Create “sandwich” in transfer apparatus

1 sponge, 1 filter paper, Gel, Nitrocellulose (roll to get good contact with gel), 1 filter paper, 1 sponge

5. Put sandwich in transfer bath with cooling unit and stir bar on stir plate.

6. Fill with

7. Run at 75 volts for 1 hour

Blot for protein of interest (ERK, p38, B-actin)

1. Remove nitrocellulose from sandwich and place protein side up in dish (I use pipette tip box lids)

2. Incubate in 5% blotting grade blocker+0.1% Tween 20 in PBS for 1 hour at room temperature or overnight at 4°C on orbital shaker

If blotting for p38 or phospho-p38, rinse 3X5 minutes in 1X tris buffered saline + 0.1% Tween 20 (TBST)

3. Add primary antibody, incubate for 1 hr at room temperature or overnight at 4°C – see dilutions below:

pERK and tERK (rabbit): 1:2000 in blocking solution

p38 and p-p38 (rabbit): 1:1000 in 5% Bovine serum albumin (BSA) in TBST

B-actin (mouse): 1:5000 in blocking solution

4. Rinse 3X5 minutes in TBST

5. Add secondary antibody corresponding to the primary (mouse or rabbit) 1:2000 (all diluted in blocking solution) and incubate for 1 hour at room temperature

6. Rinse 2X5 minutes in TBST

7. Rinse 1X5 minutes in TBS

8. Inclubate in 6 mL ECL solution for 3 minutes

9. Put in film cassette, expose film, and develop

To strip and re-blot

1. Rinse 1X5 minutes in TBS

2. Rinse 1X15 minutes in Stripping buffer

3. Rinse 2X5 minutes in TBST

4. Block, and re-blot

Equipment and Reagents:

Name	Company	Product Number
2X Laemmli sample buffer	Biorad	161-0737
DTT (Dithiothreitol)	Amresco	0281
Heat block	Fisher Scientific	
Mini centrifuge	Costar	
4-20% gradient gels	Biorad	456-1096
Gel box and power supply	Biorad	
10X Tris/Glycin/SDS Buffer	Biorad	161-0732
Precision plus dual color protein standard	Biorad	161-0374
Gel loading pipette tips	Biorad	223-9915
CAPS	Sigma Aldrich	C2632-100G
Transfer sponges	Biorad	170-3933
Filter paper	Whatman	1003-917
Nitrocellulose (Protran)	University Stores	NBA085C001EA
Cooling unit	Biorad	170-3934
Blotting grade blocker	Biorad	170-6404
Tween 20	Sigma Aldrich	P1379
Phosphate buffered saline (PBS)	Gibco by Life Technologies	14190-144
Orbital Shaker	Midwest Scientific	S2030-LS
Bovine Serum Albumin (BSA)	Amresco	0175-25G
Tris buffered saline	Thermo Scientific	28358
Total ERK (p44/42) antibody	Cell Signaling Technology	9102S
Phospo ERK (p-p44/42) antibody	Cell Signaling Technology	9101S
Total p38 antibody	Cell Signaling Technology	9212S
Phospho p38 antibody	Cell Signaling Technology	9211S
B-actin antibody (mouse)	Sigma Aldrich	A5441
Seconday Rabbit IgG- HRP Linked	GE Healthcare	NA934-100UL
Secondary Mouse IgG – HRP Linked	GE Healthcare	NA931-100UL
ECL: Luminata Classico	EMD Millipore	WBLUC0100
Genemate Blue Film, 5X7	University Stores	CX24355
Film Cassette	Fisher Scientific	FBCA 57
Restore Plus Stripping Buffer	Thermo Fisher Scientific	46430

C.4. Tissue Harvest, Lysis, and RNA Purification for PCR

NOTE: Throughout purification, keep work area clean and wipe down all equipiment/surfaces with RNase Away

1. Harvest tissue and store at 4°C in RNALater in 1.2 mL microcentrifuge tube until you're ready to proceed
2. Remove RNALater using a micropipette
3. Add 350ul or 600 ul of RLT Buffer (+DTT) to each sample, following the instructions in the RNeasy Plus Mini Kit (see Table 1 for appropriate volume)
4. Sonicate the tissue in the buffer for 20 seconds at 60% max power
5. Spin for 3 minutes at 13,000 rpm at room temperature, remove the supernatant and use it in the following steps
6. Complete steps 2-8 in the RNeasy mini kit instructions
7. Submit sample of purified RNA to BMGC for quantitation on the Nanodrop – see current submission instructions at http://www.bmgc.umn.edu/
8. Store RNA at -20°C

Equipment and Reagents:

Name	Company	Product Number
1.2 mL Microcentrifuge tubes	USA Scientific	
RNase Away Spray	Sigma Aldrich	83931
RNAlater Stabilization Reagent	QIAGEN	76104
RNeasy Plus Mini Kit	QIAGEN	74134
DTT (Dithiothreitol)	Amresco	0281
125 Volt Sonicator System	QSonica LLC	Q125
Microcentrifuge (Biofuge pico)	Heraeus	

C.5. cDNA Synthesis for PCR

NOTE: Throughout synthesis, keep work area clean and wipe down all equipiment/surfaces with RNase Away

1. Combine up to 5 ug total RNA (I try to use a constant amount, based on BMGC quantitation), 1uL Random Hexamers, 1uL Annealing Buffer, and RNase/DNAse free water to 8 uL total volume in a 0.2 mL PCR tube
2. Vortex and centrifuge to collect sample in bottom of tube
3. Heat to 65°C for 5 minutes using thermal cycler
4. Place on ice for 1 minute
5. Add 10 uL 2X first strand reaction mix and 2 uL SuperScript III/RNaseOUT Enzyme Mix to each tube
6. Vortex and centrifuge to collect sample in bottom of tube
7. Using thermal cycler, heat tubes to 25°C for 10 minutes, followed by 50°C for 50 minutes, then 85°C for 5 minutes
8. Store cDNA at -20°C.

Equipment and Reagents:

Name	Company	Product Number
0.2 mL PCR tubes	University Stores	CX13127
RNase Away Spray	Sigma Aldrich	83931
SuperScript® III First-Strand Synthesis SuperMix (Contains all components that get added to the RNA)	Life Technologies	18080-400
Vortex	Fisher	12-812
Mini Centrifuge	Costar	
Thermal Cycler (Shen Lab)	Thermo	

C.6. PCR

1. Thaw SYBR Green on ice (and in dark). Thaw primers, and cDNA on bench top
2. Make a "master mix" for each primer containing (per well)

    6.25 uL SYBR Green

    0.0075 uL forward primer

    0.0075 uL reverse primer

    ddH20
3. Pipette 11.5 uL of the appropriate master mix into each well on 384 well PCR plate
4. Add 1 uL of the appropriate cDNA sample to each well on the PCR plate
5. Cover with RNAse/DNAse free plate cover, keep on ice and protected from too much light
6. Run on Agilent

    Cycles:

        10 minutes at 95°C

        40 repeats of (30s at 95°C, 1 min at 55°C, 1 min at 72°C)

        10 minutes at 72°C

Equipment and Reagents:

Name	Company	Product Number
KicQStart SYBR Green	Sigma Aldrich	KCQS02
Primers – sequences in thesis At 100 µM in ddH20	BMGC	
PCR Plate	Life Technologies	4309849
Optical Plate Cover	Agilent Technologies	4360954
Plate centrifuge (Hall Lab)		
qPCR Machine (Hall Lab)	Applied Biosystems	7900HT

C.7. Casting 22mm Tubular Constructs

NOTE: This should all be done sterilely, in the hood

1. Assemble molds – glass mandrels + 2 plungers + Teflon tape
2. Autoclave molds, outer casings, culture jars, extra Teflon tape, ejector rod, Dacron cuffs (2 per VRE)
3. Soak molds in 5% Pluronic F-127 in water for 1-3 hours
4. Lay out molds to dry on sterile drape in the hood for ~1 hour
5. Prepare solutions (36 mL/VRE, may want to make extra if molds are extra long)

    For 1 VRE

    Fibrinogen: 4.8 mL lot SLBF fibrinogen stock (at 30 mg/mL) + 19.2 mL of 20mM HEPES in saline solution

    Thrombin: 1.2 mL thrombin stock + 4.8 mL DMEM+HEPES + 90 uL 2M $CaCl_2$

    Cells: 6 mL of passage 7 nhdfs at 6 million/mL concentration
6. Assemble molds with Dacron cuffs, and place in outer casings – make sure you have a good fit
7. Mix solutions 4:1:1 by volume (Fibrinogen:Thrombin:Cells)

    First add cells to fibrinogen and mix well, then add thrombin and mix again
8. Using a syringe and needle, inject solution into mold, being careful to avoid bubbles
9. Let sit in the hood for 6 minutes
10. Place in incubator for 24 minutes to continue gelation (I usually put all molds in 1000mL beaker and cover with foil to prevent contamination from incubator)
11. Add 250 mL of medium (DMEM+10% FBS + 1% anti/anti+2 ug/mL insulin + 50 ug/ml ascorbic acid) to each culture jar
12. Using Teflon ejector rod, eject VREs 1 at a time from mold into PBS containing petri dish and transfer with sterile gloved hands into culture jars
13. Culture in incubator (37°C, 5% CO_2, 95% humidity)

Equipment and Reagents:

Name	Company	Product Number
Glass tube mandrels, 0.625" inner diameter	McMaster Carr	8729K47
Polycarbonate outer casing	McMaster Carr	
Syringe plungers (washed in contrex, branson, and water)	Kendall Monoject	
Teflon tape, Commercial Grade, ½"	TaegaSeal	
Dacron cuffs	From St. Jude, special arrangement	
Pluronic F-127	Sigma	P2443-250G
Sterile drape	MediChoice	MDRP1001
Fibrinogen, lot SLBF	Sigma	Lot SLBF
1M HEPES solution	Corning	25-060-CI
0.9% Saline Solution	Hospira	RL-2099
Thrombin (25U/mL in 20mM HEPES)	Sigma	
DMEM+HEPES	Gibco by Life Technologies	10564-011
Calcium Chloride	Sigma	383147-100G
Neonatal human dermal fibroblasts (lot 554)	Invitrogen	Lot #: 1165554
Sterile 30mL syringe	Norm-ject	
Needle, 15G, sterile	Monoject	
Culture jar	Nalgene	
Ejector rod (12 inch Teflon rod, 20mm diameter)		
Petri dish	Corning	430597
PBS (Phosphate buffered saline)	Gibco by Life Technologies	14190-144
Incubator	Nuaire	5500
DMEM	Gibco by Life Technologies	11995-065
FBS (fetal bovine serum)	Hyclone	Lot AXK51176
Antibiotic/Antimycotic	Gibco	15240-062
Insulin	Sigma	I9278
Ascorbic Acid	Sigma	A5960-100G

C.8. Mounting Tubular Constructs in Biroeactors

NOTE: This should all be done sterilely, in the hood

1. Sterilize latex sleeves: Sonicate 1 hr in Branson, 1 hr in water, then soak in 70% isopropanol for at least 4 days
2. Autoclave the following: bioreactor jars and lids with 3 way valves, ULTEM end pieces, scissors, fine tweezers, ½ inch Teflon tape, cable ties (2 per bioreactor), male and female luer lock caps, Masterflex tubing
3. At least 1 hour before bioreactor mounting, lay out latex sleeves on a sterile drape in the hood, and allow the isopropanol to evaporate.
4. Working with sterile gloves on, in the hood, wrap the ULTEM end pieces with a single layer of Teflon tape
5. Place the latex tube over one end piece, and secure with a cable tie
6. Remove a VRE from its mandrel carefully, trying to avoid putting undue stress on the tissue
7. Use sterile scissors to cut off the Dacron cuffs from both ends of the tissue
8. Slide the tissue over the latex – sometimes wetting the latex with medium helps this process
9. Cut the latex to the appropriate length
10. Place the other end cap in the latex tubing and secure with a cable tie
11. Attach upper end piece to jar lid
12. Use a 24 mL (or larger) syringe to pump medium in through the 3-way valve to fill the tubing and lumen of the latex sleeve – try to remove all air bubbles from the construct interior
13. Fill bioreactor jar with medium (~220 mL DMEM+10%FBS+)
14. Screw lid tightly onto jar
15. Attach sterile syringe filter to port on jar lid
16. Cap top of 3-way valve before placing the bioreactor jar into the incubator (37°C, 5% CO_2, 95% relative humidity)

17. Fill lines: Using large (>30 mL) syringe, fill lines with medium. Cap one end, and place medium-filled smaller syringe on the other end (usually 5 or 10 mL syringe)
18. Place tubing in through side point of the incubator and connect to 3-way valve on bioreactor jar
19. Secure syringe in reciprocating syringe pump and start the pump
20. Watch carefully for leaks over the first 30 minutes

Equipment and Reagents:

Name	Company	Product Number
Masterflex PharMed BPT Tubing	Cole-Parmer	EW-06508-16
Bioreactor jar (Tall 250 mL jar)	Nalgene (ports added using Dremel)	
ULTEM end pieces	McMaster Carr (machined by CSE shop)	
Teflon tape, Commercial Grade, ½"	TaegaSeal	
Scissors	Ustores	
Fine tweezers	Ustores	
Sterile drape	MediChoice	MDRP1001
Sterile gloves	Medline Industries	
Sterile syringes	Norm-ject	
Cable ties	McMaster Carr	
3 way valve	Nordson Medical	DCV125-001
Sterile syringe filter	Millex	SLGP033RS
Male and female luer lock caps	Value Plastics	Female: FTLLP-1 Male: LP4-1
Syringe pump	Various, modified by CSE shop	
Incubator	Nuaire	5500
DMEM	Gibco by Life Technologies	11995-065
FBS (fetal bovine serum)	Hyclone	Lot AXK51176
Antibiotic/Antimycotic	Gibco	15240-062
Insulin	Sigma	I9278
Ascorbic Acid	Sigma	A5960-100G